Final Report

Application of the SEBAL Methodology for Estimating Consumptive Use of Water and Streamflow Depletion in the Bear River Basin of Idaho through Remote Sensing

Idaho Department of Water Resources
University of Idaho, Department of Biological and Agricultural Engineering

Submitted to

The Raytheon Systems Company
Earth Observation System Data and Information System Project

December 15, 2000

Anthony Morse
Idaho Department of Water Resources

Masahiro Tasumi
University of Idaho

Dr. Richard G. Allen
University of Idaho

William J. Kramber
Idaho Department of Water Resources

Contents

1.0 Introduction

1.1 History of the Project

1.1.1 NASA's Earth Observing System

NASA's Earth Observing System (EOS) is a satellite-based monitoring tool for supporting research on global environmental change. With the successful launch of two satellites and the initiation of an operational EOS Data and Information System (EOSDIS) ground system, there is now an established basis for collecting and monitoring global change research data. Although research remains the system's primary focus, the data and underlying technologies are potentially valuable for many other commercial and federal/state/local government uses.

Under NASA sponsorship, the Raytheon Company is working with several universities and state/local agencies within the United States to explore non-research uses for EOS data and its technologies. Raytheon and its university partners are focusing on making data more readily available for civil uses including urban planning, disaster management, agriculture, environmental monitoring and natural resource management. The University of Idaho (UI) and the Idaho Department of Water Resources are developing a water-resource application through their cooperative project application of the Surface Energy Balance Algorithm for Land (SEBAL) methodology for mapping evapotranspiration.

1.1.2 SEBAL

SEBAL is an image-processing model comprised of twenty-five computational steps that calculates the evapotranspiration (ET) and other energy exchanges at the earth's surface using digital image data collected by Landsat or other remote-sensing satellites measuring visible, near-infrared and thermal infrared radiation. SEBAL algorithms predict a complete radiation and energy balance for the surface along with fluxes of sensible heat and aerodynamic surface roughness. ET is computed as a component of the energy on a pixel-by-pixel basis. A general schematic of the SEBAL process is illustrated in Figure 1.1.2-1. A detailed description of the model is provided in Appendices A, B, and C.

ET for periods in between satellite overpasses is computed by applying ratios of ET from SEBAL to ET from ground-based weather stations to the ET from the ground-based stations for intervening periods. These ratios are essentially customized "crop coefficients" that are determined uniquely for each pixel of an image. Each Landsat image is comprised of about 30 million pixels.

1.2 Participants

The research component of this project is being led by Dr. Richard G. Allen of the University of Idaho, Departments of Biological and Agricultural Engineering and Civil Engineering. Dr. Allen is assisted by Mr. Masahiro Tasumi, graduate student of BAE. The end-user of the results of the research is the Idaho Department of Water Resources (IDWR).

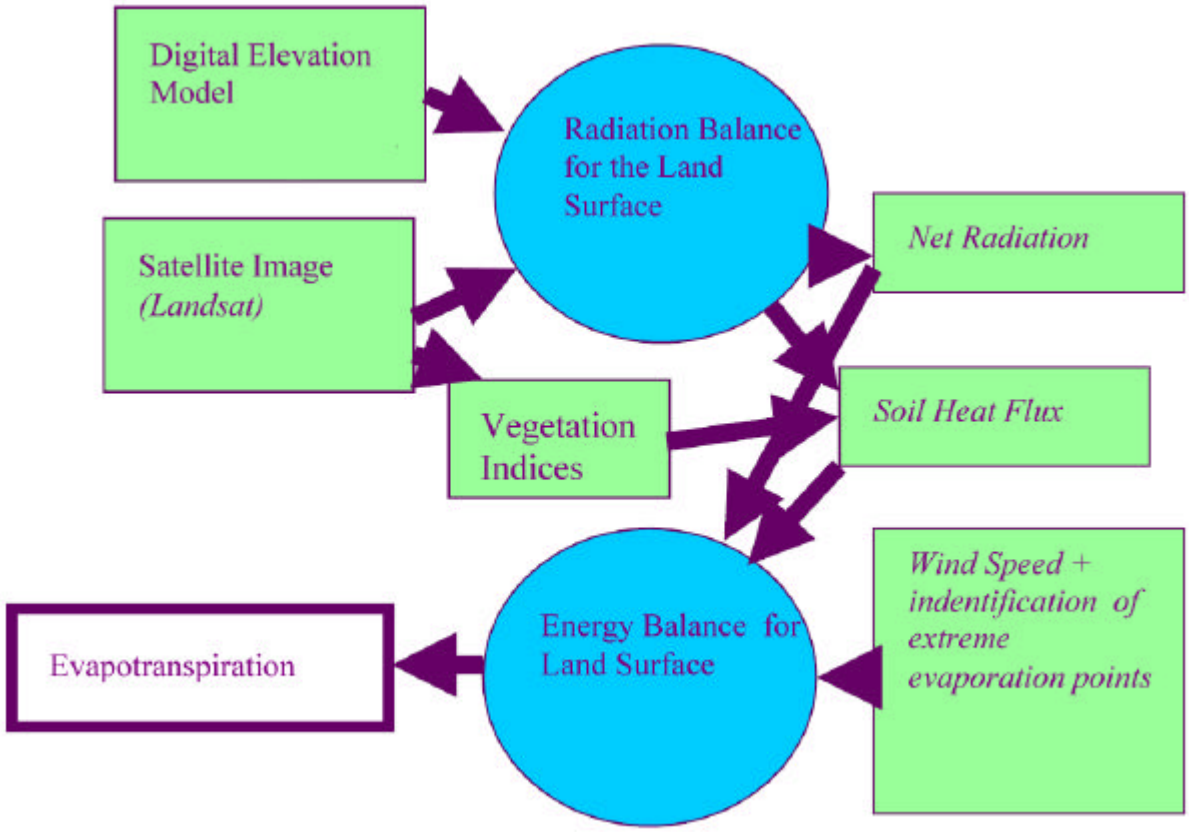

Figure 1.1-1. Schematic of the general computational process for determining evapotranspiration using SEBAL.

1.3 Institutional Roles of Participants

1.3.1 The Idaho Department of Water Resources

The role of IDWR in this project is appropriate from two perspectives. IDWR is responsible for water management in Idaho, and IDWR is the lead state agency for remote sensing and geographic information systems, and houses the Idaho Geographic Information Center.

The Department's mission statement reads as follows:

"*The Idaho Department of Water Resources is a public agency established to serve the people of Idaho and protect their welfare by ensuring that water and energy are conserved and available for the sustainability of Idaho's economy, ecosystems, and resulting quality of life. We will pursue our mission through:*

(1) controlled development, wise management, and protection of Idaho's surface and ground water resources, stream channels, and watersheds, and
(2) *promotion of cost-effective energy conservation and use of renewable energy sources*."

IDWR's role in geospatial technology is defined by provisions of Executive Order 96-24. The provisions of the Executive Order, spell out several functions, including that IDWR (1) promote the operational applications of digital image analysis and geographic information systems; (2) cooperate with, receive, and expend funds from other sources for the continued development and utilization of image and geographic information techniques; (3) cooperate with Idaho universities and other research institutions for the development and implementation of improved capabilities resulting from research activities; and (4) as resources permit, provide a centrally coordinated, spatial data clearing-house.

1.3.2 The University of Idaho

The role of the University of Idaho covers both education and research. University of Idaho faculty from Biological and Agricultural Engineering are housed in The Twin Falls Research and Extension Center at Kimberly, Idaho. The Center supports Cooperative Extension System and agricultural research programs in south central Idaho. These faculty scientists are supported by staff and work with the people of Idaho to address locally identified needs. Major programs are conducted in agriculture, natural resources, youth, family, community, and environmental issues. Center faculty and staff have worked for many years on issues related to evapotranspiration in southern Idaho.

1.4 Statement of Problem

IDWR currently has procedures used to compute ET. These procedures use remote sensing and GIS tools to map crop types, and use the resulting information as one input to ET equations (Allen and Brockway, 1983). However, these procedures are cumbersome, slow, expensive to implement, and yield results of uncertain accuracy**.** IDWR needs an efficient, accurate, and inexpensive procedure that can predict the actual evaporation fluxes from irrigated lands throughout a growing season.

In particular, IDWR needs a procedure that can predict total, net depletion of water from the Bear River system. The Idaho Department of Water Resources is the representative for Idaho to

the three-state Bear River Commission. The commission annually reviews the predicted depletions of water from the Bear River within each state. Depletions for irrigated agriculture are defined as the differences between gross diversions and net returns to the river system via ground water. Because the net returns from un-evaporated diversions are in diffused form, they are impossible to measure. Therefore, net depletions for the Bear River are predicted using predictions of evapotranspiration from irrigated lands less any evapotranspiration that would have occurred from natural range conditions in the absence of any irrigation or agriculture.

Improvement in accuracy of predicting past, present and future ET in the Bear River basin will facilitate better water management and equity among the parties to the Bear River compact. In addition, as other needs and interests in streamflows of the Bear increase over time, for example for water quality enhancement, recreation, fisheries, wildlife and endangered species, members of the Bear River compact will require ever-increasing information on disposition, fluxes, and hydrology of the water resources of the basin.

In addition to improving the monitoring and regulation of developments in irrigated agriculture, having the capability to predict ET using remotely sensed images will provide valuable information for calculating complete water balances for river basins and for calibrating and operating ground-water flow models. These models require input of information on the flux of water at the ground surface. This requires knowledge of both precipitation and ET. Prediction of ET for rangeland and natural systems is poorly developed for weather-based systems and is severely limited by the sparseness of weather stations. A remote-sensing based approach would provide spatially distributed estimates of ET that would greatly improve the resolution and certainty of river-basin water balances.

1.5 Project Goals

The proposal for this project listed six criteria for success:

1) the ability to predict evapotranspiration fluxes from irrigated areas of the Bear River basin of Idaho as determined by comparison of ET estimates with previous measurements made using drainage lysimeters and with estimates made from water balances of the river basin;

2) the ability to compute evapotranspiration fluxes during future periods with no additional calibration or modification to the remote sensing model and on an enhanced spatial scale;

3) the ability to compare total ET predictions for agricultural areas of the Bear River basin of Idaho among years, after correction for differences in weather influences;

4) the ability to predict evapotranspiration fluxes in near real time and using reasonable amounts of human resources;

5) success within the INSIDEIdaho program will be measured by use of INSIDEIdaho data by the project and the use of project data deposited into INSIDEIdaho;

6) use of the SEBAL method by the Bear River Commission.

These goals have largely been met. Goal #1, the comparison between SEBAL and lysimeter measurements of ET were successful. That success allows meeting Goals #2, #3, and #4. Arrangements are being made with INSIDE Idaho to transfer the images. Whether or not the project will succeed in meeting Goal #6 awaits evaluation of results by the Bear River Commission Technical Advisory Committee.

1.6 Criteria for Success

The end user groups under this proposal are the Idaho Department of Water Resources and the Bear River Commission. If successful, this remote-sensing application will result in changes in the way that ET is predicted, monitored, and used for administration of the Bear River Compact and for other IDWR business processes.

Insufficient time has passed since the completion of this project for IDWR to integrate SEBAL into its appropriate business processes and evaluate the results. However, The Director of IDWR is evaluating SEBAL, and has scheduled an extended presentation by Dr. Allen as part of his SEBAL and its potential role in the department's business. Some insight into the potential utility of SEBAL to IDWR can be gained from the fact that IDWR has requested spending authority from the Idaho Legislature for $100,000 in each of the next three years for SEBAL-related work.

SEBAL presents a unique opportunity for The Bear River Commission to use an objective means to quantify depletion from the three participating states. The preliminary results of this project have been presented to the Technical Advisory Committee of the Commission, and to the operations Committee. An expanded presentation is scheduled after completion of this project. The Commission will not take any action on SEBAL until the project is completed and the results can be presented in their entirety.

A direct benefit of the project to the University of Idaho is that the project directly supports a graduate student. Masahiro Tasumi began working on this project in May, and has worked a forty-hour week as part of his graduate studies. This work he is accomplishing on this project, which is contained in Appendices A, B and C, will be the core of his Ph.D. dissertation.

1.7 Project Resources

1.7.1 Budget

The budget for this project is composed of funds from three sources: 1) federal funds from the NASA EOS program and administered by the Raytheon Company; 2) State of Idaho funds provided through the budgets of IDWR and 3) the University of Idaho, Department of Biological and Agricultural Engineering. The total budget is $53,992.

	Source of funds		
	IDWR	U Idaho	NASA
Personnel			
U Idaho		$5,300	$2,500
IDWR staff	$9,000		
Grad. Student			$14,000
Consultant			$6,500
Travel			$5,000
ERDAS software			$5,200
Indirect Cost	$3,222	$795	$2,475
Total Cost	**$12,222**	**$6,095**	**$35,675**

Table 1.7.1-1. Budget categories and source of project funds .

1.7.2 Personnel

University of Idaho personnel accounted for the majority of personnel time spent on this project. Mr. Tasumi worked almost full-time for six months. Dr. Allen worked part time. IDWR personnel worked part-time. Dr. Bastiaanssen, the consultant, worked seven days.

1.8 SEBAL

1.8.1 Concept

The SEBAL procedure consists of a suite of algorithms, in this case implemented in the ModelMaker module of the ERDAS software. The algorithms solve the complete energy balance:

$$\lambda ET = R_n - G - H$$

where λET is latent heat flux (the energy used to evaporate water), R_n is net radiation at the surface, G is soil heat flux, and H is sensible heat flux to the air. R_n is computed for each pixel using albedo and transmittances computed from short wave bands and using long wave emission computed from the thermal band. Soil heat flux is predicted using vegetation indices computed from combinations of bands and net radiation. Sensible heat is calculated from several factors: surface temperature and a wind speed measurement from ground data, and estimated surface roughness and surface-to-air temperature differences predicted from vegetation indices. All computations are made specific to each pixel in the image. Iterative predictions of sensible heat are improved using atmospheric stability corrections based on Monin-Obukhov. Endpoints for H within a satellite image are bounded by known evaporative conditions at key reference-points. These reference point include pixels having little or no evaporation, for example, for recently burned areas (where $H \sim R_n - G$), desert areas having depleted soil water ($H \sim R_n - G$), shallow water bodies ($H \sim 0$), and well irrigated fields (where $H \sim 0$ so that $\lambda ET \sim R_n - G$). Evapotranspiration (ET) is finally calculated from λET by dividing by the latent heat of vaporization, λ.

Details of application are given in Bastiaanssen, et al. (1998a and in Appendices A, B, and C). The SEBAL algorithm can be applied with little or no ground-based weather data. When data are available, however, as they are for southern Idaho, predictions by the procedure are improved, for example by the use of actual measurements for solar radiation and wind speed on the day of the image. Comparison of the SEBAL procedure with three other remote-sensing based procedures for predicting ET from satellite data are presented in a series of papers in a special 2000 issue of the Journal of Hydrology (issue 229) and in Bastiaanssen (2000).

1.8.2 Previous Work

The SEBAL method has been used in various studies to assess evapotranspiration rates in Spain, Italy, Turkey, Pakistan, India, Sri Lanka, Egypt, Niger, and China (Bastiaanssen, et al., 1998a; Bastiaanssen, et al., 1998b; Bastiaanssen and Bos, 1999). In addition, Bastiaanssen (in preparation) has compiled a comparison of predictions of ET and sensible heat flux (H) by SEBAL with measurements made by eddy covariance and scintillometer systems. Confidence intervals have been determined. Comparisons with the measured fluxes confirm robustness of the SEBAL procedure.

The various applications have demonstrated the ability of SEBAL to estimate daily evapotranspiration accurately. In application of the SEBAL method, there is no need for intensive ground, meteorological or land use information. Only routine, widely available air temperature measurements are required for estimation of reference (potential) ET for interpolation between satellite overpasses. Two primary articles that describe the background and computational procedures of SEBAL are Bastiaanssen et al. 1998a and Bastiaanssen et al. 1998b.

1.9 Approach

1.9.1 The Bear River Basin

The Bear River Basin covers 7,465 square miles of Idaho, Utah, and Wyoming and contains about 470,000 acres of crop and pasture land. The Bear River flows from the Uinta Mountains in northern Utah north into Wyoming, then west into Idaho, and then back into Utah, where it empties into the Great Salt Lake. The river meanders through a basin that covers 7,465 square miles Water from the river and its tributaries is used primarily for irrigation within the basin.

During the period 1982 to 1988, a relatively intensive monitoring of weather was made in the Bear River Basin in all three states of Utah, Wyoming and Idaho (Hill et al., 1989). Five automated weather stations were installed along the Bear River during this period to complement the eleven National Weather Service volunteer stations in the basin. The automated weather stations collected data on solar radiation, air temperature, humidity, wind speed and precipitation. In addition to the weather data collection, three locations along the Bear River were instrumented with drainage-type lysimeters by which ET was directly measured on approximately weekly time-steps. Three lysimeters were located in the Idaho portion of the Bear River basin, near Montpelier.

These lysimeters were planted to different mixtures of vegetation that were representative of the irrigated meadow fields surrounding the installation. Each lysimeter was approximately 1.5 sq. meters in area. Additional lysimeters were installed near Randolph, Utah and Evanston, Wyoming (Hill et al., 1989).

The original intent of the project was to focus on data sets from two hydrologic years, including data collected throughout the 1985 growing season. The data-sets that were ultimately analyzed were different from those proposed due to shortfalls in both time duration of the study and availability of cloud-free images for some periods.

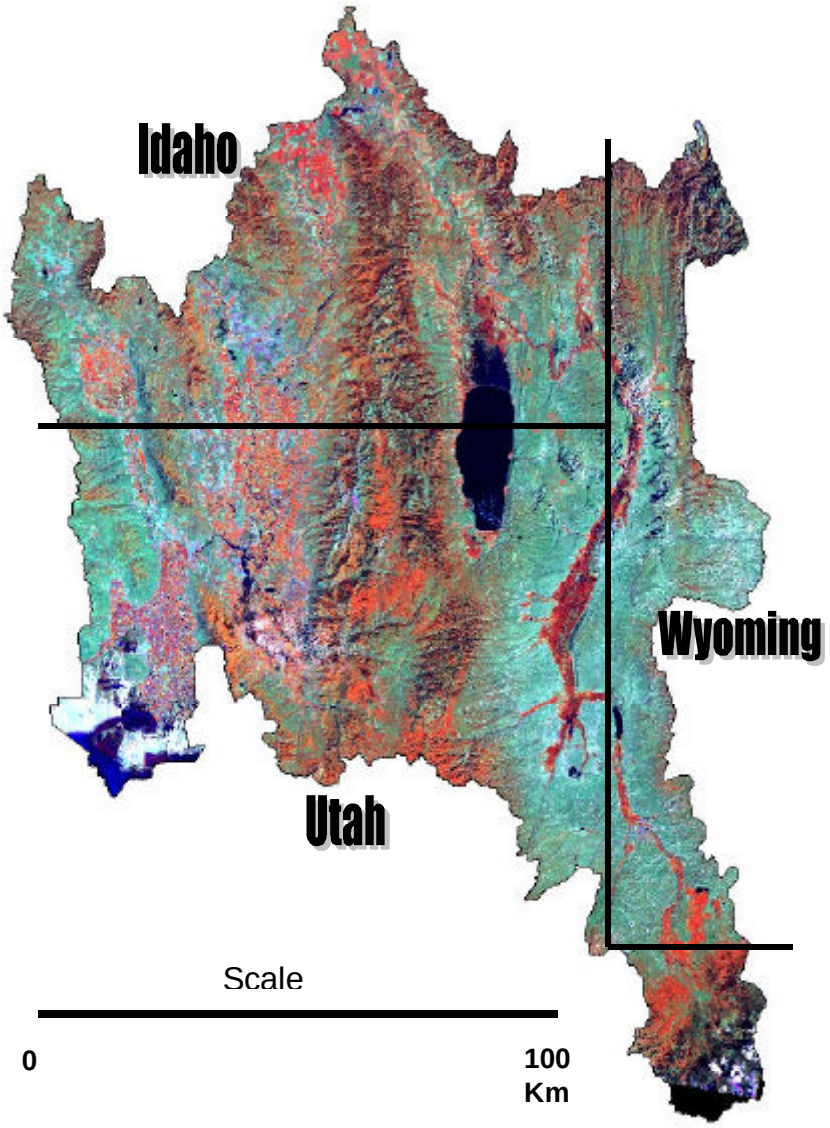

Figure 1.9.1-1 Landsat TM image of the Bear River Basin

The first data set was taken from the period 1982 to 1988, during which time ET data are available from a ground-based lysimeter system that was operating during this period (Hill et al., 1989). The year 1985 was selected based on relatively high measurements of solar radiation during the summer of that year which would help to improve the likelihood of obtaining cloudless Landsat images. The second data set was proposed for the year 2000 during which images from the new Landsat-7 satellite were available. Processing and evaluation of ET estimates from Landsat-7 data will enable the comparison of fluxes between Landsat-5 and Landsat-7 to insure compatibility between use of the two satellite platforms. It will also provide an indication of increases or changes in irrigation within the Idaho portion of the Bear River basin during the 15 year interval. However, time restrictions and decisions to focus on other aspects of the study, including modifications to SEBAL, prevented the processing of the Landsat-7 data for the year 2000. These images will be processed under Phase 2 if funded. During Phase I, only 1985 Landsat-5 data were processed.

The intent of this application is to produce estimates of monthly evapotranspiration and consequently net streamflow depletions for the Bear River basin. Agricultural crops develop and change with the time of the growing season, especially wheat and potato crops that are grown in the study area. These crops begin with bare soil and over the course of a few months obtain full ground cover. Then, depending on variety, nutrient and water management, and location, the vegetation begins to senesce until it is harvested. Therefore, it is important to process satellite images frequently enough in time to capture the changes in vegetation cover and vigor. A monthly time-step during the summer period seems to be required to capture the changes in vegetation. Images were not available for some months due to cloud cover during some spring and early summer overpasses.

Although there are only four available Landsat overpass dates between July 14th and the end of the growing season, cumulative ET can nevertheless be computed. The Kimberly Penman equation (Wright, 1982) for computing reference crop ET for an alfalfa reference was used to interpolate evapotranspiration fluxes between the Landsat overpass dates. The Kimberly Penman method, developed for Idaho and surrounding conditions, uses routine weather data for which reference evapotranspiration is computed on a daily time scale. The reference ET data were taken from the study area, and had already been processed for 1985. In the remote sensing procedure, the reference evapotranspiration information was multiplied by evapotranspiration ratios developed for the days having satellite data. The temporal interpolation includes the impact of all weather, including cloudy days, during the intervening periods.

1.9.2 Lysimeter Data

The lysimeters used for measuring ET were installed in the early 1980's as a part of a three-state study of evapotranspiration in the Bear River basin (Hill et al., 1989). The lysimeters, in essence, function as a large "flower pot." The lysimeters are large steel tanks, about 4 ft. x 4 ft. (1.2 x 1.2 m) on a side and about 4 ft (1.2 m) deep, as illustrated by Figure 1.9.2-1. They were

installed so that the vegetation planted inside of the tanks was level with that outside. An approximately 6 inch (15 cm) lip extended around the top of the lysimeter tank above the ground surface to prevent water from entering the lysimeter from outside. Figure 1.9.2-2 shows a typical lysimeter installed. The amount of evapotranspiration between weekly visits was computed by measuring the change in water content of the soil inside of the lysimeters using a neutron moisture probe and by measuring the change in the water table inside the lysimeter during each weekly site visit (Hill et al., 1989).

Figure 1.9.2-1. A lysimeter before installation in the ground.

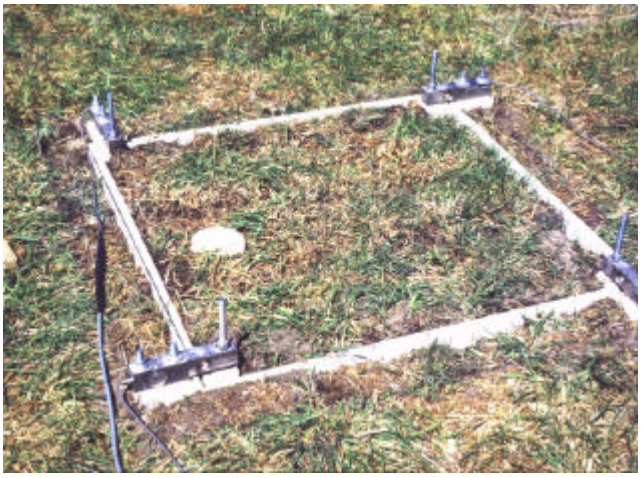

Figure 1.9.2-2. The lysimeter shown in Figure 1.9.2-1 after installation in the ground.

The three lysimeters at the Montpelier, Idaho site were planted to a forage crop that was characteristic of the area and identical to the local surroundings. The forage was characterized as a sedge type of plant. The vegetation in the lysimeters and surroundings was harvested once during late July and was then allowed to re-grow before grazing by cattle during the late summer and fall. The lysimeters were irrigated similar to surrounding fields beginning in June of each year.

The ET values derived from lysimeter data in the Bear River study were subject to some random error that varied from reading to reading. Sources of the random error included random error in measurement of the soil water contents of the lysimeters, depths to the water table, depths of water added during irrigation, and minor differences between vegetation inside lysimeters and vegetation outside. The lysimeter vegetation was managed and cultured to resemble the vegetation of the surrounding fields (and Landsat pixels), however, on occasion, the vegetation inside the lysimeters may have been less dense or more dense or shorter or taller than surroundings. These differences can impact the measurement of ET. ET values from the three lysimeters were averaged to reduce the random error components and uncertainties of the ET measurements.

2.0 ET in IDWR Business Processes

2.1 The Bear River Project

ET estimates for the Bear River Basin were last done in 1990 (Kramber, et al.,1993). Initially, the effort attempted to map land cover using mage processing of Landsat MSS data because that was the only remotely sensed information that covered the Bear River Basin in all three states in 1976. However, the spatial accuracy of the resulting maps was inadequate. Therefore, U.S. Geological Survey (USGS) 1:24,000-scale orthophoto quads (OQs) were used as base maps for the land-cover mapping

Color-infrared (CIR) aerial photography from 1990 at a scale of 1:120,000 was used to map the classes water, wetlands, irrigated cropland, non-irrigated cropland, urban, and other. The changes in land cover that occurred between 1976 and 1990 in the Idaho portion of the central division were photo interpreted from U.S. Department of Agriculture (USDA) Agricultural Stabilization and Conservation Service (ASCS) 35 millimeter color aerial slides. The slides were projected onto the 1:24,000-scale OQs, and changes that occurred between 1976 and 1990 were drawn onto overlays. Photo interpretation took about 10 weeks. Two people spent four weeks performing field verification

Data conversion involved developing land cover, the Public Land Survey System (PLSS), and Compact Division and sub-basin boundaries into ARC/INFO (Environmental Systems Research Institute, Redlands, California, USA) coverages. Those layers were required to develop the baseline 1976 land-cover data base and to link the land-cover and water-rights data bases to estimate the acreage of new and supplemental irrigated land that has occurred since 1976.

In Idaho, water rights are referenced by their legal description down to the PLSS quarter-quarter (QQ) section. Therefore, we developed a PLSS coverage to the QQ level so it could be overlaid with the land cover and linked to the water rights data base. Ninety-four townships were processed. One person completed the entire process in 10 weeks.

The purpose of linking the land-cover and water-rights data bases was to identify and calculate the acreage of land that had come under new or supplemental (additional) irrigation since January, 1976. We assumed that if the land-cover acreage was *greater* than the water-rights acreage, all the water-rights acreage was supplemental. That would be accurate more often than the alternative assumption: that all the water rights acreage was new. If the land-cover acreage was *less* than the water-rights acreage, we made an assumption shown by the following example. If the land-cover database showed 20 acres and the water rights showed 25 acres, 20 acres would be termed supplemental and 5 acres as new. These assumptions were made because the water rights data base only contains information to the QQ level, so for water rights having acreage less than the size of a full QQ, there is no way to know what land inside the QQ the water right actually covers. Such information is stored only in water-rights paper files and on field maps; it is not in digital form.

Acreage values calculated from the landcover and water-rights data bases for new and supplemental irrigated acreage were totaled by compact division and sub-basin. For new irrigated acreage, the totals were multiplied by the sub-basin depletion rates determined by the lysimeter study of Hill et al. (1989). For supplemental irrigated acreage, the depletion rates developed by Hill et al. were multiplied by an adjustment coefficient because the land already had some portion of a full water supply and the application of the supplemental water only increases the depletion some fraction of the total potential depletion. The adjustment coefficients are only estimates and are not based on empirical data. These coefficients represent the percentage of time supplemental water rights are used within a sub-basin over the long term. Sub-basin depletion totals were then summed by division. In summary, the complexity of data identification and scale bring significant uncertainty into the estimates made for total water consumption and the consequent stream flow depletion.

The Bear River Commission Technical Advisory Committee has identified the need for a study to develop more accurate adjustment coefficients for calculating supplemental depletions. Other issues that will be discussed during meetings to determine the final procedures concern the frequency for recalculating depletions and updating the base maps, and whether the central and lower divisions require different methodologies.

GIS technology provided the tools to input and analyze the various data sets required for the water rights project. However, the process was long and costly, requiring two years and approximately $100,000 to complete.

2.2 Water-Use Data

In 1990, IDWR estimated consumptive water-use (ET) by irrigated agriculture throughout Idaho as part of a cooperative agreement with the U.S. Geological Survey, Water Resources Division. ET was estimated with the FAO Blaney-Criddle equation using as input irrigated acreage, weather, and crop-specific data. IDWR expended considerable time and effort to generate the ET estimate.

IDWR used GIS for data integration and management. Five data layers were input to the GIS: section corners of the Public Land Survey, the irrigated stratum as interpreted from Landsat FCC images, county boundaries, hydrologic unit boundaries, and corners of 7 1/2 minute quads. The data were combined to generate a 5% random sample of irrigated sections within a county. Personnel traveled to each county field office of the Agricultural Stabilization and Conservation Service to use 35-mm, color, aerial slides of irrigated land. The slides were interpreted to map completely each sample section as either irrigated or non-irrigated. The field boundaries were delineated on a 1:24,000-scale orthophotoquad (OQ), and both irrigated and non-irrigated areas for each sample section were computed. The nominal crop percentages from each County Extension Agent were multiplied by the estimate of irrigated acreage to get an estimate of each crop acreage.

ET is estimated using the FAO Blaney-Criddle method as adapted specifically for Idaho by Allen and Brockway (1983). The Idaho-adapted FAO Blaney-Criddle equation uses mean monthly air

temperature to compute a reference, or potential, ET. Reference ET is then multiplied by an appropriate crop coefficient to output crop ET, which is used as the measure of water use.

2.3 Hydrology Models

ET is a critical part of the hydrologic model of the Eastern Snake River Plain Aquifer developed at IDWR. In the most basic sense, aquifer recharge is the difference between the amount of surface water diverted minus ET. IDWR closely regulates and measures the amount of surface water diverted, but can only estimate ET. The present method of estimating ET for input to the Eastern Snake River Plain aquifer model is similar to the method outlined for the Bear River Basin. The Idaho water-rights file was used to generate total acreage of irrigated agriculture by Public Land Survey System sections. The section acreages were aggregated to the 5-km cells of the model. The FAO Blaney-Criddle equation was used to compute ET.

3.0 Results

3.1 Introduction

The first, and most important goal of this study, was to assess the ability …"to predict evapotranspiration fluxes from irrigated areas of the Bear River basin of Idaho as determined by comparison of ET estimates with previous measurements made using drainage lysimeters and with estimates made from water balances of the river basin." Using SEBAL, we had to demonstrate, refine for application, and validate to the extent possible, within time and budget constraints, a remote sensing methodology to directly compute accumulated evaporation fluxes from satellite measurements without having to solve water-balance terms explicitly. All other project objectives depended on success in meeting this first goal.

The first goal was successfully accomplished using data from the Montpelier, Idaho lysimeters. A second set of lysimeters that had been installed during the same study in the 1980's at Randolph, Utah were found to have an assortment of shortcomings in the data. Analysis of the Randolph lysimeter data using SEBAL confirmed these shortcomings that were previously suspected (R. Allen, pers. communication), but were not able to be confirmed. SEBAL provided an independent means to identify and confirm the general "integrity" of the Randolph data..

When satellite images are used in an analysis, the results can be affected by the accuracy of the geo-referencing of the images. This is true for this project, as well. Therefore, a subset of the TM image, approximately 1 Km, around the lysimeter was examined to determine whether the area surrounding the lysimeter was a homogeneous or heterogeneous evaporating area. If the area is homogeneous, than exact coordinates are less important. If the area is heterogeneous, it becomes necessary to exercise care in identifying the representative pixels.

3.2 Montpelier Lysimeter

3.2.1 Location

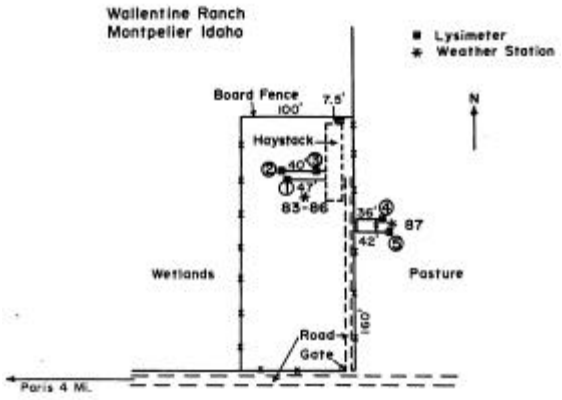

Figure 3.2.1-1. Sketch map showing location of the Montpelier, Idaho lysimeter system.

Figure 3.2.1-2. Aerial photo showing location of Montpelier, Idaho lysimeter system.

3.2.2 Montpelier Results

3.2.2.1 Data

Table 3.2.2-1 compares values of crop coefficients (K_C) based on lysimeter measurements with those derived from SEBAL for the Montpelier, Idaho lysimeter system. K_C is defined as the ratio of observed ET to reference ET. K_C values are compared between lysimeters and SEBAL, rather than ET, so as to normalize the ET data for differences caused by weather-induced changes in ET resulting from differences in time scales of measurements (SEBAL produces ET for the day of the image and the lysimeter system produced 7-day ET for the enveloping measurement period). Variation in ET due to weather was factored into the reference ET calculations.

Results for four satellite images (July 14, August 15, September 16, and October 18, 1985) are compared in Table 3.2.2-1. The data compare very well for the K_C values for the latter three dates. The earlier date (July 14, 1985) compares well, also, when it is examined in context of the impact of precipitation that preceded the Landsat overpass date, as discussed later.

Landsat date	7-day Lysimeter ET, mm/d	Equivalent 24-Hour Lysimeter ET, mm/d	24-hour SEBAL ET, mm/d	7-day Reference ET, mm/d	7-day K_C Lysimeter	7-day K_C Lysimeter for next closest period	24-hour Reference ET, mm/d	SEBAL K_C
July 14	5.3	5.1	6.5	6.9	0.78	1.11	6.6	0.98
Aug 15	3.5	3.8	4.2	6.2	0.57	0.60	6.6	0.59
Sept 16	1.9	2.4	2.6	3.7	0.53	0.52	4.6	0.57
Oct 18	0.7	1.1	1.0	1.3	0.56	0.51	2.0	0.49

Table 3.2.2-1. ET values from the lysimeter and SEBAL ET for 7-day lysimeter measurement periods enveloping the satellite images and the next adjacent period. SEBAL ET represents the value of evapotranspiration for the day and associated crop coefficient relative to the 1982 Kimberly Penman alfalfa reference equation.

It is important to note that the lysimeter K_C for each date is a seven-day average K_C for the seven-day period surrounding the Landsat date. The values for K_C varied, sometimes substantially, from one 7-day period to the next. Our analysis assumes that the K_C on the Landsat date is exactly the same as the seven-day K_C for the enclosing period. However, this may not always be entirely true, since the K_C can vary within the period due to wetting from precipitation, various day-to-day vegetation changes, soil moisture availability, or interactions with weather. Precipitation totals by date for Bear River Basin weather stations are summarized in Table 3.2.2-2

The 24-hour SEBAL ET for July 14 at first seems anomalously high, but is actually quite reasonable because of a 25 mm rain event that occurred on July 12. This rain resulted in a wet soil surface for three or more days that would have elevated ET on the day of the Landsat image to values that were higher than the average ET as measured by lysimeter for the 7-day period representing July 9-15. The ET occurring on July 14 would have been relatively higher than ET before July 12. It is also noted that the K_C for the following 7 day period (July 16 - 22) was 1.11, was very close to the K_C determined by SEBAL. It is reasonable to assume that the K_C was increasing daily during July due to fairly rapid vegetation development during that period. Therefore, on July 14, the K_c probably tended toward the 1.11 value rather than the 0.78 value. With the addition of precipitation impacts, the K_C would be higher still. The other periods did not experience the large change in K_C during the encompassing 7-day periods or into the next closest period since there was little or no rain and there was more stability in the vegetative growth.

The decrease in the ratios of ET to reference ET on about day 210 (~August 1) was likely due to cutting (harvest) of the lysimeter and surrounding crop. A –3 ^{o}C (26 F) frost occurred at Montpelier on August 10 (day 222) and a –7 ^{o}C (20 F) frost occurred on September 20, 1985 (day 263). These frosts probably retarded regrowth of vegetation somewhat in August and in total in October.

In summary, the deviation of SEBAL predictions for the July 14 date can be satisfactorily explained by the antecedent rainfall and rapid growth of lysimeter vegetation during that date. The agreement between SEBAL and lysimeter for the other three dates was very good.

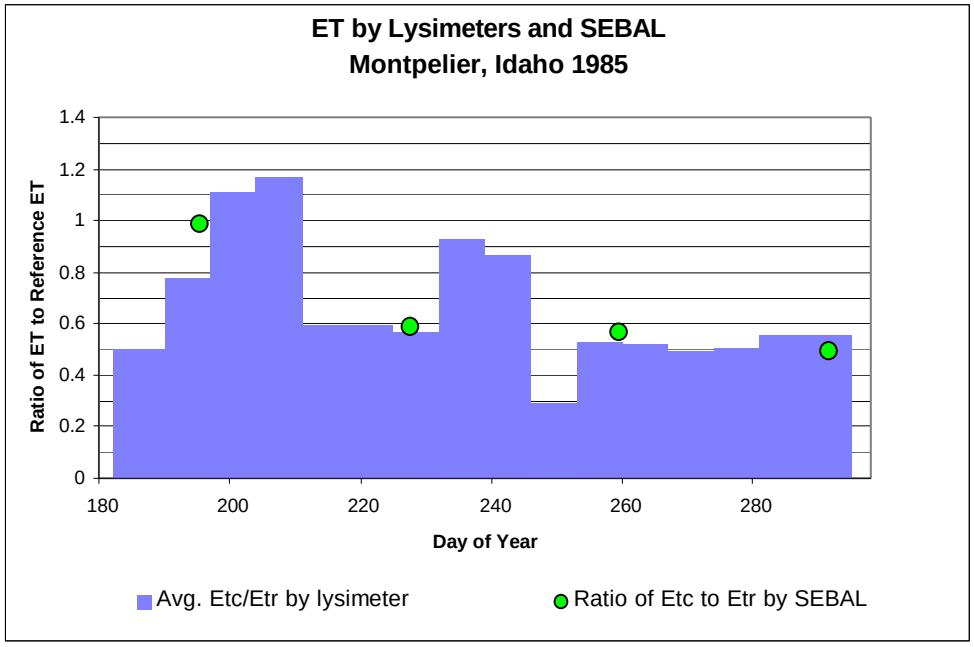

Figure 3.2.2-1. Comparison of K_C values derived from 7-day lysimeter measurements at Montpelier, Idaho during 1985 and K_C values derived from 24-hour ET from SEBAL for four Landsat dates, based on the 1982 Kimberly Penman alfalfa reference equation.

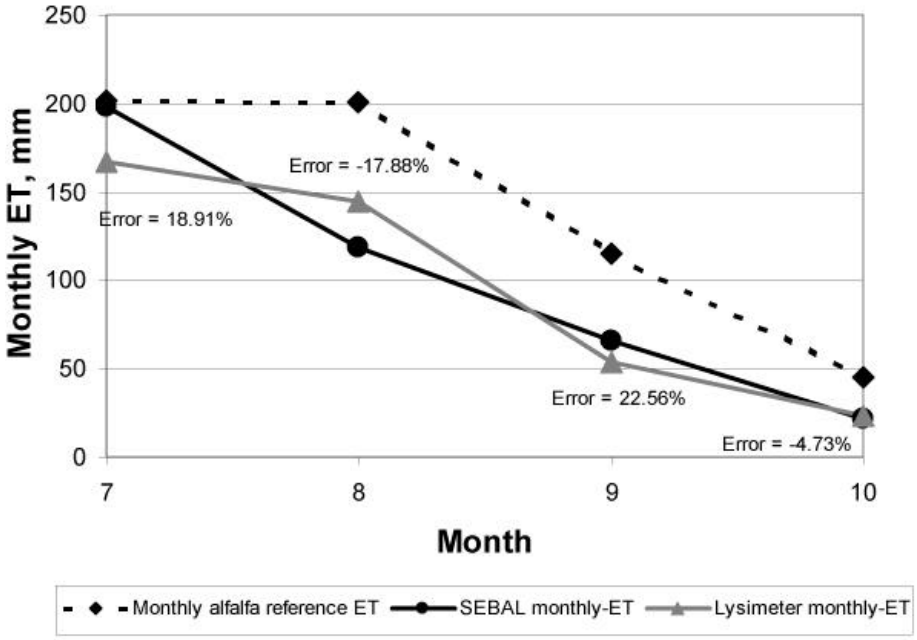

Figure 3.2.2-2. Comparison of the monthly ET predicted by SEBAL, the monthly ET measured by lysimeter, and the monthly alfalfa reference ET for the Montpelier site.

Date		Precipitation (mm) Montpelier, ID	Randolph, UT
7/5/85	7/5/85	0	0
7/6/85	7/6/85	0	0
7/7/85	7/7/85	0	0
7/8/85	7/8/85	0.3	0
7/9/85	7/9/85	0	0
7/10/85	7/10/85	0	0
7/11/85	7/11/85	0	0
7/12/85	7/12/85	25.7	2.0
7/13/85	7/13/85	0.3	0
7/14/85	7/14/85	0	0
8/6/85	8/6/85	0	0
8/7/85	8/7/85	0	0
8/8/85	8/8/85	0	0
8/9/85	8/9/85	0	0
8/10/85	8/10/85	0	0
8/11/85	8/11/85	0	0
8/12/85	8/12/85	0.3	0
8/13/85	8/13/85	0	1.0
8/14/85	8/14/85	0	0
8/15/85	8/15/85	0	0
9/7/85	9/7/85	0	0
9/8/85	9/8/85	1. 8	0
9/9/85	9/9/85	2.3	0
9/10/85	9/10/85	0	0
9/11/85	9/11/85	3.0	3.0
9/12/85	9/12/85	3.0	0
9/13/85	9/13/85	1.0	0
9/14/85	9/14/85	0	0
9/15/85	9/15/85	0	0
9/16/85	9/16/85	0.3	0
10/9/85	10/9/85	0	0
10/10/85	10/10/85	0	0
10/11/85	10/11/85	0	0
10/12/85	10/12/85	1. 8	1.0
10/13/85	10/13/85	Missing	0
10/14/85	10/14/85	Missing	0
10/15/85	10/15/85	0	0
10/16/85	10/16/85	0	0
10/17/85	10/17/85	Missing	0
10/18/85	10/18/85	Missing	0

Table 3.2.2-2. Precipitation in millimeters by date for the two Bear River Basin lysimeter systems evaluated. Landsat overpass dates are highlighted.

3.3 Randolph Lysimeter

3.3.1 Location

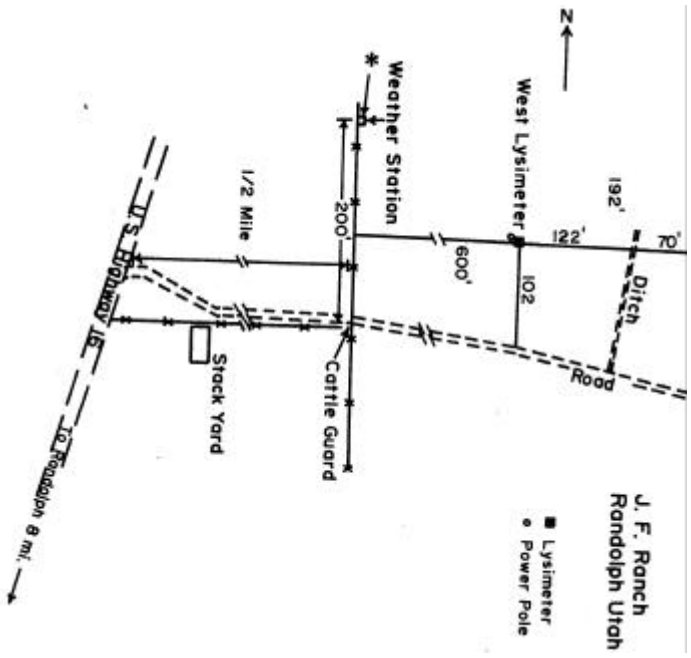

Figure 3.3-1. Sketch-map showing the location of the Randolph lysimeter system (from Hill, et al., 1989

Figure 3.3-3. Aerial photo showing interpreted location of Randolph, Utah lysimeter system.

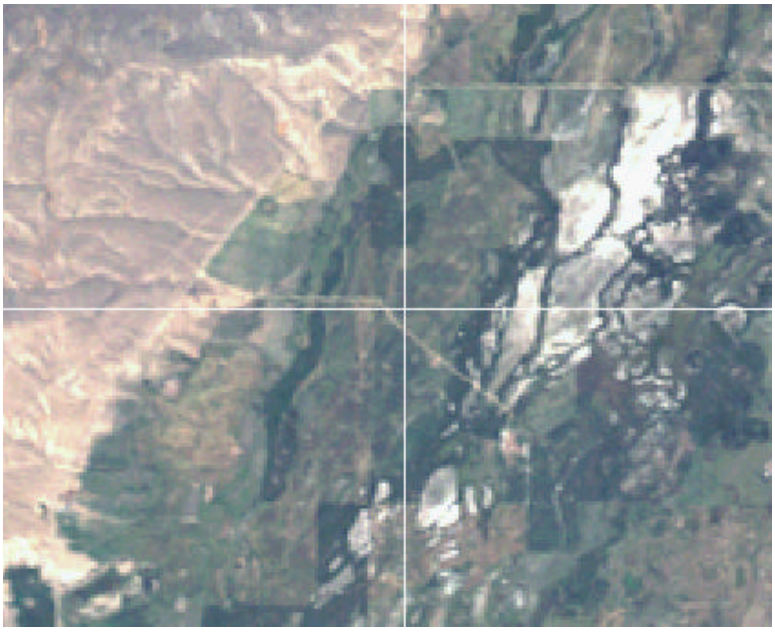

Figure 3.3-2. The location of the Randolph lysimeter system is at the cross-hair in the Landsat TM data.

3.3.2 Randolph Lysimeter Results

The results of SEBAL for the Randolph lysimeter are graphed against lysimeter measurements for weekly periods in Figure 3.3.2-1b. Data for the Montpelier site are plotted in Figure 3.3.2-1a to provide for a side-by-side comparison. The SEBAL estimate for July 14 is missing due to cloud cover over the Randolph site on that day. Values based on lysimeter measurements vary substantially from week to week as shown in Figure 3.3.2-1b and do not follow the trends observed for Montpelier that were explained by cultural practices and weather. The ET values reported from the Randolph lysimeter cast some suspicion on the quality of the lysimeter data set. The large amount of "bounce" in the K_c values from date to date was acknowledged by Dr. Robert Hill of Utah State University (2000, personal communication), who set-up the lysimeters at Randolph. Dr. Hill speculated that the source of error might have been hysteresis or side flex in the lysimeters that impacted measurements of total water content of the lysimeters.

Some of the variation in lysimeter data was probably random and therefore partially cancels when averaged over longer periods. Monthly values computed from weekly lysimeter measurements and from the SEBAL predictions are presented in Table 3.3.2-1. Much of the variation in lysimeter measurements was reduced and lysimeter measurements for August were only 12% greater than those based on SEBAL. The month of July was missing from SEBAL for Randolph due to cloud-cover on the day of the satellite image.

Large deviations occurred between lysimeter measurements and SEBAL for September and October, where SEBAL predicted ET that was about 2/3 of that reported for the lysimeters. The

ratios (i.e., K_c's) predicted by SEBAL for Randolph are more in line with those measured and predicted at Montpelier (Table 3.2.2-1) and are more reasonable considering the frosts at Randolph (-5 ºC (22 F) on August 10 and –9 ºC (16 F) on September 23). Monthly K_c's predicted by SEBAL for August, September and October were 0.74, 0.48 and 0.79 at Randolph as compared to 0.85, 0.76 and 1.0 predicted from lysimeter measurements. K_c's of 1.0 would be highly unlikely in October, when the vegetation has been heavily damaged by frost. K_c's from the lysimeter at the Montpelier site for August, September and October were 0.60, 0.52 and 0.51.

In summary, SEBAL confirms some suspicion that the investigators of this and the Bear River lysimeter study had concerning the integrity and representativeness of the Randolph lysimeters. Comparisons were not made for the Evanston, Wyoming site (located at Hillyard Flats).

	Monthly Lysimeter ET mm/day	SEBAL ET on day of image mm/day	SEBAL ET for the month mm/day	Lysimeter K_c	SEBAL K_c	Lysimeter Cumulative ET mm	SEBAL Cumulative ET mm	Difference between SEBAL and Lysimeters
July	4.2	cloud	cloud	0.62	Cloud	130	cloud	--
August	5.8	5.5	5.1	0.85	0.74	181	159	-12%
September	3.7	3.1	2.1	0.76	0.48	112	62	-45%
October[1]	2.7	1.4	1.8	1.00	0.79	57[1]	38	-33%
Ave./Total for Aug.-Oct.[1]	4.3	3.6	3.2	0.90	0.67	350[1]	259	-26

Table 3.3.2-1. Comparison of monthly ET values and crop coefficients measured by the Randolph lysimeter and estimates by SEBAL.

[1] Data for October represents days 1 – 21, only, as this was the extent of the lysimeter record.

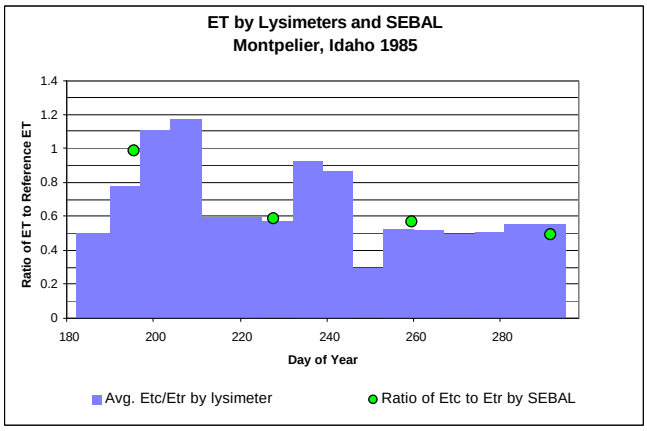

Figure 3.3.2-1a. Weekly K_c values for theMontpelier, Idaho lysimeter system.

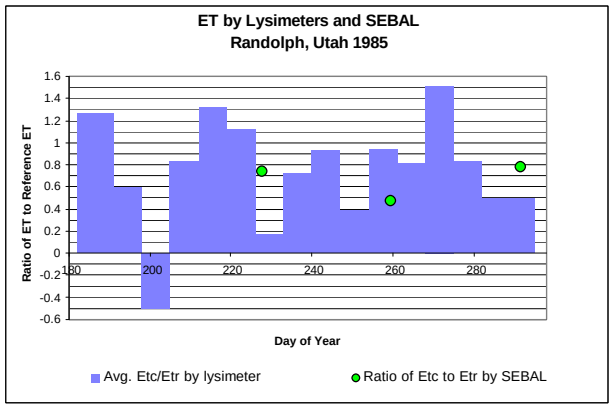

Figure 3.3.2-1b. Weekly K_c values for the Randolph, Utah lysimeter system.

3.3.3 ET Images

3.3.3.1 Evapotranspiration for Twenty-Four Hour Periods

SEBAL makes its primary calculation of ET for the instant of the satellite overpass, which is generally between 10 and 11 am. ET for the 24-hour period (i.e., day) of the image is based on the use of the evaporative fraction (EF) that is computed on a pixel-by-pixel basis. The evaporative fraction is defined as the ratio of ET to the difference R_n – G. SEBAL assumes that the value for EF is constant throughout the day. This assumption is supported by a large number of field studies (Bastiaanssen et al., 1998ab). However, EF can very under some conditions. Soil heat flux, G, is computed for the instantaneous image based on the value for R_n and the computed vegetation image for the pixel. G for 24-hour periods is assumed to be nearly zero due to the canceling effect of positive G during daylight and negative G during nighttime.

Figure 3.3.3-1 shows a mosaic of two Landsat TM images along path 38, rows 30 and 31 to illustrate the spatial coverage of the Bear River Basin. The image date for the mosaic is August 15, 1985. This image is a false color composite comprised of Landsat bands 2, 3, and 4. The red colors indicate areas of relatively high densities of active vegetation.

Figure 3.3.3.1-2 shows images of twenty-four hour ET as computed by SEBAL for the same the image mosaic as shown in Figure 3.3.3-1. ET values were converted in ERDAS from real numbers to 8-bit integers to facilitate presentation as false colors for use with legends.

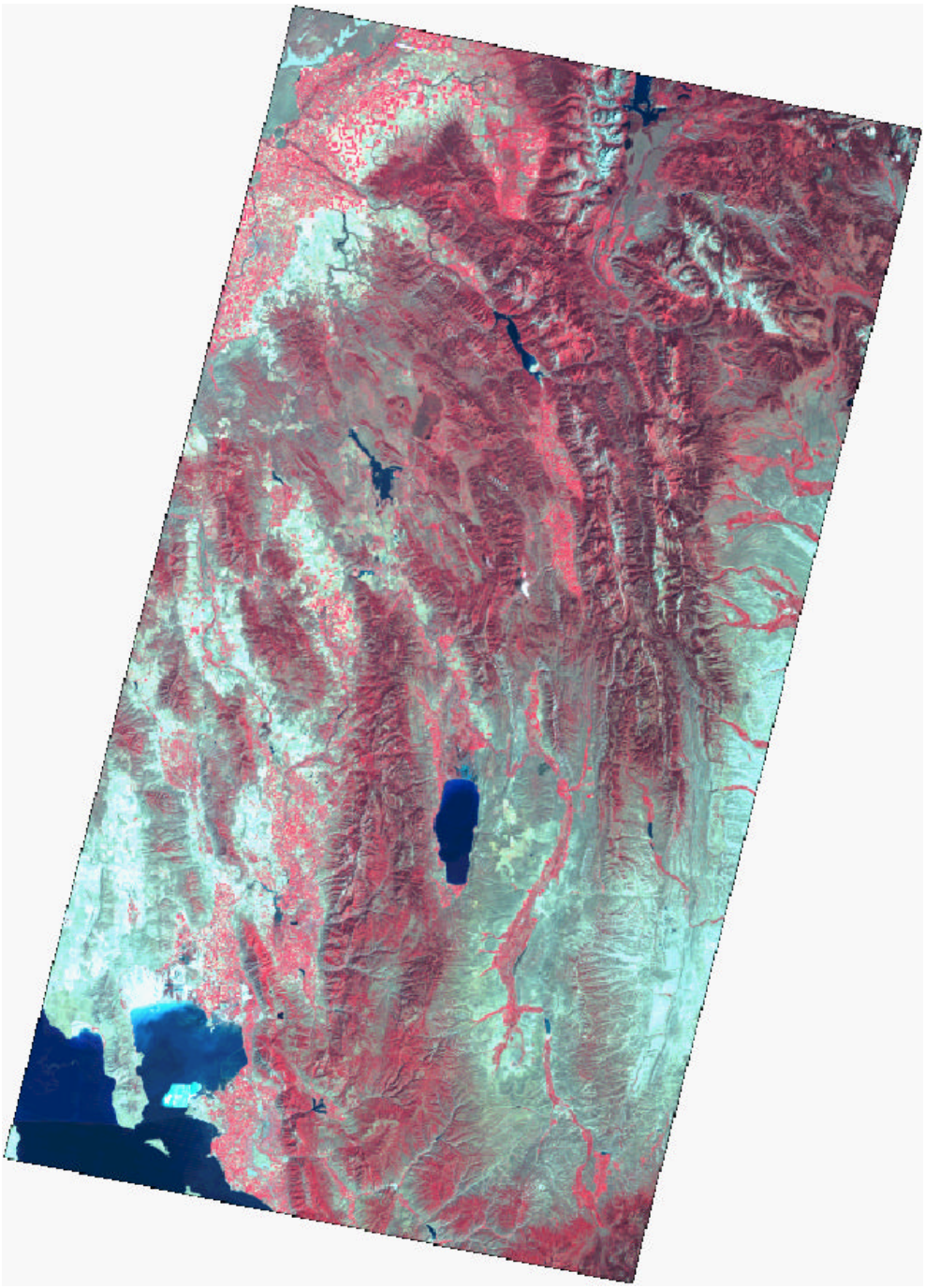

Figure 3.3.3.1-1. An example of the spatial coverage of the two-image mosaics of Landsat TM images that were used as input to SEBAL. This image shows Landsat bands 2, 3, and 4 composited into a false color image. Bear Lake is in the lower center of the image and the Great Salt Lake is shown in the lower lefthand corner. The Montpelier lysimeter site was a short distance directly north of Bear Lake.

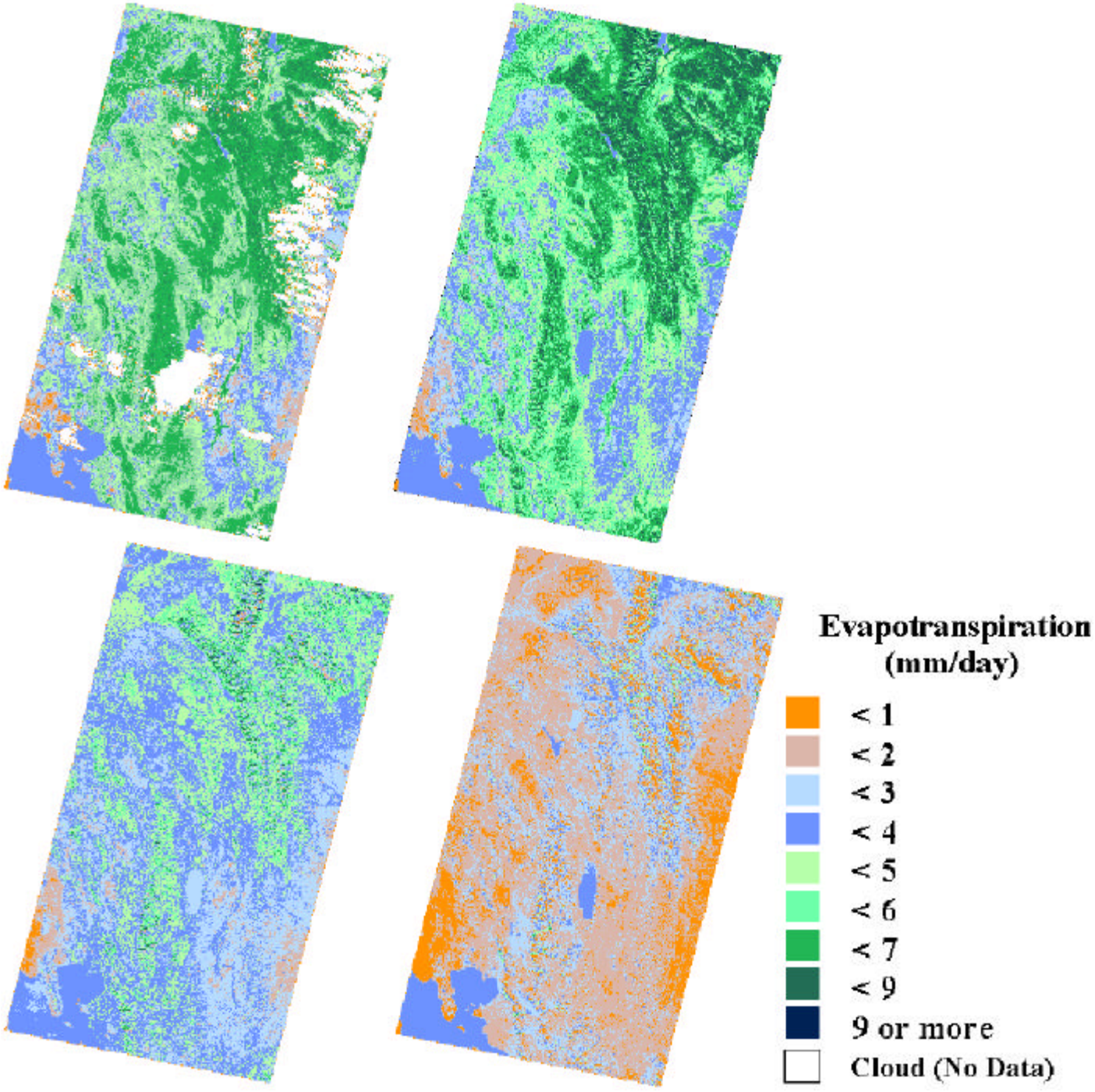

Figure 3.3.3.1-2. Image mosaics color-coded to show twenty-four hour ET. Starting clockwise from the upper left, image dates are July 14 ; August 15; September 16; and October 18; all from 1985.

3.3.3.2 Seasonal ET Image

Figure 3.3.3.2-1 is an image showing cumulative ET for the measurement period beginning July 1, 1985 and ending October 21, 1985. Cumulative ET was computed using monthly crop coefficients that were based on the 24-hour SEBAL ET computed for the four image dates and a standard reference ET equation, as described in Section Three. A detailed explanation of the process is give in Appendix A. A brief explanation follows:

The first step in computing season ET is to delineate the time period to be represented by each ET image. In this case, the July 14th image was assigned to represent July, the August 15th image to represent August, the September 16th image to represent September, and the October 18th image to represent October.

The second step in the cumulative ET process is to compute the alfalfa reference ET_r for the period represented by each image. The ET_r data for this study were taken from Hill, et al. (1989) for 1985. The values were confirmed using the University of Idaho REF-ET software. The values for ET_r are summarized in Table 3.3.3.2-1.

The third step in the process is to compute the multiplier K_m for each period to use to convert ET for the day of the image into ET for the month. K_m is computed as the ratio of cumulative reference ET_r for the period to 24-hour reference ET_r. Values K_m used for 1985 are summarized in Table 3.3.3.2-2 and were based on ET_r computed at the lysimeter site at Montpelier, Idaho.

Date	July14	August15	September 16	October 18
Cumulative ET_r for the month (mm)	202	201	115	45
ET_r on image date (mm)	6.6	7.1	4.6	2.0

Table 3.3.3.2-1. Values of alfalfa reference ET, ET_r, and cumulative for the Bear River Basin in 1985.

Period	July 1-31	August 1-31	September 1-30	October 1-21
K_m	30.5	28.3	25.2	22.1

Table 3.3.3.2-2. Values computed for K_m, for the Bear River Basin in 1985.

The fourth step of the cumulative ET process is to compute cumulative, seasonal ET. The equation for this computation is

$$ET_{cumulative} = \sum_{i=1}^{n} \left(ET_{SEBAL-24}\right)_i \left(K_m\right)_i$$

where $ET_{SEBAL-24}$ is the 24-hour ET predicted by SEBAL for each pixel and K_m is the multiplier for ET for the representative period. n is the number of satellite images processed. Units for $ET_{cumulative}$ will be in mm when $ET_{SEBAL-24}$ is in mm/day.

Final results for $ET_{July-October}$ for the Bear River Basin are presented in Figure 3.3.3.2-1. The white areas are locations where there was cloud cover on one or more of the images. In an operational mode where computations are done on a GIS platform, for example with ArcInfo, these areas can be masked out or filled in using a nearest neighbor approach.

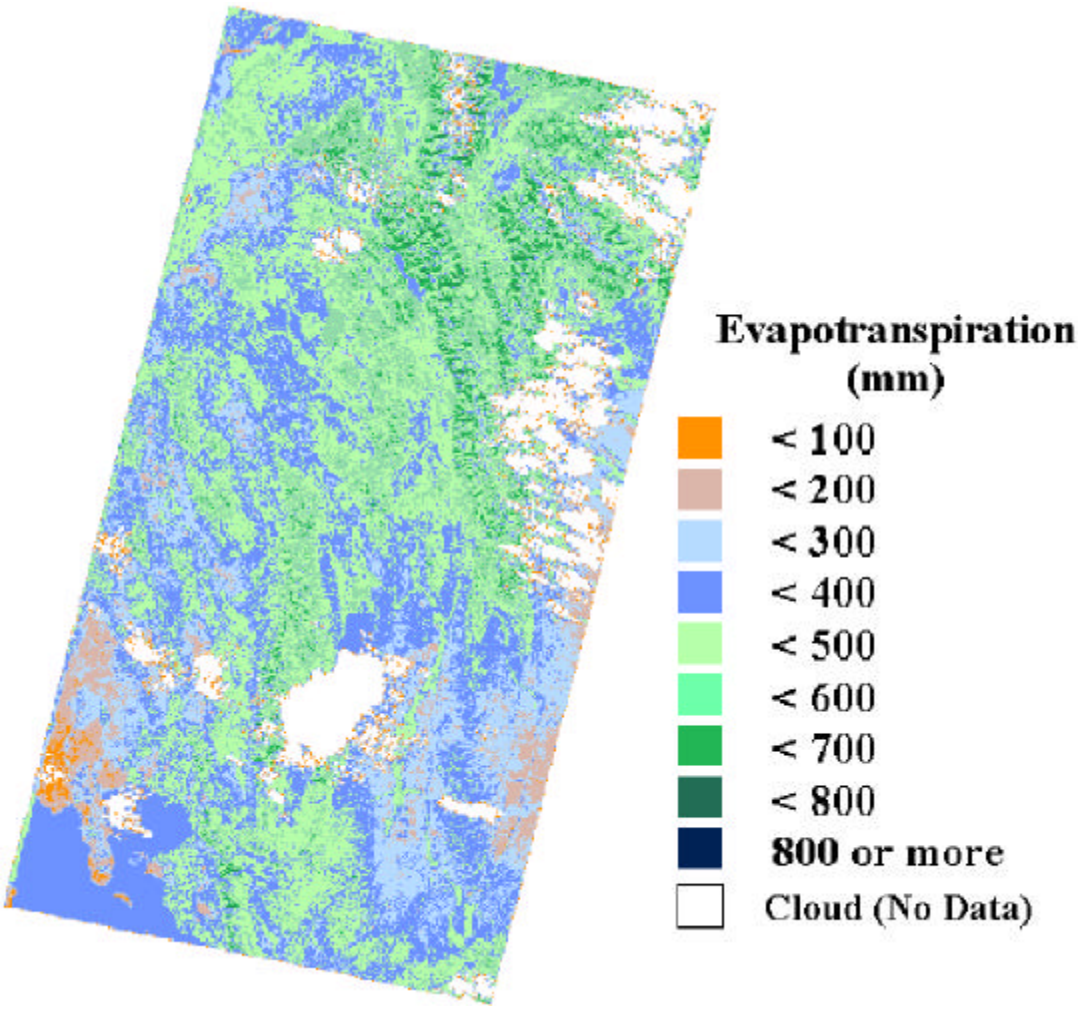

Figure 3.3.3.2-1. An image of the Bear River Basin area showing cumulative ET for the period July 1 through October 21, 1985.

3.4 Sources of Error

3.4.1 Lysimeter Errors

The SEBAL measurements of ET did not precisely match the lysimeter measurements of ET for locations in the Bear River basin, which is not surprising. However, comparisons are judged to be very good for the Montpelier, Idaho location, which has the best data integrity. Given the sparseness of the SEBAL observations, (only four during the growing season) and only a single valid ground-truthing location, it is difficult to do an exhaustive error analysis. Nevertheless, some general observations are possible. There are three types of SEBAL estimates that were made during the study and three corresponding types of errors. These errors are those associated with daily, weekly, and cumulative (or seasonal) timesteps.

Results from the Bear River Basin, and elsewhere, suggest that the 95% confidence intervals for the ET estimates on the day of the Landsat overpass are approximately +/- 1 mm/day for well-watered, irrigated areas (Bastiaanssen et al., 1998b, Bastiaanssen, 2000, pers. communication). For the Bear River Basin, daily ET for well-watered, irrigated areas is typically 6 to 8 mm/day during the peak of the growing season. Therefore, the +/- 1 mm/day confidence interval would translate into +/- 15% of ET.

For non-irrigated areas the uncertainty is also approximately +/- 1 mm/day, but the confidence as a percentage of baseline ET is larger, since the ET for non-irrigated areas is less, averaging approximately 2.5 mm/day. Therefore, the error for any particular pixel or land use type may be as large as +/- 40%, which is this is 1 part in 2.5. For the growing season, the error would be equivalent to about +/- 20%.

It is important to bear in mind that these are 95% confidence intervals, so that they represent 2 standard deviations from the mean, assuming that the population of errors is normally distributed. Approximately 83% of the estimates will be within 1 standard deviation of the mean, so that the confidence intervals would be half-as much, so that 83% of estimates should be within +/- 10% of actual ET for irrigated areas and +/-20% of actual ET for nonirrigated areas, respectively.

A comparison of errors for weekly periods is made using lysimeter data from Montpelier in Table 3.4-1. Based on the weekly periods enveloping the four Landsat overpass dates, the standard deviation of errors for each week for the lysimeter site (based on column 5) is 0.6 mm/day or 15%. If these values are multiplied by a factor of 2 to create the 95 % confidence intervals, then these confidence intervals become +/-1.2 mm/day and +/- 30%. One limitation of this analysis is that there are only four observations and therefore three degrees of freedom, which is statistically scanty.

An assessment of errors in monthly ET estimates can be made using the right-hand half of Table 3.4-1. The standard deviation of errors for each monthly period for the lysimeter site is 0.7 mm/day or 17%. Multiplying these values by the factor of 2, the 95 % confidence interval predicted for monthly ET estimated by SEBAL becomes +/-1.4 mm/day and +/- 34%.

An additional expression of confidence can be made regarding the impact of estimating monthly ET using a K_c from a shorter period. This can help to predict the impact of change in vegetation and/or the evaporative fraction over the course of a month on the error in the monthly estimate. This error assessment is done by comparing the weekly lysimeter K_C (column 6 in Table 3.2.2-1) with the whole-month lysimeter K_c (column 9 in Table 3.4-1). This analysis shows that average error among the four months is only 1%. However, the standard deviation of the errors for individual months is 13%, which indicates that uncertainty induced in extrapolating the K_C from a SEBAL image to a monthly period may average 13% for about 80% of occurrences for an individual month, but, because it is a random type of error, the error for the season would nearly cancel.

It is important to understand that some of the error that is calculated above is due to the lysimeters and not the SEBAL estimate. There are reasons not to rely heavily on the accuracy of the lysimeter measurements**.** In all likelihood, the quality of the lysimeter measurements at Montpelier is about the same as that for SEBAL. Therefore, one could multiply the weekly and monthly confidence intervals computed above by 0.5 in assigning error to SEBAL. Therefore, for monthly data, one could suggest that for any particular pixel, there is a 83% probability that one will be within 8% of the true answer and a 95% probability that one will be within 15% of the true answer, and these confidence intervals become similar to those for daily. The reason for this is that some of the error associated with a daily value may reduce over the course of a month, but other errors may enter in, such as extrapolation of the K_C.

When pixels are aggregated, the confidence interval will be reduce, but not in proportion to the standard error of the mean, as would be expected for independent measurements. Because the aggregation over a field or irrigated area will likely contain some systematic types of errors that are biased in the same direction, which is especially the case for a single field, the error will not reduce in proportion to the square root of the number of observations, as one would expect for normally distributed random errors. The same goes for combining monthly ET based on more than one Landsat image to get an annual estimate. The random component will reduce in proportion to the square root of the number of images combined, but any systematic bias due to errors in interpretation or prediction by SEBAL, or by the user, will linger at full strength.

	Lysimeter ET 7-day average mm/day	SEBAL K_C	7-day SEBALET mm/day	Difference in 7-day ET (SEBAL – Lys) %	Monthly Alfalfa Reference ET mm	SEBAL Monthly ET mm	Lysimeter Monthly ET mm	Monthly K_c for Lysimeter	Difference in monthly ET (SEBAL-Lys) %	Seasonal Error
(1)	(2)	(3)	(4)	(5)	(6)	(7)	(8)	(9)	(10)	(11)
July 14	5.3	0.98	6.8	28%	202	198	167	0.83	19%	
Aug 15	3.5	0.59	3.7	6%	201	119	145	0.72	-18%	
Sept16	1.9	0.57	2.1	10%	115	66	54	0.47	22%	
Oct 18	0.7	0.49	0.6	-14%	45	22	23	0.51	-5%	
Ave./Total	2.9	0.73	3.3	_15%	563	405	388	0.69	4%	4.3%

Table 3.4-1. Summary of SEBAL- and lysimeter-derived ET values for weekly and monthly periods at Montpelier, Idaho, and the associated error.

3.4.2 Errors induced by the user of SEBAL

SEBAL is comprised of more than 20 computational steps or submodels. Some of these steps require decision-making by the user, for example, during the selection of the dry and wet indicator pixels, determination of prediction algorithms for surface roughness, characteristics of the weather surface and selection of ground-based weather data, and development of prediction equations for surface to air temperature differences.

To determine the impact of user-induced error in ET prediction, the Landsat 5 image for July 14, 1985 was reprocessed by a second person at IDWR independent from the primary processor. In addition, a different computer system and version of ERDAS Imagine software was used. Decision making concerning selection of indicator pixels and appropriate prediction algorithms was also independent. A total of 440 pixels were randomly selected from the processed images of 24-hour ET by the two users, out of 30 million pixels total. Locations of selection were chosen so that the sampled pixels represented a wide range of land-use types. Results are shown in Figure 3.4.2-1.

The agreement in ET between the two independent applications of SEBAL is considered to be very good, having an r^2 of .978. Predictions follow a 1:1 line closely, with about 1% deviation from the line, on average. Some difference in estimates occurred for locations having relatively low ET. However, these differences appear to be random and would average out over a wide range and number of pixels. Therefore, it appears that the prediction of ET by SEBAL is relatively immune to the user. However, it should be noted that both users were trained in the use of SEBAL at the same time by Dr. Bastiaanssen and therefore were exposed to similar recommendations that may have been unique to that training. One of the users is a trained agriculturalist/hydrologist and the other is a trained remote sensor.

The graph shows three outlyers. The two data points farthest above the line are water pixels. The data point farthest below the line is a rangeland pixel. The differences in water pixels are understandable; water pixels in the UI data were adjusted in post-processing, while the IDWR data were unadjusted. The reason for the difference in the rangeland pixel is unclear.

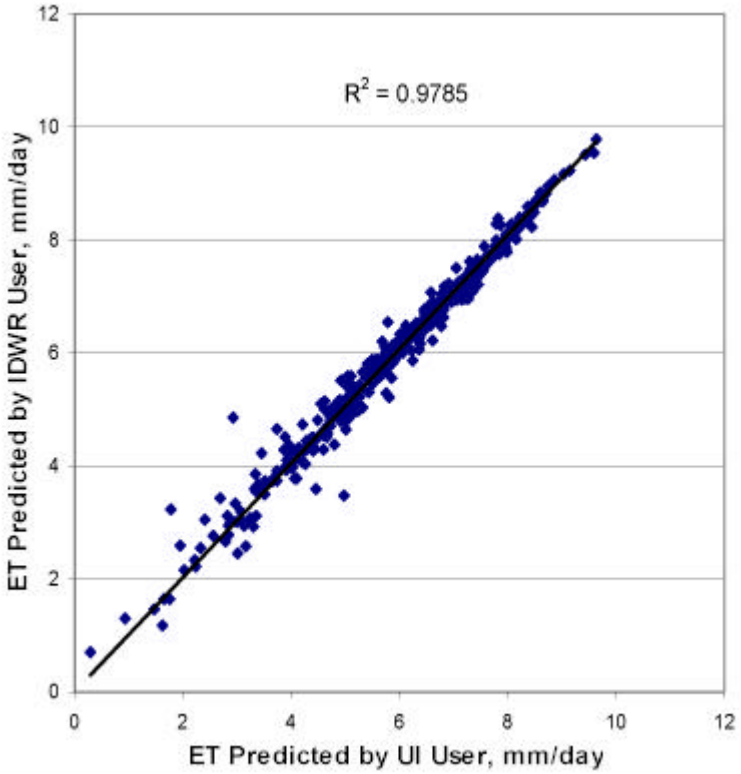

Figure 3.4.2-1. Comparison of 24-hour evapotranspiration predicted for July 14, 1985 in the Bear River basin by two different users of SEBAL.

3.5 Lessons Learned

There were four significant lessons learned from this project. The first lesson is that SEBAL has weaknesses that need to be investigated. The second lesson is that there are weaknesses in the lysimeters used for the analysis. And the third lesson is that the processing of SEBAL is robust and can be done with good consistency by an analyst using Appendix C as a guide, and without experienced supervision. The fourth lesson is that for SEBAL to be adopted for operational use, more validation will be needed.

The weaknesses in SEBAL were 1) the assumption of uniform, flat terrain, and 2) the assumption of no 24-hour heat carry-over for water bodies. These weaknesses and the ways in which they were addressed are documented in Section 4.2.2

The weaknesses in the Lysimeter data impacted the data analysis. These weaknesses are discussed in Section 3.4.

The robustness of the SEBAL process is addressed in Section 3.4.2. The SEBAL operation manual, Appendix C, provides clear and effective guidance in running the model.

Based on the results of the Montpelier, Idaho lysimeter, the results from SEBAL are very encouraging. Nevertheless, the results are based on data from one lysimeter and cannot be considered as definitive. Rather than adopt SEBAL immediately, IDWR has requested funding authority from the Idaho Legislature to further study SEBAL. Specifically, IDWR wants to understand how well SEBAL will perform on the Snake River Plain, and to compare SEBAL results to a more extensive lysimeter data set and to extensive data that IDWR has gathered over the last five years on the amount of ground water pumped by specific water right. Clear results based on a large amount of varied data will be needed to convince potential users to make the commitment to SEBAL.

4.0 Future Directions

4.1 ET in Future IDWR Business Processes

This section describes the various future applications that are being planned or recommended for SEBAL in Idaho and surrounding states.

4.1.1 Ground-water Modeling

IDWR has begun re-calibrating the Eastern Snake River Plain ground water model. The re-calibrated model will be used in support of conjunctive management of ground and surface water. One of the major goals of the re-calibration is to get better estimates of aquifer recharge as input to the model.

Recharge from both irrigated and non-irrigated lands is a major component in developing the long-term water balance for the model, and is the amount of water remaining after ET is subtracted from the amount of water diverted from surface-water sources plus precipitation. An improved ET estimate (spatially, temporally and magnitudinally) would significantly reduce the uncertainty involved in computing the net recharge input term for the model. An accurate recharge term is a critical part of model re-calibration. SEBAL will allow IDWR to compute the agricultural ET component of the model in an efficient and inexpensive way, and to compute the wildland ET component for the first time.

4.1.2 The Bear River Commission

In 1958 the Bear River Compact was developed to establish how the three states would equitably distribute and use water from the Bear River. Eighteen years later, interested parties entered into six years of negotiation to resolve concerns about the original compact, and in February 1980 the Amended Bear River Compact was signed into federal law. The Bear River Commission is the administrative authority that oversees and enforces the compact.

The compact assigns a depletion (i.e. ET) allotment to each state and directs the commission to develop and implement "approved procedures" to account for and calculate the amount of water depleted. The role of IDWR is to compute depletion for the Idaho part of the Basin to support Idaho's position in negotiations with the other two states. IDWR will continue to refine and apply SEBAL in the Bear River basin to assist in administration of the Bear River Compact.

4.1.3 Water Rights Management

Managing water rights and irrigation on the Snake River Plain and tributary basins presents a particular challenge to IDWR. Water for irrigation comes from both surface and ground sources. For various historical reasons, the use of surface water has been directly measured and regulated by IDWR while the use of ground water has not. This situation began to change in 1995 when the Water Measurement Program was established within IDWR to measure ground-water use.

IDWR has dedicated considerable resources to water measurement, including three full-time positions to monitor some 5,000 points of diversion, mostly wells. As useful as these data are, they do not provide all the information necessary for effective management of the resource. Information regarding the ET or consumed fraction of diversions is needed. SEBAL can be used in conjunction with Water Measurement data in an efficient program to help manage water development, use and stewardship. SEBAL can cover large areas inexpensively and efficiently, thereby extrapolating Water Measurement Data, and the Water Measurement data, in turn, can be used to validate the SEBAL results.

This combined program offers several advantages over present methods. First, it offers the ability to monitor whether or not water has actually stopped being used for irrigation after a water shut-off order has been issued. Second, It can discover if more water has been used than is authorized. Third, It can quantify and be used as proof of beneficial use of a right. Fourth, it can be used as an unbiased, quantitative record of historic use. Fifth, the consumed fraction and return of nonevapotranspired water to the resource can be quantified. Sixth, estimations of yield and productivity can be made to assess benefits of water development and tradeoffs.

4.1.4 Performance of irrigation projects

ET maps created using SEBAL can be aggregated over individual irrigation projects in the western US and ground-water districts in other parts of the U.S. Aggregated ET can be compared with recorded irrigation diversions to assess the performance of the project or district in its water use, including the consumed fraction of diversions with time. ET predictions, coupled with diversion records and estimates of groundwater pumpage may allow the evaluation of:

a) relative performance of projects (i.e., fraction of diverted water that is evaporated)
b) distribution in space and time of incidental recharge (residual of diversions not consumed)
c) locations of “hot spots” where fluxes of nitrates and other soluble agro-chemicals may be occurring
d) changes in timing within a year and in between years for various performance indicators
e) prediction of crop yields and identification of areas where education and extension information may be useful

f) overlay of ET variation with land cover and land use types and soil maps to assess relative variation in ET that may be caused by cultural practices and other factors.

4.1.5 Separation of estimates of evaporation from transpiration

Many methods have been proposed to predict or measure changes in evaporation from the soil surface that result from changes in the type of irrigation system or in management of a system. Questions concerning the amount of evaporation from soil are becoming critical, since this portion of evapotranspiration can generally be reduced, during water conservation programs, for example in the Central Valley of California, without reducing crop health and total yield. Crop yield is generally tied to transpiration of water through the crop and is largely independent of evaporation from soil. Various irrigation system types (for example, surface irrigation, sprinkler irrigation, center pivot irrigation, drip irrigation, and subsurface drip irrigation) have varying portions of evaporation. However, these portions are closely tied to the management of the systems and with the frequency of water application.

Most methods that have been proposed to predict evaporation from soil have large amounts of uncertainty. The uncertainty may be more than can be tolerated in studies of water conservation measures and future planning. Many prediction methods have a systematic bias. For example, soil based measurements of evaporation are perplexed by diffusive evaporation from below the soil surface and interactions with water extraction via transpiration. Microlysimeters have systematic biases and limitations.

The commonly used crop coefficient – reference ET approach, although evolving with the improved methodology for assessing the impact of variation in the fraction of soil surface watered and frequency of watering, still has uncertainty and subjective biases. These uncertainties and biases also apply to “direct” ET prediction methods such as the Penman-Monteith or sophisticated multi- layer canopy models. However, these models do provide a vehicle for assessing relative differences among systems and for extending field measurements once they are calibrated to the local conditions and system behavior. The calibration might be accomplished using input from SEBAL.

The most reliable method for obtaining an integrated and absolute estimate of the evaporation component from irrigated systems will be to use micrometeorological systems, for example, eddy correlation. However, these systems provide total measurements of ET and do not easily provide for separate measurement or prediction of evaporation. For evaporation assessment, one would need to set up paired stations in nearly identical fields of the same crop, with one field irrigated and one unirrigated over a relatively short period of time. Differences in total ET measurements can then be compared and interpreted to predict the evaporation component. Results can then be used to calibrate the predictive weather based models to extend in space and time. However, micrometeorological systems are expensive and require large amounts of time for operation, integrity assessment and data reduction. Therefore, their application is limited to only a small sampling of types of crops and irrigation systems and management cultures. Measurements

by these systems can be used in conjunction with SEBAL, however, to both validate SEBAL predictions and to extrapolate micrometeorological estimates to large regions.

SEBAL can be used to predict ET for large areas using Landsat, NOAA-AVHRR and MODIS images. It is possible that combinations (associations) of fields could be identified that have the same type of crop and having the same amount of biomass (this can be done using remote sensing techniques with the satellite image). Given a sufficient number of observations within a particular crop-soil-growth stage association, there will be a distribution and range in the relative dryness or wetness of soil among the fields due to randomness of irrigation scheduling. The SEBAL predicted ET will reflect these differences and can quantify differences due to differences in soil evaporation at the time of the satellite overpass. Statistical processing of the distributions in evaporation for a specific irrigation system type can provide information on the percentages of fields belong to various "wetness" categories. This would provide

a) an indication of the increase in evaporation following a wetting event (i.e. irrigation),
b) an indication of the time interval between irrigations (wettings) and therefore means to quantify the total volume of water from a region resulting from evaporation from soil.

The application of SEBAL can also provide a means for monitoring/correcting, in time, weather/soil water balance based predictions for evaporation that are run continuously for individual fields having recorded irrigation events. The SEBAL predictions of evaporation fluxes can be used to confirm accuracy of the underlying ET modeling procedure.

4.1.6 Water balances of total river basins

Water resources planning is often constrained by uncertainties regarding the total flow of water within and out of a river basin or water shed. In many basins and subbasins, the underflow of ground-water from the basin is unknown, and can not be quantified due to uncertainties in total evapotranspiration from the basin and uncertainties in precipitation over the basin. Application of SEBAL to large basins can improve the confidence in estimates of the ET component of the water balance, thereby allowing the prediction of ground-water underflow to be more accurately predicted.

4.1.7 Health of natural vegetation

The health of natural systems, such as forests, rangeland and wetlands, is closely tied with transpiration of water through the vegetation. Often transpiration is reduced by external stresses on vegetation caused by pests and disease. ET mapping using SEBAL can provide information on the magnitude and spatial extent of infestations of diseases and pests and on reductions in ET and subsequently plant health and vigor due to drought. There is strong interest in the western states for improved tools, such as SEBAL, that can provide information on water usage over large land areas and vegetation types.

4.2 SEBAL Research

4.2.1 Further Validation

Previous work with SEBAL has shown it to be an effective predictor of ET in Africa and Asia (Bastiaanssen et al, 1998b). The results of the work in the Bear River Basin, while somewhat equivocal, indicate that SEBAL can perform well in North America, as well. Further research on SEBAL is needed if SEBAL is to become an operational tool at IDWR.

SEBAL is an emerging technology, and suffers from some uncertainties that should be eliminated or reduced if SEBAL is to become operational. These uncertainties are in the form of 1) uncertainties created by extrapolating the ET predicted at the time of the satellite overpass to longer periods of time; 2) uncertainties created by the need to refine SEBAL to account for slope, aspect, and elevation, and to account for ET from water bodies and snow; and 3) uncertainties in precisely how SEBAL can be integrated into IDWR business processes and processes by other entities, for example the federal Bureau of Reclamation, Bureau of Land Management, Geological Survey, agencies in other states, and local users, for example canal companies and cities

The application and accuracy of SEBAL is potentially limited by uncertainties created by extrapolating the ET predicted at the time of the satellite overpass to the entire day of the overpass, as well as to the period between overpasses, which in the case of Landsat, is 8 or 16 days. Further work is needed on SEBAL to test and refine the means for using SEBAL to extrapolate ET from an instantaneous observation to longer periods. More work is needed to understand if the ET is constant over a typical day in Southern Idaho, or if some adjustment is needed to extrapolate the ET from midday to the entire day. The use of soil-water balance models and more frequent, yet more coarse AVHRR or MODIS images to extrapolate in time should be pursued.

For SEBAL to become operational, there needs to be demonstrated utility to IDWR (and other entity) business processes, particularly in regard to water rights management and ground-water modeling and planning. The question to be asked by water rights management is in how the utility of SEBAL measurements is affected by 1) pixel size and 2) repeat cycle. For ground-water modeling, the question is in regard to how aggregated ET for irrigation projects compares with recorded irrigation diversions. ET predictions, coupled with diversion records and estimates of ground-water pumpage, may allow the evaluation of 1) the relative efficiency of projects (i.e., fraction of diverted water that is evaporated); 2) the distribution in space and time of incidental recharge, which is a residual of diverted water; 3) the change in time of year and between years for these various performance indicators; and impacts of timing of return flows from irrigation projects on downstream discharges and consequent predictions for salmon recovery and impacts on other endangered species.

4.2.1.1 Additional Lysimeter Measurements

Precision weighing lysimeter systems present an excellent means for providing ground truth for validating and refining remote sensing-based procedures. Precision weighing lysimeter systems for evapotranspiration measurement were in place at Kimberly, Idaho from 1968 to 1992, at Utah State University, Logan, UT from 1988 to 1994 and at Bushland, Texas from 1986 to the present time. The Kimberly lysimeter system was operated by Dr. James Wright of the USDA-ARS (Wright, 1982, 1996) and measured evapotranspiration (ET) fluxes each 5 minutes. The Logan lysimeter system was operated by Dr. R.G. Allen (Allen and Fisher, 1990) and measured ET fluxes each 30 minutes. The Bushland lysimeter system is operated by Dr. Terry Howell of the USDA-ARS (Howell et al, 1995, 1997) and measures ET each 30 minutes. Much of the data from the lysimeter systems have been processed to daily totals of ET, and in many instances have been reported as hourly totals. The ET data are supported by measurements of solar radiation, humidity, air temperature, wind speed, soil moisture, soil temperature, vegetation height and leaf area, and in many cases by measurements of net radiation and sensible heat to the ground. The original 5 minute and hourly lysimeter summaries at Kimberly and 30 minute summaries from Logan and Bushland can be retrieved for the times of Landsat overpasses to provide concurrent measurements of ET fluxes.

In this application, the pixel size for Landsat Thematic Mapper reflective bands is 30 m by 30 m, and for the thermal band, 120 m by 120 m. The size of fields surrounding the lysimeter crops at Kimberly were characteristically 120 x 210 m, so that each crop grown on the lysimeter represents 28 pixels within a Landsat image, with the lysimeter toward the center. The lysimeters at Bushland were typically surrounded by about 400 m of similar vegetation. The Logan lysimeter was surrounded by 100 acres of grass forage. The size of surrounding vegetation provides a substantial number of degrees of freedom with regard to resolution and pixels in Landsat images for testing remote-sensing based algorithms for evapotranspiration prediction.

The lysimeter systems at Kimberly, Logan, and Bushland were operated night and day, 365 days per year. They represent precision measurements of ET. Crops grown on the Kimberly and Bushland lysimeters were irrigated crops common to the western US and represent well-watered conditions typical of irrigation projects. The Logan lysimeter was always planted to grass forage.

Most remote-sensing based ET prediction algorithms require information in the thermal as well as visible spectrum. The Thematic Mapper was placed onboard Landsat-4 and has provided thermal information since about 1982. Previous Landsat satellites used the Multi-Spectral Scanner (MSS) that had no thermal band vital for remotely-sensed ET work. The Kimberly lysimeter data span ten years of Thematic data and the Logan data span seven years of TM data. The Bushland data span 15 years of TM data An alternate source of spectral information is available from the NOAA AVHRR satellite. These data have coarser (1 km) resolution, but are less expensive to purchase than Landsat data.

The lysimeter data sets at Kimberly, Logan, and Bushland represent extremely valuable data sets in that they represent absolute measurements of ET fluxes spread over a long period of

time. They provide valuable information to verify procedures used to extrapolate SEBAL and other remote sensing algorithms over various land use categories. These data sets include typical climatic conditions as well as years having weather anomalies that can be used to test remote sensing estimates under dry and wet conditions. In addition, periodic measurements of net radiation components, soil heat flux and plant canopy parameters have been made at these sites. These data can be used to improve and/or validate various components of the SEBAL modeling process.

4.2.2 Model Refinement

Two refinements will make SEBAL more useful to IDWR. These refinements are 1) validation for ET from water bodies and snow; and 2) correction for differing slope, aspect and elevation. SEBAL as formulated by Basitaanssen, et al. (1998a) assumes all vegetation is growing on a relatively flat surface. In applying SEBAL to entire watersheds, especially those in Idaho and the west, this assumption clearly is not valid, and affects the ET estimates. In the arid, western United States, ET from lakes, reservoirs and wetlands can be significant. As a follow-on to this project, a commitment for partial funding has been secured to research these two refinements.

4.2.2.1 Evaporation from Water Bodies

Water evaporates from lake surfaces as well as from soil. However, the dynamics of evaporation from water bodies are different than those from soil. This project briefly examined the issue of water-body evaporation in the context of work done on the subject by Yamomoto and Kondo (1968) and of Amayreh (1995). The complicating factor with water bodies is the absorption and storage of solar energy by the water column. It is unclear precisely how time affects evaporation due to stored heat.

In SEBAL, G is the heat flux penetrating the surface. For the most part, G is the soil heat-flux, since SEBAL is normally applied to land surfaces. However, lakes are part of the landscape, and water is evaporates from their surfaces. Because the energy-balance dynamics of water bodies and soil are different, G needs to be treated differently for lakes than for soil.

For soil surfaces, SEBAL assumes essentially no 24-hour heat carry-over for soil. Some portion of net radiation is stored in the soil as heat during the day, and that stored heat is then discharged during the night, resulting in a positive G during the day and a negative G at night. Thus, SEBAL approximates the 24-hour G as zero for a land surface, although the instantaneous G is not zero.

The problem with using zero as the 24-hour G-value for a deep, clear lake such as Bear Lake, is that solar energy is absorbed by the water column and stored. The 24-hour G cannot be assumed to be zero. Amayreh (1995), reported the evaporation from Bear Lake to be very low, for this reason. Work by Yamamoto and Kondo (1965) has indicated similar findings.

Amayreh (1995) measured the seasonal aspect of heat exchange for Bear Lake. Yamamoto and Kondo (1965) reported that the seasonal trend of evaporation from a deep Japanese lake is substantially influenced by the heat storage of the lake. In the spring, water temperature is lower than the air temperature, and during the day, solar radiation penetrates the water column and is absorbed throughout the column. The energy enters the water and is counted as G. The radiation that enters into the lake heats the cold water, and much of the energy is not returned to the air during the night; rather it is stored in the water for a longer period of time. Therefore, in spring and much of the summer, the 24-hour G for water may have a large positive value every day.

During summer, the temperature difference between water and air is lower because water has been heated during the spring. The 24-hour G for water is still positive because solar radiation is strong in summer, and the water may still be heating up.

During the fall, there is a relatively large thermal contrast between the heated water and the cooling air. The 24-hour G for water becomes negative as stored heat is lost to the cool, fall air by convection to the water surface.

During the winter, there is still a relatively large thermal contrast between the still-warm water and the cold, winter air. The G for water therefore exhibits a large negative value.

The precise dynamics of the seasonal variation in G for deep, clear systems such as Bear Lake are difficult to quantify. However the measurements of G by Amayreh (1995) are markedly similar to the variation in G described for lakes in Japan studied by Yamamoto and Kondo (1965). This issue of predicting G for deep, clear lakes is described in more detail in Section 8 of Appendix A.

4.2.2.2 Corrections for Slope, Aspect, and Elevation

Previous applications of SEBAL have been limited to agricultural areas having no significant relief. However, the topography of the Bear River Basin, and of the western United States in general, has a wide range of slopes and aspects. Figure 4.2.2.2-1 illustrates both some of the varied terrainfound in the Bear River Basin, and the results of SEBAL processing for the corresponding area. ET estimation has not been validated by any actual ET measurements for areas of natural vegetation on different slopes and aspects. Therefore, it is likely that there is some error in ET predicted for mountainous regions in the Bear River basin resulting from assumptions presently in SEBAL.

Figure 4.2.2.2-1a. A shaded relief image of a mountainous area in the Bear River Basin

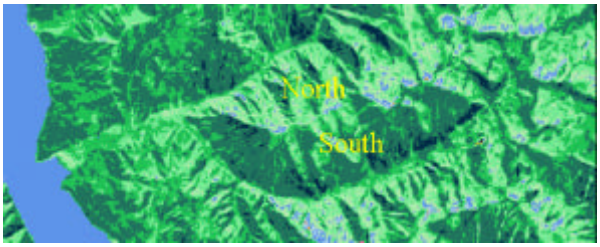

Figure 4.2.2.2-1b. Landsat data corresponding to Figure 1a color-coded for ET flux. The colors represent the same ET ranges as is Figure 3.3.3.1-2

Since SEBAL was designed for flat surfaces, it misinterpreted the temperature differential between north and south aspects when no distinction concerning slope and aspect was made. The 24-hour radiation is typically much higher on a south slope than on a north slope in the northern Hemisphere. The effect of not correcting for slope, aspect, and elevation is that SEBAL will compute higher than actual ET from north slopes because the cooler surface temperatures on north slopes are incorrectly interpreted by SEBAL as very wet (therefore cool) areas. However, cooler surface temperatures on north-facing slopes result not from the surface being wet, but from the lapse in temperature caused by higher elevations and smaller amounts of incident solar radiation.

Elevation and slope-aspect data were incorporated into SEBAL during phase I of this study. This substantially improved estimates of ET and other energy balance components in mountainous terrain. However, more development work and testing is needed. For example, improvement is needed in the prediction of air flow and wind velocity over mountainous terrain. Wind velocities in mountainous areas can be higher than that predicted in SEBAL using friction velocity and classical turbulent profile theory due to the effects of orographic drainage of air caused by differential cooling in mountainous terrain, by the acceleration of air streams passing over mountains due to the Venturi effect, and by impacts of drag by undulations in the land surface.

4.2.3 Using SEBAL with Other Satellites

The application and accuracy of SEBAL is limited by uncertainties caused by extrapolating ET predicted at the time of the satellite overpass to the entire day of the overpass, and of ET predictions for the period between overpasses. In the case of Landsat, the repeat cycle is 16 days (or 8 days if both Landsat 5 and Landsat 7 images are used after 1998). SEBAL can potentially use data from several other satellites with shorter repeat cycles.

Several satellites are available with repeat cycles equal to or shorter than Landsat's 8 or 16 days. NASA's Terra mission carries two potentially useable instruments for SEBAL: ASTER and MODIS. Terra was launched in December 1999, and was activated for science operations in February, 2000. Beta versions of its data products are now available for order from the CERES, MISR, and MODIS sensors. In addition to ASTER and MODIS, AVHRR images are available from NOAA.

4.2.3.1 AVHRR

The AVHRR has been used successfully for SEBAL by Bastiaanssen, et al., (1998b). It has a 2399-Km square image, and has five spectral bands between 0.58 and 12.5 micrometers. AVHRR images have a relatively large pixel size of one square kilometer. This maybe problematic for some IDWR applications, but suitable for others. The pixels are too large for applications involving the management of water rights, where ET needs to be assessed on a field-by-field basis. However, AVHRR images may be useful for extrapolating Landsat-based image in time by auto-correcting for changes in evaporative fraction over time. The AVHRR pixel size would pose no problem for applications involving ground-water modeling of the Eastern Snake River Plain Aquifer since the ground-water model uses a cell size of 5 Km. In fact, AVHRR's frequent repeat cycle and complete coverage of the Snake River Plain make this satellite attractive for aquifer modeling. Initially, ET maps predicted by Landsat may be useful during development of SEBAL applications for a region that are based on AVHRR by helping to identify and select the various “indicator” pixels required to apply SEBAL.

4.2.3.1 ASTER

ASTER stands for the Advanced Space-born Thermal Emission and Reflection Radiometer. It has fourteen spectral bands between 0.52 micrometers and 12.0 micrometers. Images are approximately 60 Km square. The spatial resolution for the visible and near infrared bands is fifteen meters, thirty meters for the short-wave infrared bands, and ninety meters for the thermal infrared bands. The repeat cycle is sixteen days, similar to that of Landsat. ASTER will have limited utility for IDWR due to selective scheduling of the approximately 750 scenes collected per day and due to the large number of scenes needed to cover IDWR's area of interest..

4.2.3.3 MODIS

MODIS stands for Moderate Resolution Imaging Spectrometer. MODIS has 36 channels between 0.4 micrometers and 14.4 micrometers. Images are approximately 2230 Km in size. The pixel size varies with band: from 250 meters (bands 1-2, the red and near infra-red), to 500 m (bands 3-7) to 1000 m (bands 8-36). MODIS offers the best choice for further SEBAL application based on the 1-2 day return cycle, large areal coverage, and 250-meter pixel size.

5.0 Bibliography

Allen, R.G. and D.K. Fisher. 1990. Low-Cost Electronic Lysimeters. *Trans. ASAE*, Vol 33(6):1823-1833.

Bastiaanssen, W.G.M. 2000. SEBAL-based sensible and latent heat fluxes in the irrigated Gediz Basin, Turkey. *J. Hydrology* 229:87-100.

Bastiaanssen, W.G.M., R. Sakthivadivel and A. Van Dellen, 1999a. Spatially delineating actual and relative evapotranspiration from remote sensing for modeling non-point source pollutants, in (eds.) D. Corwin et al, Geophysical Monograph 108, American Geophysical Union (special issue after joint AGU Chapman/SSSA Outreach Conference, USDA Salinity Lab, Riverside): 179-196

Bastiaanssen, W.G.M., T. Thiruvengadachari, R. Sakthivadivel and D.J. Molden, 1999b. Satellite remote sensing for estimating productivities of land and water, International Journal of Water Resources Development, vol. 15, nos. 181-196.

Bastiaanssen, W.G.M., 1998. Remote sensing in water resources management: the state of the art, International Water Management Institute, Colombo, Sri Lanka: 118 pp.

Bastiaanssen, W.G.M., M. Menenti, R.A. Feddes and A.A.M. Holtslag, 1998a. The Surface Energy Balance Algorithm for Land (SEBAL): Part 1 formulation, J. of Hydr. 212-213: 198-212

Bastiaanssen, W.G.M., H. Pelgrum, J. Wang, Y. Ma, J. Moreno, G.J. Roerink and T. van der Wal, 1998b. The Surface Energy Balance Algorithm for Land (SEBAL): Part 2 validation, J. Of Hydr. 212-213: 213-229

Bastiaanssen, W.G.M., H. Pelgrum, P. Droogers, H.A.R. de Bruin and M. Menenti, 1997. Area-average estimates of evaporation, wetness indicators and top soil moisture during two golden days in EFEDA, Agr. and Forest Met. 87: 119-137

Bastiaanssen, W.G.M., T. Van der Wal and T.N.M. Visser, 1996. Diagnosis of regional evaporation by remote sensing to support irrigation performance assessments, Irrigation and Drainage Systems, vol. 10, no. 1: 1-23

Bastiaanssen, W.G.M., D.H. Hoekman and R.A. Roebeling, 1994. A methodology for the assessment of surface resistance and soil water storage variability at mesoscale based on remote sensing measurements, IAHS Special Publications, No. 2, IAHS Press, Wallingford, Oxfordshire, UK

Hill, R.W., et al. 1989. *Duty of Water Under the Bear River Compact: Field Verification of Empirical Methods for Estimating Depletion.* Research report 125. Utah Agricultural Experiment Station, Utah State University, Logan, Utah.

Howell, T.A., A.D. Schneider, D.A. Dusek, T.H. Marek, and J.L. Steiner. 1995. Calibration and scale performance of Bushland weighing lysimeters, *Trans. ASAE* 38(4):1019-1024.

Howell, T.A., J.L. Steiner, A.D. Schneider, S.R. Evett, and J.A. Tolk. 1997. Seasonal and maximum daily evapotranspiration of irrigated winter wheat, sorghum, and corn – Southern High Plains. *Trans. ASAE* 40(3):623-634.

Hurk, van den, B.J.J.M., W.G.M. Bastiaanssen, H. Pelgrum and E. van Meijgaard, 1997. A new methodology for initialization of soil moisture fields in weather prediction models using METEOSAT and NOAA data, J. of Applied Met., 36: 1271-1283

Kramber, W.J., H.N. Anderson, M. Verdun, G. Astiguy and B. Ondrechen, 1993. Idaho's system for monitoring water use in the Bear River Basin, GeoInfo Systems, vol. 3(5):48-52.

Pelgrum, H. and W.G.M. Bastiaanssen, 1996. An intercomparison of techniques to determine the area-averaged latent heat flux from individual in-situ observations: A remote sensing approach using the European Field Experiment in a Desertification-Threatened Area data, Water Resources Research, vol. 32(9): 2775-2786

Roerink, G.J., W.G.M. Bastiaanssen, J. Chambouleyron and M. Menenti, 1997. Relating crop water consumption to irrigation supply by remote sensing, Water Resources Management 11: 445-465

Wang, J., W.G.M. Bastiaanssen, Y. Ma and H. Pelgrum, 1998. Aggregation of land surface parameters in the oasis-desert systems of Northwest China, Hydrological Processes.

Wright, J.L. 1982. New Evapotranspiration Crop Coefficients. *J. of Irrig. and Drain. Div.* (ASCE), 108:57-74.

Wright, J.L. 1996. Derivation of Alfalfa and Grass Reference Evapotranspiration. in. Evapotranspiration and Irrigation Scheduling, C.R. Camp, E.J. Sadler, and R.E. Yoder (ed.). Proc. Int. Conf., ASAE, San Antonio, TX. p. 133-140.

6.0 Appendix A

The Theoretical Basis of SEBAL

M. Tasumi and R.G. Allen
University of Idaho
and
W. Bastiaanssen
International Institute for Aerospace Survey and Earth Sciences
Enschede, the Netherlands

This appendix describes the theory and background for the various computational steps that are involved in the SEBAL process. Many of these steps are based on the development work of Bastiaanssen et al (1998a,b) and Bastiaanssen (2000). Other steps were added or modified during application of SEBAL to the Bear River basin during the current study. The index numbers associated with the steps are the same as the index numbers used in the ERDAS programming applications that are described in Appendix C.

0.1. Intermediate files for slope/aspect correction

In this step, the sine and cosine of the surface slope and aspect are made for each pixel of the image. These outputs are used for slope/aspect correction in SEBAL. The procedures used in this step are relatively simple. However, the user should exercise care in regard to the definition of the slope and aspect.

We have defined the units for the input/output images as follows:

Input

Slope :

In degrees (not in percent or in radians) The range of values in the image is from 0^o to 90^o.0^o means that there is no slope (= flat), and 90^o means that the land surface profile is vertical.

Aspect :

In degrees, where North is zero, and with values increasing positively in a clockwise direction. There is no sense of aspect when the slope of the surface is zero. The number 361 is given to the pixels that have no slope. Therefore, the range of values in the images is from 0 to 361. 0^o indicates a north facing slope, 90^o indicates an east facing slope, 180^o is a south facing slope, 270^o is a west facing slope, and 361 indicates that there is no aspect, since there is no slope.

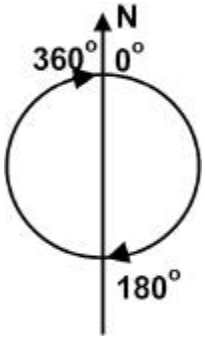

Output

Sin(slope) and Cos(slope) : The range of the output image is from 0 to 1.

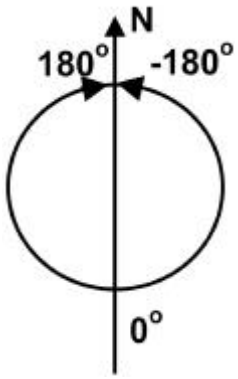

Sin(aspect) and Cos(aspect) : We defined the aspect in the output as South=0, West= positive. Therefore, the range of aspect is from –180 to 180 degrees.

The input file with the above defined units can be automatically derived from a DEM using ERDAS's Topographic Analysis function. If the available input files have a different definition for units, then the user must modify the model to obtain output files having the appropriate definition for units.

0.5. Cosine of solar incidence angle, cos?, for instantaneous incoming short-wave radiation Kin

This step adds slope and aspect corrections.

In SEBAL, the slope/aspect correction is carried out based on an assumption that the land surface acts as a Lambertian reflector. The solar incidence angle ? is the angle between the solar beam and a vertical line perpendicular to the land surface. If the land surface is horizontal, then the solar incidence angle ? is computed as:

$$?= 90^{o} – (\text{Sun Elevation}) \quad \text{…Equation 0.5.1}$$

where the sun elevation above the horizon. If there is any slope in the land surface, ? changes depending on the slope and aspect of the solar radiation and the land surface.

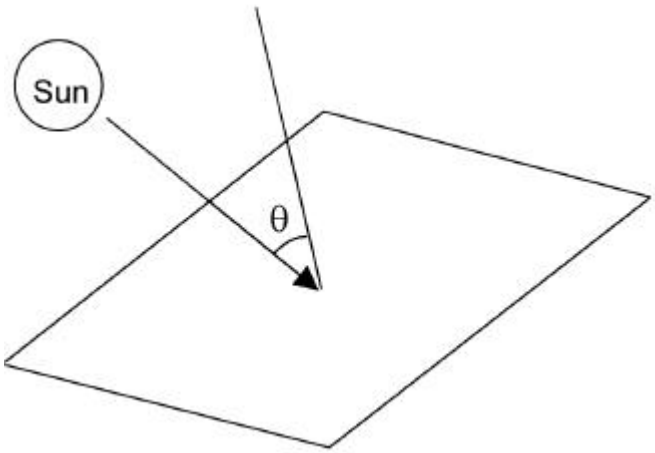

The ERDAS Field Guide gives the equation to compute the cosine of the incidence angle as follows (Ref. ERDAS Field Guide p383 “Lambertian Reflectance Model”):

$$\cos q = \cos(90 - q_s)\cos q_n + \sin(90 - q_s)\sin q_n \cos(f_s - f_n) \quad \text{Equation 0.5.2}$$

where
$?_S$ = the elevation of the sun above the horizon
f_S = the azimuth of the sun
$?_n$ = the slope of each surface element
f_n = the aspect of each surface element.

Equation 0.5.2 gives the cosine of the incidence angle for a particular date and time. However, one must integrate the equation for daily timesteps by tracking the sun as shown later in Step 0.7. Equation 0.5.2 is not suitable for integration because the location of sun is not an independent constant in this equation. Therefore, we use the following general equation for the calculation of incident angle:

$$\begin{aligned}\cos q = {} & \sin(d)\sin(f)\cos(s) - \sin(d)\cos(f)\sin(s)\cos(g) \\ & + \cos(d)\cos(f)\cos(s)\cos(w) \\ & + \cos(d)\sin(f)\sin(s)\cos(g)\cos(w) \\ & + \cos(d)\sin(f)\sin(s)\sin(w)\end{aligned} \quad \text{… Equation 0.5.3}$$

where,

d	declination of the earth (positive in summer in northern hemisphere)
f	latitude of the pixel (positive for northern hemisphere)
s	slope in radians, where s=0 is horizontal and s=p/2 is vertical downward (s is always positive and represents a downward slope in any direction)
?	surface azimuth angle. ? is the deviation of the normal to the surface from the local meridian, where ? = 0 for aspect that is due south, ? = - for east and ? = + for western aspect. ? = -p/2 represents an east-facing slope and ? = +p/2 represents an west-facing slope. ? = -p or ? = p represents a north-facing slope.
?	hour angle. ? = 0 at solar noon, ? is negative in morning and ? is positive in afternoon

For more detail on computing the cosine of the solar incidence angle, the reader is referred to Appendix B “Derivation of an equation to compute incoming solar radiation over 24-hour period for sloping surfaces”.

In this step, the value of cos? calculated by equation 0.5.3 is divided by the cosine of the slope, cos(s). Cos? is used for the calculation of incoming solar radiation for each band of the Landsat TM (E_{in}), and the reflectance is calculated from the reflected radiation observed by the satellite.

Usually the incoming and outgoing solar radiation for a band (E_{in}, E_{out} or reported as a whole (K_{in}, K_{out})) are expressed as energy per unit area, W/m^2.

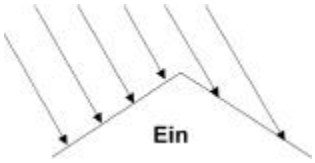

For incoming radiation, the unit area is expressed along a plain parallel to the sloped surface.

Since outgoing radiation is observed by the satellite's sensors for an essentially flat surface, the intensity of outgoing radiation is rederived as energy per unit area where the unit area is in an horizontal equivalent. In SEBAL, the factor cos? that represents the effect of the solar angle is divided by cos(s) to adjust the incoming solar radiation to energy per unit area where the area is a horizontal equivalent.

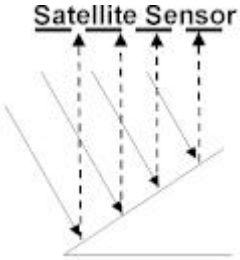

All of the fluxes that are computed for the energy balance, including radiative fluxes, are analyzed on a horizontal-equivalent basis in SEBAL.

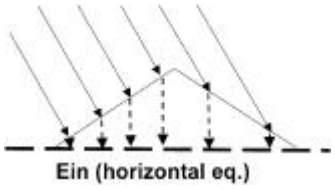

0.7. Twenty-Four Hour Extraterrestrial Radiation, Ra_{24}

The twenty-four hour extraterrestrial radiation, $Ra_{24,}$ is the daily incoming solar radiation unadjusted for atmospheric transmittance. The estimation of atmospheric transmittance is described later in Step 3.

Ra_{24} is derived by the following equation;

$$Ra_{24} = Gsc * d_r * \int_{w_1}^{w_2} \cos(q)\, dw \quad \ldots \text{ Equation 0.7.1}$$

where
Gsc is the solar constant, 1367 W/m^2,
d_r is inverse relative distance Earth-Sun (See Step 1 of the Appendix C for the d_r calculation).

In equation 0.7.1, $\int_{w_1}^{w_2} \cos(q)\, dw$ is the integration of the cosine of the solar incidence angle which was given as Equation 0.5.3. For more detail of the computation of the Twenty-four Hour Extraterrestrial Radiation, see the Appendix B "Derivation of an equation to compute incoming solar radiation over 24-hour period for sloping surfaces".

1. Spectral reflectance (unadjusted for transmittance)

In this step, reflectance is calculated for all pixels of each band 1-5 and 7 (band 6 is the thermal band). The reflectance of a band is computed as

$$R(\text{band}) = \frac{E_{out}(\text{band})}{E_{in}(\text{band})} \quad \text{... Equation 1.1}$$

where E_{out}(band) is the outgoing energy (radiation) of the band measured at the top of atmosphere by the satellite, and E_{in}(band) is incoming energy (radiation) of the band at the top of atmosphere. The outgoing energy is recorded by the satellite's sensors, and incoming energy is based on theoretical values for various wave lengths of solar radiation.

E_{in}(band) is computed as:

$$E_{in}(\text{band}) = G_{sc}(\text{band}) \times \cos(q) \times d_r \quad \text{... Equation 1.2}$$

where, G_{sc}(band) is the solar constant for the band, the values for which are given in Table 1.1; cos? is the cosine of the solar incident angle derived in Step 0.5., and d_r is inverse relative distance Earth-Sun. The value for d_r averages 1.0 and ranges from about 0.97 to 1.03.
E_{out}(band) is computed as

$$E_{out}(\text{band}) = \left(a + (b-a)\frac{DN}{255} \right) p \quad \text{... Equation 1.3}$$

where, a and b are constants (See. Table 1.1), DN is the original digital number for the pixel in the satellite image. In equation 1.2, inverse squared relative distance Earth-Sun d_r is computed as

$$d_r = 1 + 0.033 \cos\left(DOY \frac{2p}{365} \right) \quad \text{... Equation 1.4}$$

This value for d_r is dimensionless, and DOY is the sequential day of year (i.e., Julian date). The unit of the angle argument (DOY * 2p / 365) is in radians. (Ref. FAO56 (Allen et al., 1998), p46, Equation 23)

The calibration constants used in Equation 1.2 and 1.3 are as follow;

Table 1-1. Calibration constants for Landsat 5 (in mW/cm^2/μm for G_{sc}, and in mW/cm^2/star/ μ m for a and b) (note that calibration constants are different for Landsat 7 images)

	Band1	Band2	Band3	Band4	Band5	Band7
G_{SC}(band)	195.7	182.9	155.7	104.7	21.93	7.452
a	-0.15	-0.28	-0.12	-0.15	-0.037	-0.015
b	15.21	29.68	20.43	20.62	2.72	1.44

G_{SC}(band): Markham,B.L. and J.L. Barker, 1986
Constants a and b: Markham, B.L and J.L. Barker, 1987

2. Surface albedo at the top of atmosphere, a_{toa}

Albedo is the ratio of reflected to incident solar radiation at the surface and is computed initially as

$$a = \frac{K_{out}}{K_{in}} \quad \text{... Equation 2.1}$$

where, a is albedo, K_{in} is incoming short wave radiation (solar radiation) and K_{out} is outgoing short wave radiation. Short wave radiation is defined as the wave-lengths between 0.17 and 4 micrometers.
In this step, we calculate albedo as observed at the top of atmosphere (unadjusted for transmittance) using the reflectance of each band calculated in the previous step. This albedo at the top of the atmosphere is converted into a surface albedo in the following step. The meaning of Equation 2.1 is basically same as Equation 1.1. The only difference is in the range of the wavelengths used. Equation 2.1 targets whole range of short wave radiation, by essentially adding the magnitudes (E_{out}) of the individual short-wave bands.

The basic concept of calculating a_{toa} is to use weight coefficients on the summation of individual bands:

$$a_{TOA} = \Sigma[c(band) \times Radiation(band)] \quad \text{... Equation 2.2}$$

where, c(band) is weighting coefficient for a particular band

In equation 2.2, Sc(band) = 1

The ratio of potential incoming energy in each band is determined by the ratio of solar constant G_{SC} in each band (See. Table1.1). Therefore,

$$c(band) = \frac{G_{sc}(band)}{\Sigma G_{sc}(band)} \quad \text{... Equation 2.3}$$

where, c(band) is the weighting coefficient for the band given in Table 2.1

For example, since $SG_{sc}(band) = 668.4$, $c_1 = 195.7 / 668.4 = 0.293$

Table 2.1. Weighting coefficients c(band) for Landsat 5.

	Band 1	Band 2	Band 3	Band 4	Band 5	Band 7
c(band)	0.293	0.274	0.233	0.157	0.033	0.011

3. Surface albedo, a_0

In this step, SEBAL estimates surface albedo, a_0, from the "surface albedo at the top of atmosphere, a_{toa}" that was calculated in the previous section.

Since the atmospheric transmittance is not taken into account in a_{toa}, the adjustment of the albedo value by transmittance is the task in this step.

The reader is referred to the following sketch.
There are three differences between radiation (and albedo) at the earth's surface and at the top of the atmosphere:
(1) Incoming radiation (i.e., solar radiation) is higher at the top of atmosphere and lower in the land surface because a portion of radiation is absorbed or reflected by air. The amount of the absorption or decrement is explained by using a (one-way) transmittance of air.
(2) The outgoing short wave radiation generated by reflectance at the surface is reduced by the time it arrives at the top of atmosphere because a portion of radiation is absorbed by air. The amount of the absorption or decrement is also explained by using the (one-way) transmittance of air.
(3) There is additional reflectance that is observed by sensors above the top of atmosphere because a portion of incoming radiation is reflected, rather than absorbed, before it reaches the earth's surface. This component is called albedo path radiance.

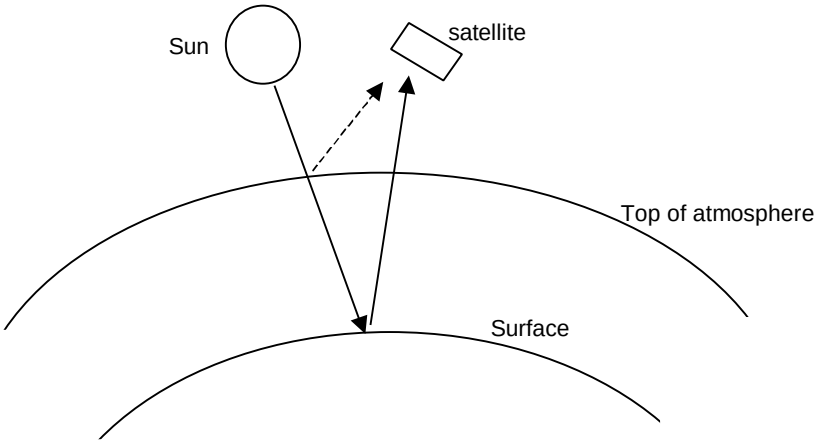

Figure 3.1. Sketch of solar radiation and the reflectance

Therefore, surface albedo is calculated as

$$a_0 = \frac{a_{toa} - a_{path\_radiance}}{t_{sw}^2} \quad \text{… Equation 3.1}$$

where, $a_{path\ radiance}$ is albedo path radiance, and $t_{sw} * t_{sw}$ is the two-way transmittance.

Usually, $a_{path\ radiance}$ has a value between 0.025 to 0.04.

A general value for the one-way transmittance in clear-sky can be predicted for clear, relatively dry atmospheric conditions as:

$$t_{sw} = 0.75 \times 2 \times 10^{-5} \times z \quad \text{… Equation 3.2}$$

where, z is elevation above sea level in m. (Ref. FAO56 P51 Equation 37). More complicated expressions are available for transmittance in FAO56 and elsewhere (Allen, 1996) that consider sun angle and absorption by water vapor. Transmittance can also be determined for a locality using measurements of solar radiation on clear days. However, it is important the the pyranometer used be well-calibrated and maintained.

As an example for the Bear River application, since two-way transmittance is the square of one-way transmittance, if the elevation is 1800m,

$t_{sw} = 0.75 + 2 * 10^{-5} * 1800 = 0.786$,

then,
$t_{sw}^2 = 0.786^2 = 0.618$

A set of reference albedo values is given in the albedo part of Appendix C. The user can also refer the following albedo information for comparison with predictions by SEBAL:

Fresh snow 0.8-0.85
Old snow and ice 0.3-0.7
Black soil 0.08-0.14
Clay 0.16-0.23
White-yellow sand 0.34-0.4
Gray-white sand 0.18-0.23
Paddy field (rice) 0.17-0.22
Grass or pasture field 0.15-0.25
Maize field 0.14-0.22
Forest (coniferous) 0.1-0.15
Forest (deciduous) 0.15-0.2
Water (solar elevation=10degree) 0.348
Water (solar elevation=30degree) 0.06
Water (solar elevation=50degree) 0.025
(Agricultural Meteorology, 1992)

4. Normalized Difference Vegetation Index, NDVI

The NDVI (Normalized Difference Vegetation Index) is an index of vegetation that is often computed using Landsat TM data as follows:

$$NDVI = \frac{Band4 - Band3}{Band4 + Band3} \quad \text{… Equation 4.1}$$

However, reflectance of band 3 and 4 are used in SEBAL, instead of the brightness of the original bands:

$$NDVI = \frac{r4 - r3}{r4 + r3} \quad \text{… Equation 4.2}$$

where, r3 is reflectance of band 3 computed in Step 1, and r4 is reflectance of band 4 computed in Step 1.

5. Thermal infrared surface emissivity, e_0

Emissivity of an object is the ratio of the energy radiated by that object at a given temperature to the energy radiated by a blackbody at the same temperature. Since the thermal radiation of the surface is observed in the TM thermal band (band 6), one can compute the surface temperature from band 6 if the emissivity of the land surface is estimated.

In SEBAL, surface emissivity is estimated using NDVI and an empirically-derived method:

$$e_0 = 1.009 + 0.047 \ln (NDVI) \quad \text{… Equation 5.1}$$

where NDVI > 0. Otherwise, emissivity is assumed to be zero (for example, for water).(Ref. Van de Griend and Owe (1993))

6. Surface temperature, T_0

In this step, surface temperature is estimated by Band 6 (thermal band).

The Stefan-Boltzman law explains the relationship between temperature and radiation of a object:

$$B = sT^4 \quad \text{... Equation 6.1}$$

where, B is radiation from a black body, s is the Stefan Boltzman constant 5.67 * 10^{-8} ($W/m^2/K^4$), and T is surface temperature of a black body.

However, the thermal band of Landsat TM is too narrow to use as a representation of B in equation 6.1. The range of the radiation used in the Stefan Boltzman relationship is 3.0 – 300 µm, and the range of TM band 6 is 10.4 – 12.4 µm. Therefore, SEBAL uses the Plank equation which is given in the following:

$$B_l = \frac{2\ phc^2}{l^5 \times \exp\left(\frac{hc}{k\ lT}\right) - 1} \quad \text{… Equation 6.2}$$

where, $B_?$ is intensity of radiation which has a wave length ? (W/m^2), h is the Plank constant 6.626*10^{-34} Js, c is speed of light 2.998*10^8 m/s, k is Boltzman constant 1.381*10^{-23} J/K, T is surface temperature of the black body in K.

From equation 6.2, the following equation is derived with a modified Plank constant for TM band 6 from Landsat 5 (coefficients for Landsat 7 are different):

$$T = \frac{1261}{\ln\left(\frac{60.8}{L6} + 1\right) e_0^{0.25}} \quad \text{… Equation 6.3}$$

where,

$$L6 = 0.0056322DN + 0.1238 \text{ … } 6.4$$

DN is digital number of band 6 (Ref. Wukelic, 1989, for equation 6.3 and 6.4)

Surface temperature T_0 is then calculated by T and e_0 with the following equation:

$$T_0 = \frac{T}{e_0^{0.25}} \quad \text{… Equation 6.5}$$

From equation 6.3 to 6.5, the surface temperature T_0 can finally be calculated for Landsat 5 images by:

$$T_0 = \frac{1261}{\ln\left(\frac{60.8}{0.0056322DN + 0.1238}\right) e_0^{0.25}} \quad \text{… Equation 6.6}$$

6.5 Apparent Surface Temperature for a Reference Elevation for calculation of sensible heat flux

Generally, air temperature decreases 6.5^{o}C when elevation increases by 1 km under neutral stability conditions. Since surface temperatures are in strong equilibrium with air temperature, one can usually observe similar decreases in surface temperature. During the prediction of the surface-to-air temperature difference (dT) during steps 10-19, SEBAL assigns a value for dT as a function of surface temperature. However, the surface temperature that is used needs to be uniformly adjusted to a common reference elevation for accurate prediction of dT. Otherwise, high elevations that appear to be "cool" may be misinterpreted as having high evaporation. Therefore, in this step, a "lapsed" (and artificial) surface temperature map is made for purposes of computing surface-to-air temperature differences by assuming that the rate of decrease in surface temperature by the orographic effect is the same as that for a typical air profile. Elevation data are taken from U.S. Geological survey Digital Elevation Model (DEM) data. The "fictitious" lapse-adjusted surface temperature is referred to as a DEM corrected surface temperature.

The DEM corrected surface temperature is calculated by the following equation;

$$T_{0\_dem} = T_0 + 0.0065\Delta z \quad \text{… Equation 6.5.1}$$

where, ?z is the difference of a pixel's elevation from the datum in meters. The term ?z is positive if the elevation of a pixel is higher than the datum.

7. Net radiation, Rn

Net radiation is given by the surface radiation balance by the following equation:

$$R_n = (K_{in} - K_{out}) + (L_{in} - L_{out}) \text{ ... Equation 7.1}$$

where, K_{in} is incoming short wave radiation, K_{out} is outgoing short wave radiation, L_{in} is incoming long wave radiation, and L_{out} is outgoing long wave radiation.

Using Equation 2.1, Equation 7.1 can be rewritten as:

$$R_n = (1- a) K_{in} + (L_{in} - L_{out}) \text{ ... Equation 7.2}$$

In equation 7.2, K_{in} is predicted, assuming cloud-free conditions, as:

$$K_{in} = G_{sc} \times \cos q \times d_r \times t_{sw} \text{ ... Equation 7.3}$$

where G_{sc} is the solar constant expressed as 1367 W/m^2, cos? is the cosine of the solar zenith angle, d_r is the inverse relative distance Earth-Sun, and t_{sw} is one-way transmittance.

In Equation 7.2, the Stephan Boltzman equation (explained in Equation 6.1) is applied for long wave components L_{in} and L_{out}.

L_{in} is calculated by the following equation from Bastiaanssen et al. (1998) for cloud-free conditions:

$$L_{in} = 1.08 (-\ln t_{sw})^{0.265} s T_{0ref}^4 \text{ ... Equation 7.4}$$

where, T_{0ref} is the surface temperature at a reference point, generally selected to be a well-watered pixel so that surface temperature and air temperature are similar.

Since L_{out} is the long wave radiation from the surface, it is calculated by applying Equations 6.1 and 6.5:

$$L_{out} = e_0 s T_0^4 \text{ ... Equation 7.5}$$

However, in equations 7.2 to 7.5, surface reflectance of incoming long wave radiation is not taken into account. This reflectance is estimated as $(1 - e_0)L_{in}$. Therefore, Equation 7.2 becomes

$$R_n = (1- a) K_{in} + (L_{in} - L_{out}) - (1 - e_0)L_{in} \text{ ... Equation 7.6}$$

8. Soil heat flux, G_0

Net radiation is the net radiant energy that the land surface actually receives and loses from or to the atmosphere. Usually R_n is positive during the day and negative at night. Some of the net energy is used to evaporate soil water, some energy is used to heat the air, and the rest of the net energy is stored in the ground (or a water body).

The following equation describes the surface heat balance:

$$Rn = ?E + H + G_0 \ldots 8.1$$

where, ?E is latent heat flux, H is sensible heat flux, and G_0 is soil heat flux. Other minor terms, such as energy absorbed by photosynthesis or advected horizontally, are relatively very small in value, and are ignored.

This step focuses on the estimation of ground heat flux as illustrated in the following figure. Ground heat-flux is explained as

$$G_0 = l_s \frac{dT}{dz} \quad \ldots \text{Equation 8.2}$$

where, $?_s$ is the thermal conductivity of the soil, dT_s is temperature difference between T_0 and T_1, dz is the depth difference between z_0 and z_1

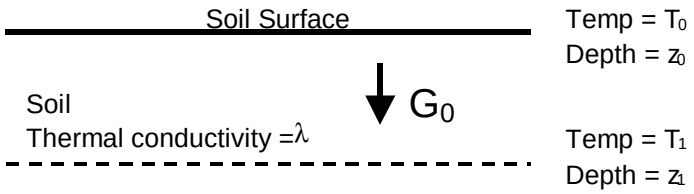

Figure8.1. Soil Heat Flux

However, Equation 8.2 cannot be applied to SEBAL because we do not know T_1 and ?. Therefore, in the Idaho application, an empirical equation is applied to estimate G_0, and a general equation that utilizes the normalized vegetation index is given as

$$G_0 = 0.30(1 - 0.98\mathrm{NDVI}^4)R_n \quad \ldots \text{Equation 8.3}$$

This equation was derived from actual measurements as reported in Bastiaanssen et al. (1998) and was used in place of the more extended equation recommended in Bastiaanssen (2000) that uses surface temperature and albedo, due to some question regarding the applicability of the extended equation to Idaho conditions. Strictly speaking, Equation 8.3 is applicable only to a vegetated land surface, and the equation for water and snow would be quite different. In the application of SEBAL to Idaho, G_0 for snow surface was predicted for daytime periods as

$$G_0\text{snow} = 0.5Rn \ldots \text{Equation 8.4}$$

This is a very crude estimate for G and assumes that one-half of net radiation incident to snow penetrates the snow surface in the form of light and is absorbed into the snow mass as G. Additional research and literature review is needed in this area.

The equation for G_0 on a water surface is difficult to define since there is very limited information. As discussed in the text, short-wave solar radiation penetrates into a water body according to the transparency of the water and is absorbed at a range of depths below the surface where it is converted into heat (G). Therefore, this component of G, although not a surface phenomenon, must never-the-less be included in total G for the water body. The depth of penetration will vary with sun angle and turbidity of the water body. The Bear River Basin has a large, deep lake called Bear Lake that is the primary water surface in the study area. Therefore, the situation of a deep lake was focused upon during development of the equation of G for a water body.

As an example of the heat balance for a deep lake, Yamamoto reported the seasonal trends within a set of actual measurements (Yamamoto and Kondo, 1968). The following graph is the plot of the monthly averages for R_n and G values which Yamamoto measured in a deep lake (mean depth was 21m) in Japan.

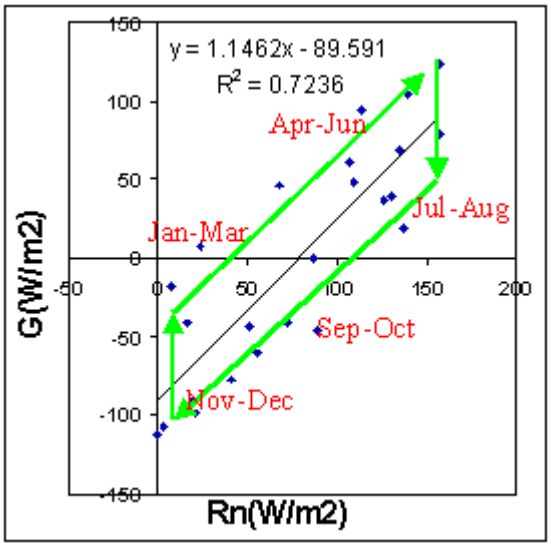

Figure 9.1. The plot of the monthly averages of R_n and G values measured in a deep lake (mean depth of 21m) in Japan (Yamamoto and Kondo, 1968).

In this project, we attempted to separate a year into two periods, January-June and July-December, and derived for each a R_n-G curve from Yamamoto's measurements for estimating G for water. Figure 9.2 is for January-June. One extreme data point in January was rejected. Figure 9.3 is for July-December. One extreme data point in July was rejected

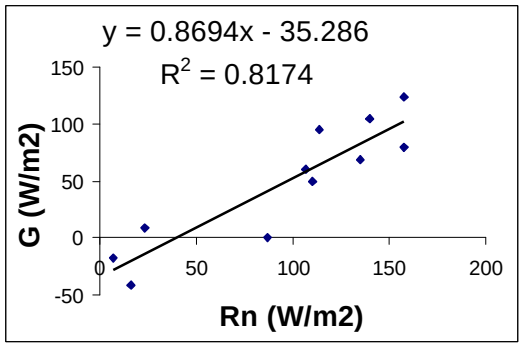

Figure9.2. An R_n-G curve and measurements for estimating G for water during the January to June period (based on Yamamoto and Kondo, 1968).

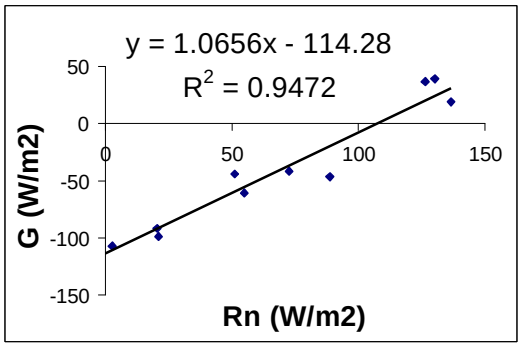

Figure9.3. An. R_n-G curve and measurements for estimating G for water during the July to December period (based on Yamamoto and Kondo, 1968).

In addition to Kondo's work, Amayreh (1995) measured G for the Bear Lake using eddy covariance and heat storage change, and reported that daily G during summer and fall could be predicted as $G = 0.984R_n - 62$ (Amayreh, 1995). This equation does not include a sense of "seasonal difference" in G vs. time, since Amayreh's work was limited to summer and fall. However, Amayreh's measurements are similar to those of Kondo's in both magnitude and trends, so that this simple prediction approach based on R_n is probably valid for deep, clear water bodies. The following equations were developed for estimating G for water, based on Yamamoto's and Amayreh's work:

For the July to December period, for instantaneous G at the time that the satellite image was taken (approximately 10:40 am):

$$G_0 water = R_n - 90 \ldots \text{Equation 8.5}$$

and for 24hr G:

$$G_0 water = R_n - 100 \ldots \text{Equation 8.6}$$

For the January – June period, for instantaneous G at the time that the satellite image was taken (approximately 10:40 am):

$$G_0 water = 0.9R_n - 40 \ldots \text{Equation 8.7}$$

and for 24hr G:

$$G_0 water = 0.9R_n - 50 \ldots \text{Equation 8.8}$$

Penetration of solar radiation into water decreases as depth of the water body decreases and/or as turbidty of the water increases. Highly turbid bodies of water and very shallow bodies of water will have G that is more in synch with R_n, so that the offsets of the above equations will be reduced or may completely disappear.

9. Surface roughness for momentum transport, z_{0m}

Surface roughness for momentum transport z_{0m} is defined as the height above the "zero-plane displacement" that the zero-origin for the wind profile just begins within the surface or vegetation cover.

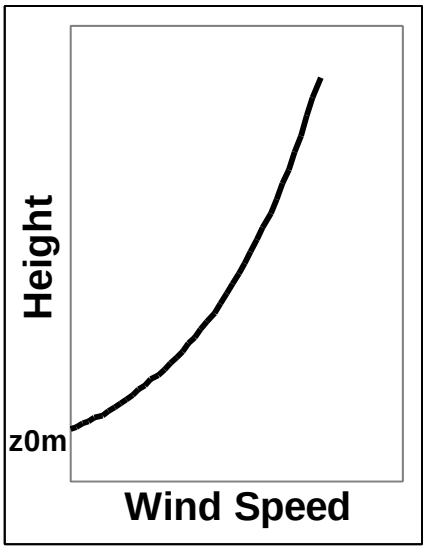

Figure 9.1. The vertical wind profile and the location of z_{0m}.

In SEBAL, surface roughness is estimated from NDVI using an empirical equation:

$$z_{0m} = \exp(a \times NDVI) + b \quad \ldots \text{ Equation 9.1}$$

where, a and b are constants. The constants a and b are derived by values of NDVI and z_{0m} for sample pixels representing specific vegetation types. The calculation method for the constants a and b is given in Appendix C. Allen (2000, personal communication) has found that using NDVI/albedo may be more effective in predicting differences in z_{0m} between forests and agricultural systems.

10-19. Estimating friction velocity (u_*), aerodynamic resistance to heat transport (rah), and sensible heat flux (H)

Steps 10 to 19 are used to estimate the sensible heat flux H. The aerodynamic transfer of heat to air, H, is commonly predicted using the following equation:

$$H = \frac{r_{air} \times Cp_{air}}{r_{ah} \times dT} \quad \ldots \text{ Equation 10.1}$$

where, $?_{air}$ is air density which is a function of atmospheric pressure; Cp_{air} is the heat capacity of air 1004(J/kg/K); r_{ah} is aerodynamic resistance to heat transport; and dT is the temperature difference between z_1 and z_2

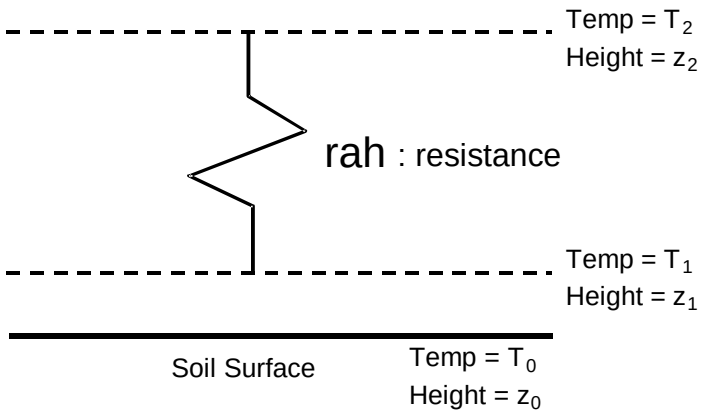

Figure 10.1. Sketch of aerodynamic heat transfer

In equation 10.1, r_{ah} is calculated as

$$r_{ah} = \frac{\ln\left(\frac{z_2}{z_1}\right)}{u_* \times k} \quad \text{… Equation 10.2}$$

where, u_* is friction velocity, k is von Karman's constant (0.41), and z_1 and z_2 are heights above the ground surface. To identify the value of u_* in equation 10.2, SEBAL requires at least one wind speed observation datum for the day when the image is taken, preferably from within the image area and near the time of the satellite image. This wind speed observation is used to predict the friction velocity for the measurement surface, which is then used to predict a surface-independent wind speed at a high level (200 m) above the earth's surface. The high level wind speed is applied to all pixels of the satellite image.

The wind profile over a stable surface shows the following relationship:

$$\frac{u_x}{u_*} = \frac{\ln\left(\frac{z_x}{z_{0m}}\right)}{k} \quad \text{… Equation 10.3}$$

where u_x is wind speed at x (m/s); k is von Karman's constant (0.41); z_x is height in m where wind u_x was observed; and z_{0m} is surface roughness for momentum transport in m.

From equation 10.3, u_* is calculated when u_x, z_x and z_{0m} are available from a meteorological station. In Equation 10.3, z_{0m} is empirically estimated from the average vegetation height around the meteorological station from the following equation.

$$z_{0m} = 0.123 \text{ (vegetation height in meters)} \quad \text{… Equation 10.4}$$

Once u_* is identified, wind velocity at an elevation of 200 meters is determined by using Equation 10.3. In this process, 200 meters is selected as the height where wind speed is no longer affected by surface roughness. The wind speed at 200 m is fixed in the image and is assumed to "float" above mountains and

other changes in terrain. For example, if the computed u_{200} is 5.3 m/s, the SEBAL application assumes that u_{200} at every pixel is 5.3 m/s. Using the computed u_{200}, SEBAL uses equation 10.3 once again to calculate u_* for each pixel. Once u_* in each pixel is computed, r_{ah} can be calculated by Equation 10.2 for the heights z_1 and z_2 that are specified. Heights z_1 and z_2 represent the heights that define the surface to air temperature difference dT. z_1 is defined as the mean height above (or within) the vegetation where radiant energy is converted into sensible heat (See. Figure 10.1).

The following conditions were considered in selection of the heights z_1 and z_2.

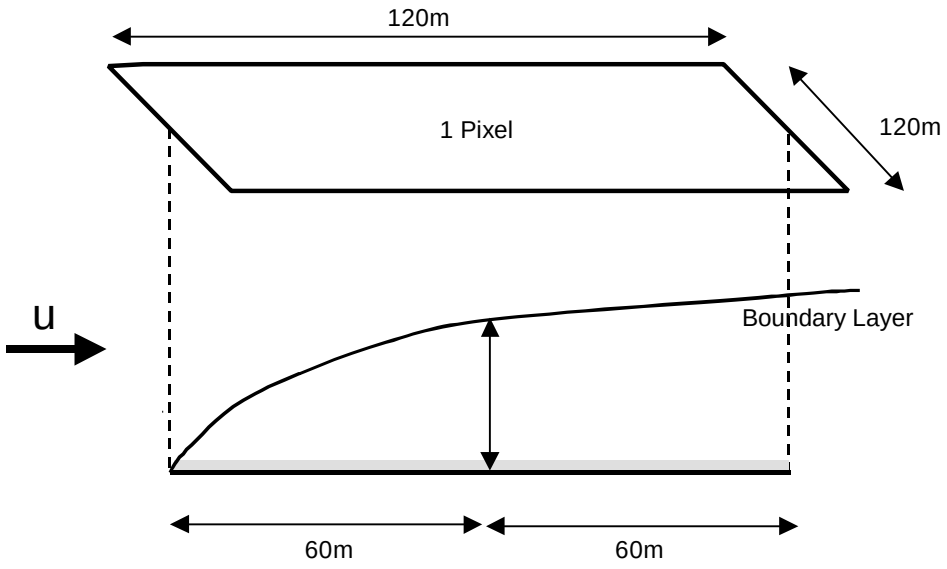

Figure 10.2. Boundary layer

As shown in Figure 10.2, a boundary layer develops above the land surface downwind of each change in surface characteristics. The information from TM band 6 only indicates the environment of the surface that is operating below the boundary layer. The height of the boundary layer is assumed to be 0.01 to 0.02 of the distance (fetch) from the beginning of a change in vegetation in a downwind direction. (e.g. if the fetch is 60m, the height of the boundary layer is 0.6 m to 1.2 m). Of course, the boundary layer height tends to be higher when the surrounding pixels have similar vegetation and water-status environment.
Ideally, heights z_1 should be defined as being just above the mean height of the crop canopy, and height z_2 should be defined as being just below the height of the boundary layer. For consistency, z_1 and z_2 are assigned values of 0.01 m and 2.0 m respectively. The value of r_{ah} is calculated using Equation 10.2 based on these two heights.

The temperature difference between z_1 and z_2 is predicted in order to estimate H from Equation 10.1. In the Equation 10.1, H and dT are both unknown factors, but are directly related to one another, as well as to the value for r_{ah}.

If the inverse of Equation 10.1 is considered,

$$dT = \frac{H \times r_{ah}}{r_{air} Cp_{air}} \quad \text{… Equation 10.5}$$

Therefore, during the SEBAL process, the user calculates dT at two extreme "indicator" pixels (endpoints) by assuming values for H at the reference pixels. The reference pixels are carefully chosen so that at these pixels one can assume that H ~ 0 at a very wet pixel (i.e., all available energy (R_n – G) is converted to ET), and that ?E ~ 0 at a very dry pixel, so that H = R_n – G_0. These assumptions from the selected pixels provide endpoints for values and locations for H so that a relationship for dT can be established.
The selection of the wet and dry pixels is somewhat subjective, but necessary to solve the energy balance. The selection of wet and dry pixels where ET = R_n – G and where H = R_n - G is easier than for pixels that lie in between these endpoints, since conditions favoring these two endpoints are generally straight-forward to identify.

Under conditions of similar available energy (R_n – G), a wet pixel will have a lower temperature than a dry pixel. The lower the temperature, relative to other pixels, the more likely that ET approaches R_n – G so that H approaches 0. Therefore, to find a very wet pixel, one should search for the coldest pixel that is situated in an agricultural setting (if possible). The assessment should be done using the DEM adjusted surface temperature image so that lapse effects do not mask the wet pixels. Usually the wettest/coldest pixels occur in wet fields just after irrigation. An agricultural setting is desired over a water body, since the aerodynamics and available energy will be more similar to other vegetative surfaces. This may be important in later steps when dT of other pixels are interpolated according to surface temperature and when the focus of SEBAL is ET from vegetation. The DEM-corrected surface temperature in the very wet pixel selected is labeled as T_{cold}.

The value of dT is presumed to be zero at the wet (T_{cold}) pixel. This assumption is generally true in a wide range of climates, except perhaps, in extremely arid regions where regional advection of sensible heat energy into irrigated projects can cause ET to exceed R_n – G. This results in negative values for H, so that according to Equation 10.5, dT may become negative. If this type of highly advective situation is known to occur, then the SEBAL user can make an assumption concerning the ratio of ET/(R_n-G) at the "wet" pixel and can then determine H and subsequently dT for the pixel. In the winter time, the coldest pixel might be below 273K (0 ^oC). However, the coldness may not necessarily indicate wetness, but is from being snow-covered, or from the ground being frozen. In such situations, a very wet pixel might have a surface temperature during midmorning (during the Landsat overpass) and under sunlit conditions of approximately 273.1 K. Since the DEM corrected surface temperature is not the actual temperature, but a fictitious lapse-corrected temperature, the actual surface temperature T must also be referred to in order to judge the actual, underlying conditions and relative wetness.

It is often more difficult to find a very dry pixel at which one can assume ?E is zero. This is especially difficult in a semihumid or humid climate having substantial rainfall so that even bare soil has some evaporation flux. Also, since the driest pixel has a large value for dT as compared to the coldest pixel in SEBAL, a good estimation is required. As an initial guess, a very hot pixel is a good candidate for locating the driest place within the image. Within the hotter pixels, man-made places such as airports or highways are more likely to be dry than a naturally vegetated location or location having bare soil. Man-made surfaces are less desirable than natural or agricultural surfaces because of larger uncertainties in the estimate for G and aerodynamic transport. A steeply sloped place should be avoided due to uncertainties in total energy. One can refer to the DEM adjusted surface temperature in the very dry pixel selected as T_{hot}.

The UTM coordinates of the driest pixel must be recorded because they are required later. Once the driest pixel is identified, the value of H at the pixel is calculated from the values of R_n and G_0 in the R_n and G_0 images since $H = R_n - G_0$ for the pixel. Then dT of the pixel can be calculated by equation 10.5 assuming an initial value for aerodynamic resistance, r_{ah} (See. Appendix C).

In SEBAL, it is assumed that dT has a linear relation to T_0 at all pixels:

$$dT = aT_0 + b \quad \text{… Equation 10.6}$$

where, a and b are constants

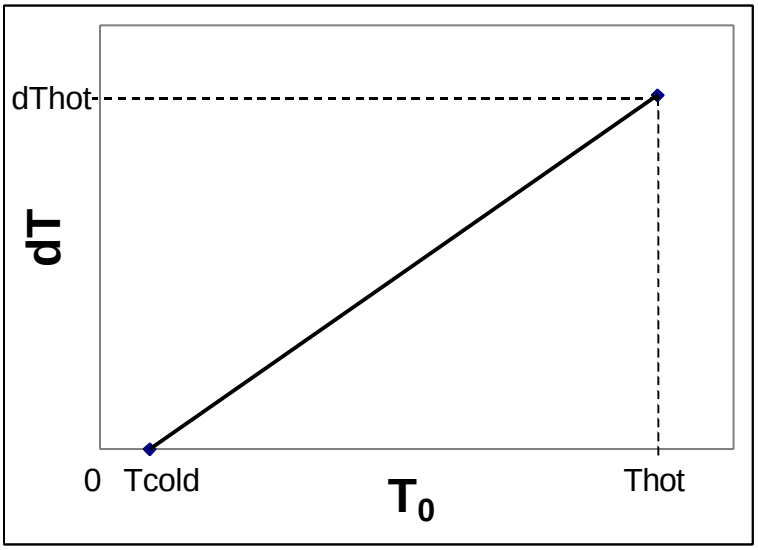

Figure 10.3. Concept of dT (temperature difference between surface and air) prediction in SEBAL

The user must determine the constants a and b in equation 10.5, using the T_0 and dT values of the wettest and the driest pixels that have been chosen for the image.

Once dT is determined, H is calculated by Equation 10.1. However, the result is only a preliminary estimate. SEBAL must internally repeat the calculation of H at least five times, as explained in the following section and in Appendix C due to the need to employ corrections to the estimates for r_{ah} due to instability (buoyancy) effects within the lower atmosphere caused by surface heating.

In Steps 12, 14, 16 and 18, the Monin-Obukov method is applied to estimate updated values for r_{ah}.

The stability corrected r_{ah} is calculated as;

$$r_{ah} = \frac{\ln\left(\frac{z_2}{z_1}\right) - \Psi_{h(z_2)} + \Psi_{h(z_1)}}{u_* \times k} \quad \text{… Equation 10.7}$$

where, z_1 and z_2 are heights which are determined in step 10, k is von Karman's constant (= 0.41), $?_h$ is the stability correction factor for atmospheric heat transfer, where $?_{h(z1)}$ is $?_h$ for the height z_1 and $?_{h(z2)}$ is $?_h$ for the height z_2.

In application of SEBAL, the component $?_{h(z1)}$ is ignored because the value is very small. Therefore, Equation 10.7 is modified as:

$$r_{ah} = \frac{\ln\left(\frac{z_2}{z_1}\right) - \Psi_{h(z_2)}}{u_* \times k} \quad \ldots \text{Equation 10.7'}$$

In equation 10.7', an updated value for u_* is computed during each successive iteration and for each pixel as;

$$u_* = \frac{u_{200} k}{\ln\left(\frac{200}{z_{0m}}\right) - \Psi_{m(200m)}} \quad \ldots \text{Equation 10.8}$$

where, u_{200} is wind speed at 200 m (if a user choses another height for the reference wind speed, then the wind speed at the reference height must be specified in Equation 10.8 instead of 200 m), $?_m$ is stability correction factor for atmospheric momentum transport. The stability correction factor for atmospheric heat transfer $?_h$ is calculated for negative values of L (i.e., for unstable conditions) as:

$$\Psi_{h(z_2)} = 2\ln\left(\frac{1 + x_{(z_2)}^{\ 2}}{2}\right) \ldots \text{Equation 10.9a}$$

where, $x_{(z2)}$ is a parameter (x) based on the z_2 height. The value for x is defined in Equation 10.11. For nonnegative values for L, the equation for stable conditions is:

$$\Psi_{h(z_2)} = -5\left(\frac{z_2}{L}\right) \ldots \text{Equation 10.9b}$$

The stability correction factor for atmospheric momentum transport $?_m$ is defined for L < 0 (unstable boundary layer) as;

$$\Psi_{m(200m)} = 2\ln\left(\frac{1 + x_{(200m)}}{2}\right) + \ln\left(\frac{1 + x_{(200m)}^{\ 2}}{2}\right) - 2ARCTAN\left(x_{(200m)}\right) + 0.5p \quad \ldots \text{Equation 10.10a}$$

where, x is defined in Equation 10.11. For stable conditions (L = 0) , the equation is:

$$\Psi_{m(200m)} = -5\left(\frac{z_2}{L}\right) \ldots \text{Equation 10.10b}$$

where the 200 represents the elevation height where u_{200} is calculated.

The x used in Equations 10. 9 and 10.10 is calculated for L < 0 as:

$$x_{(height)} = \left(1 - 16\frac{(height)}{L}\right)^{0.25} \ldots \text{Equation 10.11}$$

where (height) is the corresponding height z_2 or 200m, L is the Monin-Obukov length parameter given by equation 10.12. For L = 0, $x_{(height)} = 1$.

The Monin-Obukov length parameter L is

$$\mathrm{L} = -\frac{r_{\mathrm{air}}\mathrm{Cp}_{\mathrm{air}}\mathrm{u}*^{3}\mathrm{T}_0}{\mathrm{k\,g\,H}} \ldots \text{Equation 10.12}$$

where $?_{air}$ is air density in kg/m^3, Cp_{air} is heat capacity of air (= 1004 J/kg/K), T_0 is in K, g is gravitational acceleration (= 9.81 m/s^2), H is sensible heat flux in W/m^2.

20. Evaporative fraction, ?

Once the final (iteratively stable) values for H are calculated (by applying steps 10 through 19 four to five times), the latent heat flux ?E can be calculated from Equation 8.1 using values for H, G_o and R_n. This E represents the instantaneous evapotranspiration at the time of the Landsat overpass.

Following the computation of the evaporative fraction at each pixel of the image, one can estimate the 24-hour evapotranspiration for the day of the image by assuming that the value for the evaporative fraction ? is constant over the full 24-hour period. In this step, the evaporative friction ? is calculated for the instantaneous values in the image as:

$$\Lambda = \frac{l\mathrm{E}}{\mathrm{R_n} - \mathrm{G_0}} \ldots \text{Equation 20.1}$$

Equation 20.1 can be rewritten as

$$\Lambda = \frac{\mathrm{R_n} - \mathrm{G_0} - \mathrm{H}}{\mathrm{R_n} - \mathrm{G_0}} \ldots \text{Equation 20.2}$$

where the values for R_n, G_o and H are instantaneous values taken from processed images. Units for all flux parameters are expressed as W m^{-2}.

21. Twenty-four hour actual evapotranspiration

The 24 hour actual evaporation is calculated by the following equation:

$$ET_{24} = \frac{86400\Lambda(R_{n24} - G_{024})}{l} \quad \text{… Equation 21.1}$$

were, R_{n24} is daily net radiation; G_{024} is daily soil heat flux; 86,400 is the number of seconds in a twenty-four hour period; and ? is the latent heat of vaporization (J/kg). The latent heat of vaporization allows expression of ET_{24} in mm/day

In equation 21.1, G_{024} can be approximated for vegetative and soil surfaces as zero at the soil surface. This is because, on average, the energy stored in the soil during the daytime is released into the air at night. The value for G_{024} of snow can also generally be approximated as zero. For a water body, however, and especially in a deep lake, G_{024} does not become zero because of the high heat storage capacity of water. As discussed in Step 8, Equation 8.6 or 8.8 can be used to estimate the G_{024} for water.

In equation 21.1, the latent heat vaporization ? is defined as

$$l = \left(2.501 - 0.00236(T_0 - 273)\right) \times 10^6 \quad \text{(J/kg) … Equation 21.2}$$

The equation for calculating R_{n24} under conditions of clear sky (all day) is

$$R_{n24} = (1-a)R_{a24}t_{sw} - 110t_{sw} \quad \text{… Equation 21.3}$$

where Ra_{24} is daily extraterrestrial radiation which is calculated by Step 0.7. If the day of the satellite image is known to have had some cloudiness during periods preceding or following the time of the image, then one should use a locally (ground-based) measured value for 24-hour solar radiation (R_s) in place of $R_{a\,24}$ t_{sw} in Equation 21.3.

22. Cumulative (or seasonal) evapotranspiration

A cumulative evapotranspiration map can be derived from the 24-hour evapotranspiration maps made in Step 21 with a set of weather data.

The concept of this method is to expand 24-hour evapotranspiration proportionally to the reference evapotranspiration, where the reference evapotranspiration is derived from weather data. The fact that the reference ET is from a specific point in the image (or immediately outside the image) and therefore does not represent the actual condition at each pixel is not important for the extrapolation of the ET_{24} image in time, since the reference ET is used only as an index of the relative change in weather (and therefore ET and reference ET) for the image area. The assumption made is that the ET for the entire image area changes in proportion to the change in the reference ET at the index weather site. If this assumption is not true (for example where the image spans many mountain valleys or includes both coastal and inland areas having

different impacts by clouds or wind are not well correlated across the image), then the image should be broken down into subimages, each with its own reference ET index.

The first step in the expansion is to determine the period represented by each image. In the Bear River basin application, the July 14th image was chosen to represent the month of July, the August 15th image represented the month of August, the September 16th image represented the month of September, and the October 18th image represented the month of October.

The second step is to compute the alfalfa reference (ET_r) for the period represented by each image. In this project, we used the ET_r data that were available for 1985 from Hill, et al. (1989). Usually, a user must calculate ET_r using a Penman or Penman-Monteith reference ET equation or by means of a similar method. An alfalfa reference ET was used in the Bear River study since this type of method is common to Idaho and Utah. In other regions, as grass reference equation may be preferred, for example the FAO-56 Penman-Monteith equation or CIMIS Penman equation. Reference ET can be computed using the University of Idaho REF-ET software downloadable from the web at www.kimberly.uidaho.edu.

For the Bear River study, the values for ET_r used for monthly periods are summarized in the following Table.

Date	July14	August15	September 16	October 18
Cumulative ET_r (mm)	201	201	115	44.8
ET_r (mm)	6.6	7.1	4.6	2.0

Table22-1. Values of alfalfa reference ET, ET_r, and cumulative ET_r for the Bear River Basin in 1985.

The third step is to compute the value for K_m for each period. K_m is the ratio of cumulative reference ET to 24-hour ET, and is computed as K_m = (Cumulative ET_r) / (24-hour ET_r). For 1985, the values of K_m used are summarized in Table 22-2.

Period	July 1-31	August 1-31	September 1-30	1October 1-21
K_m	30.52	28.28	25.20	22.05

Table 22.2. Values of K_m, for the Bear River Basin in 1985.

The fourth step is to compute cumulative, seasonal ET. The equation for the computation is

$$ET_{cumulative} = \sum_{i=1}^{n} \left(ET_{SEBAL-24}\right)_i \left(K_m\right)_i$$

where $ET_{SEBAL-24}$ is the 24-hour ET predicted by SEBAL for each pixel of image "i" and K_m is the multiplier for ET for the representative period. n is the number of satellite images processed. Units for $ET_{cumulative}$ will be in mm when $ET_{SEBAL-24}$ is in mm/day.

References

Allen, R.G., L.S. Pereira, D. Raes and M. Smith, 1998, Crop evapotranspiration, FAO Irrigation and drainage paper 56, FAO

Amayreh, J.A. 1995. Lake evaporation: a model study. Ph.D. dissertation, Dept. Biological and Irrigation Engineering, Utah State University, Logan, UT. 178 p.

Bastiaanssen, W.G.M., M. Menenti, R.A. Feddes, and A.A.M. Holtslag. 1998. A remote sensing surface energy balance algorithm for land (SEBAL): 1. Formulation. *J. Hydrology* 212-213, p. 198-212.

ERDAS Field Guide – Fifth Edition, ERDAS Inc.

Horiguchi, Ikuo (Ed.) 1992. Agricultural Meteorology, Buneidou, Tokyo, Japan

Markham,B.L. and J.L. Barker, 1986. Landsat MSS and TM post-calibration dynamic ranges, exoatmospheric reflectances and at-satellite temperatures, EOSAT Landsat Tech. Notes (Aug.): 3-8

Markham, B.L and J.L. Barker, 1987. Thematic Mapper bandpass solar exoatmospherical radiances, Int. J. of Remote Sensing 8(3): 517-523

Van de Griend, A.A. and M. Owe. 1993. On the relationship between thermal emissivity and the normalized difference vegetation index for natural surfaces. *Int. J. of Rem. Sens.* vol 14(6):1119-1131.

Wukelic, G.E., D.E. Gibbons, L.M. Martucci and H.P. Foote, 1989. Radiometric calibration of Landsat Thematic Thermal Band, Remote Sensing of Environment 28: 339-347

7.0 Appendix B

Algorithms for applying SEBAL to sloping or mountainous areas

R.G. Allen and M. Tasumi
University of Idaho

This appendix describes the derivation of an equation to compute incoming solar radiation over a 24-hour period for sloping land surfaces.

Analytical Solution (Calculus-based)

A full equation for computing the instantaneous angle of incidence of beam radiation on sloping surfaces is taken from Duffie and Beckman (1980):

$$\begin{aligned}\cos(q) = &\sin(d)\sin(f)\cos(s) \\ &-\sin(d)\cos(f)\sin(s)\cos(g) \\ &+\cos(d)\cos(f)\cos(s)\cos(w) \\ &+\cos(d)\sin(f)\sin(s)\cos(g)\cos(w) \\ &+\cos(d)\sin(s)\sin(g)\sin(w)\end{aligned} \qquad (1)$$

where:

- d declination (positive in summer in northern hemisphere)
- f latitude (positive for northern hemisphere)
- s slope in radians, where s=0 is horizontal and s=p/2 = vertical downward (s is always positive and represents downward slopes in any direction)
- ? surface azimuth angle in radians. ? is the deviation of the normal to the surface from the local meridian, where ? = 0 for aspect that is due south, ? = - for east and ? = + for western aspect. ? = -p/2 represents east-facing slope and ? = +p/2 represents west-facing slope. ? = -p or ? = p represents a north-facing slope.
- ? hour angle. ? = 0 at solar noon. ? is negative in morning and ? is positive in afternoon

Total instantaneous incoming solar radiation, Kin, is computed as:

Kin = Gsc * dr * cos(?)

where G_{SC} is the solar constant and dr is the inverse of the square of the relative distance between the earth and sun.

Equation 1 can be integrated between two different sun-hour angles, ω_1 and ω_2 as:

$$\begin{aligned}\int_{\omega_1}^{\omega_2}\cos(\theta)\,d\omega &= \int_{\omega_1}^{\omega_2}\sin(\delta)\sin(\phi)\cos(s)\,d\omega \\ &- \int_{\omega_1}^{\omega_2}\sin(\delta)\cos(\phi)\sin(s)\cos(\gamma)\,d\omega \\ &+ \int_{\omega_1}^{\omega_2}\cos(\delta)\cos(\phi)\cos(s)\cos(\omega) \\ &+ \int_{\omega_1}^{\omega_2}\cos(\delta)\sin(\phi)\sin(s)\cos(\gamma)\cos(\omega) \\ &+ \int_{\omega_1}^{\omega_2}\cos(\delta)\sin(s)\sin(\gamma)\sin(\omega)\end{aligned} \qquad (2)$$

so that

$$\begin{aligned}\int_{\omega_1}^{\omega_2}\cos(\theta)\,d\omega &= \sin(\delta)\sin(\phi)\cos(s)(\omega_2-\omega_1) \\ &- \sin(\delta)\cos(\phi)\sin(s)\cos(\gamma)(\omega_2-\omega_1) \\ &+ \cos(\delta)\cos(\phi)\cos(s)(\sin(\omega_2)-\sin(\omega_1)) \\ &+ \cos(\delta)\sin(\phi)\sin(s)\cos(\gamma)(\sin(\omega_2)-\sin(\omega_1)) \\ &- \cos(\delta)\sin(s)\sin(\gamma)(\cos(\omega_2)-\cos(\omega_1))\end{aligned} \qquad (3)$$

and

$$K_{in\,24} = Gsc * dr * \int_{\omega_1}^{\omega_2}\cos(\theta)\,d\omega$$

where the integral is computed using Equation 3 and where ω_1 and ω_2 are the beginning and ending sun-hour angles where the sun's beam first strikes the surface. For a horizontal surface, ω_1 and ω_2 are equal to $-\omega_s$ and ω_s, where ω_s is the sunset hour angle.

Determining Limits for Equation 3.

For a sloping surface, the sun-hour angle where the sun's beam first strikes the slope is when cos(?) = 0. Therefore, Equation 1 can be solved for cos(?) as:

$$\cos(w) = \frac{\sin(d)\cos(f)\sin(s)\cos(g) - \sin(d)\sin(f)\cos(s) - \cos(d)\sin(s)\sin(g)\sin(w)}{\cos(d)\cos(f)\cos(s) + \cos(d)\sin(f)\sin(s)\cos(g)} \qquad (4)$$

Equation 4 has ? on both the left hand and right hand sides. Equation 4 can be reexpressed as:

$$\cos(w) = \frac{a}{b} - \frac{c}{b}\sin(w) \qquad (5)$$

where a, b, and c are constants for a given day, latitude, slope and slope azimuth:

$$a = \sin(d)\cos(f)\sin(s)\cos(g) - \sin(d)\sin(f)\cos(s) \qquad (5a)$$

$$b = \cos(d)\cos(f)\cos(s) + \cos(d)\sin(f)\sin(s)\cos(g) \qquad (5b)$$

$$c = \cos(d)\sin(s)\sin(g)\sin(w) \qquad (5c)$$

Squaring both sides of Equation 5:

$$\cos^2(w) = \left(\frac{a}{b} - \frac{c}{b}\sin(w)\right)^2 \qquad (6)$$

and using the relationship that $\cos^2(?) = 1 - \sin^2(?)$, Equation 5 becomes:

$$1 - \sin^2(w) = \left(\frac{a}{b} - \frac{c}{b}\sin(w)\right)^2 \qquad (7)$$

Solving for sin(?):

$$\left(1 + \frac{c^2}{b^2}\right)\sin^2(w) - \frac{2ac}{b^2}\sin(w) + \left(\frac{a^2}{b^2} - 1\right) = 0 \qquad (8)$$

Using the quadratic solution:

$$\sin(w) = \frac{\frac{2ac}{b^2} \pm \sqrt{\left(\frac{2ac}{b^2}\right)^2 - 4\left(1+\frac{c^2}{b^2}\right)\left(\frac{a^2}{b^2}-1\right)}}{2\left(1+\frac{c^2}{b^2}\right)} \qquad (9)$$

where a, b, and c are as defined by Equations 5a, 5b, and 5c.

Both solutions for the ± application of Equation 9 are useful, so that preliminary predictions to sin(?) are:

$$\sin(\hat{w}_1) = \frac{\frac{2ac}{b^2} - \sqrt{\left(\frac{2ac}{b^2}\right)^2 - 4\left(1+\frac{c^2}{b^2}\right)\left(\frac{a^2}{b^2}-1\right)}}{2\left(1+\frac{c^2}{b^2}\right)} \qquad (9a)$$

$$\sin(\hat{w}_2) = \frac{\frac{2ac}{b^2} + \sqrt{\left(\frac{2ac}{b^2}\right)^2 - 4\left(1+\frac{c^2}{b^2}\right)\left(\frac{a^2}{b^2}-1\right)}}{2\left(1+\frac{c^2}{b^2}\right)} \qquad (9b)$$

Refinement to the integration limits

These calculations for $?_1$ and $?_2$ serve as candidate limits for applying Equation 3, but may not always apply and must be compared against $?_s$ and against each other. The following procedure for determining the appropriate integration limits can be used:

Beginning limit ($?_1$)

a. Compute cos(?) from Equation 1 using $-?_s$+ 5 minutes (i.e., five minutes after sunrise, so that ? = $-?_s$ + 5/60*p/12). If cos(?) for this ? is positive, then $-?_s$ can serve as $?_1$ (i.e., $?_1 = -?_s$). Otherwise:
b. Compute cos(?) from Equation 1 using $?_1$ from Equation 9a + 5 minutes
(i.e., for ? = $?_{1 \text{ from (9a)}}$ + 5/60*p/12). If cos(?) for this ? is positive, then $?_{1 \text{ from 9a}}$ can serve as $?_1$ (i.e., $?_1 = ?_{1 \text{ from 9a}}$). Otherwise:
c. Use $?_1 = ?_{2 \text{ from 9b}}$
In summary, an affirmative step a indicates that the slope can “see” the sun immediately at sunrise. A nonaffirmative step a, but an affirmative step b indicates that the slope sees the sun after sunrise, but before noon. Step 3 (utilized only for steep slopes facing away from the sun) indicates that the slope does not see the sun until after noon (approximately).

Ending limit (ω_2)

a. Compute cos(?) from Equation 1 using ω_s - 5 minutes (i.e., five minutes before sunset, so that ω = ω_s - 5/60*p/12). If cos(?) for this ω is positive, then ω_s can serve as ω_2 (i.e., $\omega_2 = \omega_s$). Otherwise:
b. Compute cos(?) from Equation 1 using ω_2 from Equation 9b - 5 minutes
(i.e., for $\omega = \omega_{2 \text{ from (9b)}}$ - 5/60*p/12). If cos(?) for this ω is positive, then $\omega_{2 \text{ from 9b}}$ can serve as ω_2 (i.e., $\omega_2 = \omega_{2 \text{ from 9b}}$). Otherwise:
c. Use $\omega_2 = \omega_{1 \text{ from 9a}}$

In all cases, the following situations must be checked to insure numerical stability (these conditions all occur when slopes are steep and northerly facing so that the slope may be shaded during all times of the day):

1. The argument of the quadratic function (Equation 9a and 9b) must be limited to > 0. Therefore, if the argument is 0 or less, set it equal to 0.0001.

2. Check to insure that $\omega_1 = \omega_2$ (i.e., if $\omega_2 < \omega_1$ then set $\omega_2 = \omega_1$) (violation of this condition indicates that the slope is always shaded).

3. Check to make sure that the $\sin(\omega_1)$ and $\sin(\omega_2)$ from Equation 9a or 9b are between $-1 = \sin(\omega_1) = 1$ and $-1 = \sin(\omega_2) = 1$ before computing the ArcSines. If the $\sin(\omega_1)$ or $\sin(\omega_2)$ are outside these limits, then clip them to the limit.

Refer to the SunAngle24d spreadsheet for illustration of the application.

The logic expressed in deciding limits for integrating over the daylight period (when beam radiation is incident on the sloping surface) works well at all latitudes, dates, slopes and aspects. The only exception is for steep, north-facing aspects where the sun "sees" the slope at times near sunrise and at sunset, but, at some point in the day, the sun becomes southern enough in the sky that the slope comes into the shadow. Therefore, the slope sees the sun for a period in the morning and for a period in the evening, but not during midday. Of course, the integration equation assumes that this does not happen. This occurrence is rare and will not happen often.

The slope aspect (slope azimuth) can extend westward from 0 (south) to p (north) and can extend eastward from 0 (south) to -p (north). The slope, s, is always positive (positive slopes run downhill).

In summary, 24-hour R_a (i.e., $K_{in\ 24}$) can be computed using Equation 3 with limits predicted using Equation 9a, 9b, the sunrise and sunset hour angles, and the conditions and logic noted.

Limitations for Application to SEBAL

Besides the requirement to check the integration limits to insure numerical stability, the analytical approach assumes that all radiation reaching the surface is due to "beam" radiation, only with no diffuse component. In other words, if total short wave radiation at the surface is computed in SEBAL as: $R_{S\ surf} = R_{a24} * t_{sw}$, where t_{sw} is transmittance for the short-wave radiation, then, for periods when a slope is shaded, the above solution presumes that $R_{S\ surf} = 0$. However, there will be some diffuse radiation. An estimate of diffuse radiation for any surface is approximately 0.1 to 0.13 R_{a24_hor} where R_{a24_hor} is R_a computed for a horizontal surface. For high elevations (i.e., Bear Lake), 0.1 is appropriate. Therefore, a lower bound on $R_{S\ surf}$ could be expressed as 0.1 R_{a24_hor}.

Numerical Solution

As an alternative to applying the calculus solution previously described, the user can compute 24-hour total extraterrestrial energy by solving Equation 1 a large number of times during the day and then integrating numerically. This solution is easier to apply and requires less checking for stability and applicability of the integration limits required for the analytical solution. The numerical procedure also calculates accurately under all conditions, including those where a north-facing slope may shadow itself during midday, but receive beam radiation during early and late periods.

The numerical solution can be applied within ERDAS by making the following computations for each pixel:

For each 0.5 hour timestep during the day, and from midnight to midnight (i.e., -p <= ? <= p), apply Equation 1. In other words,

As ? is varied from -p to p by increments of 0.5 * p/12, the equation 1 is applied:

$$\begin{aligned}\cos(q)_w &= \sin(d)\sin(f)\cos(s) \\ &\quad -\sin(d)\cos(f)\sin(s)\cos(g) \\ &\quad +\cos(d)\cos(f)\cos(s)\cos(w) \\ &\quad +\cos(d)\sin(f)\sin(s)\cos(g)\cos(w) \\ &\quad +\cos(d)\sin(s)\sin(g)\sin(w)\end{aligned} \qquad (1)$$

where $\cos(?)_?$ is the value for cos(?) at each particular value for ? during the day. There will be 48 calculations during the day. Note, however, that the values for declination and latitude are constants for the date and image, so that these can be computed outside the 48 steps to reduce computation time.

After the 48 computations are made, then the following conditionals are applied to insure that 1) cos(?) is limited to a nonnegative number and 2) that cos(?) is set to zero if the hour angle is between sunset and sunrise (i.e., it is nighttime). This latter conditional is necessary because Equation1 is able to look at both sides of the slope (i.e., top and bottom). In other words, it presumes that the earth is transparent.

Therefore, for each value of $\cos(?)_?$, do the following:

If $\cos(?)_? < 0$ then $\cos(?)_? = 0$ (note that this can change to "If $\cos(?)_? < 0.1$ then $\cos(?)_? = 0.1$" to account for diffuse radiation during the daytime)

if $? < -?_s$ then $\cos(?)_? = 0$ (it is before sunrise)
if $? > ?_s$ then $\cos(?)_? = 0$ (it is after sunset).

After these computations are made, then all 48 values for $\cos(?)_?$ are summed and R_a is computed as:

$$R_{a24} = (0.5\ (3600)/10^6) G_{sc}\ d_r \sum_{i=1}^{48} \cos(q)_i$$

where R_{a24} will be in MJ/m^2/day for G_{sc} in W/m^2.

For R_{a24} in W/m^2:

$$R_{a24} = (0.5\ /\ 24)\ G_{sc}\ d_r \sum_{i=1}^{48} \cos(q)_i$$

The above values for R_{a24} are in MJ/day or Watts per m^2 of sloped surface. To express R_{a24} in energy per m^2 of equivalent horizontal plane for application in SEBAL, the following equations are used:

$$R_{a24} = ((0.5\ (3600)/10^6)/\cos(s))\ G_{sc}\ d_r \sum_{i=1}^{48} \cos(q)_i$$

where R_{a24} will be in MJ/m^2/day for G_{sc} in W/m^2.

For R_{a24} in W/m^2:

$$R_{a24} = ((0.5\ /\ 24)/\cos(s))\ G_{sc}\ d_r \sum_{i=1}^{48} \cos(q)_i$$

where s is the slope in radians and s is always = 0.

Lower limit for diffuse radiation

The above computation for R_{a24} assumes that all radiation reaching the surface is due to "beam" radiation, only, with no diffuse component. In other words, if total short wave radiation at the surface is computed as: $R_{S\ surf} = R_{a24} * t_{sw}$, where t_{sw} is transmittance for the short-wave radiation, then, for periods when a slope is shaded, the above solution presumes that $R_{S\ surf} = 0$. However, there will be some diffuse radiation. A minimum estimate of diffuse radiation for any surface will be approximately 0.1 to 0.13 R_{a24_hor} where R_{a24_hor} is R_a computed for a horizontal surface. For high elevations (i.e., Bear Lake), 0.1 is appropriate. Therefore, a lower bound on cos(?) for any daylight period should be 0.1.

Programming Implementation of the Numerical Procedure

In Visual Basic form, the numerical expression would be implemented as:

```
'programming by R.G. Allen, 2000

pi = 3.14159

'compute terms that are fixed for the entire image/date
term5=cos(decl)
term1=sin(decl)*sin(lat)
term2=sin(decl)*cos(lat)
term3=term5*cos(lat)
term4=term5*sin(lat)
omegas = pi/2 – atan((-tan(lat)*tan(decl))/((1-tan(lat)*tan(lat)*tan(decl)*tan(decl))^0.5)

FOR i = 1 to pixels

'compute terms that are used more than once in the cos(theta) equation to increase speed.
    cosslope=cos(slope)
    sinslope=sin(slope)
    cosaspect=cos(aspect)

  FOR timestep = 1 to 48
    omega =  - pi + timestep *0.5*pi/12
   cosomega=cos(omega)

'compute costheta for each of the 48 timesteps for pixel "i"
    costheta(timestep) = term1*cosslope - term2*sinslope*cosaspect +
term3*cosslope*cosomega+term4*sinslope*cosaspect*cosomega+term5*sinslope*sin(aspect)*sin(omega)

' check for negative values
    if costheta(timestep) < 0.1 then costheta(timestep)=0.1    '(0.1's represent diffuse radiation component)

'check for nighttime
     if omega < -omegas then costheta(timestep)=0
     if omega > omegas then costheta(timestep)=0

  NEXT timestep

'add up and compute Ra24 on a equivalent horizontal surface in W/m2 during the 24-hour period

  Ra24=0
  FOR timestep = 1 to 48
    Ra24=Ra24+costheta(timestep)
  NEXT timestep
   Ra24 = Ra24*Gsc * dr /48 / cosslope
   print "Ra24 for pixel "; i; " = "; Ra24
NEXT I
```

8.0 Appendix C

A Step-by-Step Guide to Running SEBAL

M. Tasumi, W. Bastiaanssen, and R.G. Allen
University of Idaho
and
International Institute for Aerospace Survey and Earth Sciences
Enschede, the Netherlands

SEBAL is the **S**urface **E**nergy **B**alance **A**lgorithm for **L**and. SEBAL was developed by Bastiaanssen (1995) and Bastiaanssen et al.(1998) and has been extended for use in mountainous and snow-covered regions of Idaho as well as for deep, clear lakes during an application to the Bear River basin of Idaho during 2000. This study was funded by the Idaho Department of Water Resources using funding provided by Raytheon, Inc. using funding provided by NASA.

The following sections describe application of SEBAL using the ERDAS Imagine image processing system. Background theory and development of SEBAL is described in Bastiaanssen (1995) and Bastiaanssen et al. (1998) and in Appendix A. Extensions of SEBAL for application to mountains (using digital elevation maps), snow, and water are described in Part II.

0.1. Intermediate files for slope/aspect correction

Input image : slope (**in degree**) and aspect (north=zero, 0~360^{o} clockwise) images derived from a digital elevation model (DEM)
Output image : sin_slope, cos_slope, sin_aspect, cos_aspect
Model : 001_slopeaspect

IMPORTANT: The area of coverage by the DEM file must be same as or larger than the TM image. Otherwise, there will be a divide by zero error in later steps.

The following three equations are for slope:

Slope in rad: n3 = $n1_slope*PI/180
sin(slope) = sin($n3_temp)
cos(slope) = cos($n3_temp)

The following three equations are for aspect:

Aspect in rad (South=0, West=positive -p~p): n9 = (($n10_aspect-180)*PI/180)
sin(aspect) = SIN($n9_temp)
cos(aspect) = COS($n9_temp)

The data type of the output file should be “Float Single”, and DO NOT set “Ignore zero” in the Stats calculation. You do not have to change anything unless the input data type is different. If the input data type was different (ex. the unit of slope was defined as percent, or the angle of aspect was defined as south=0 on your input image), you must modify the model appropriately.

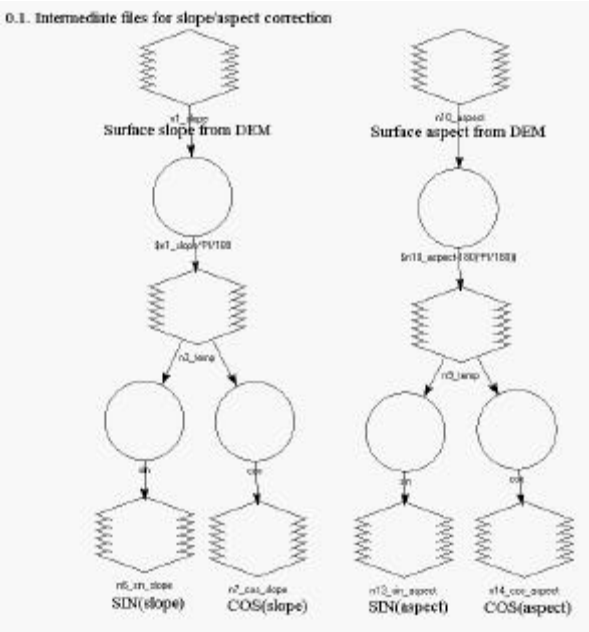

0.5. Cosine of solar incidence angle cos?, for instantaneous incoming short-wave radiation Kin

Input image : sin_slope, cos_slope, sin_aspect, cos_aspect
Output image : costheta0815
Model : 005_costheta0815

The following equations for cos?, where ? is the angle between the sun and nadir of a sloping surface is a standard equation based on trigonometry. This equation is contained in the model, and the all constants in the model must be changed for each image. The constants depend on the representative latitude of the location and the date and time of the image. The values of the constants are given in the attached MS-Excel file “Materials of slope correction.xls”.

Temporary cos? (relative to surface) = n8 = **0.15838***$n2_cos_slope - **0.1759***$n1_sin_slope*$n4_cos_aspect + **0.72203***$n2_cos_slope***0.9351** + **0.65012***$n1_sin_slope*$n4_cos_aspect***0.9351** +**0.97158***$n1_sin_slope*$n3_sin_aspect*(**-0.3543**)
cos? (horizontal equivalent) = $n8_memory/$n2_cos_slope

where the following describe how the coefficients are calculated:
0.15838 = sindsinF
0.1759 = sind cosF
0.72203 = cosd cosF
0.9351 = cos?

0.65012 = cosdsinF
0.97158 = cosd
-0.3543 = sin?

where d is declination of the earth, latitude is latitude of the location, and ? is the hour angle of the sun at when the satellite image was taken, expressed in radians (0 = noon).

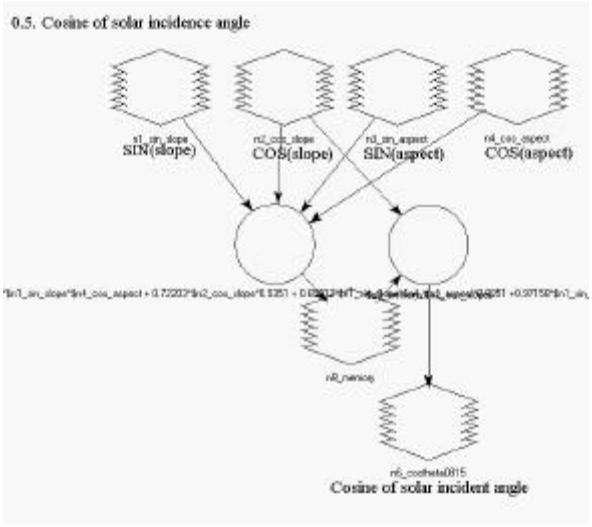

0.7 Twenty-Four-Hour Extraterrestrial Radiation, Ra_{24}

Input image : sin_slope, cos_slope, sin_aspect, cos_aspect
Output image : Ra24
Use model : 007_ra24

There are 21 equations are available in this step. Since this step has extremely complicated calculations, only information which is necessary for the calculation is given. The data type of the output file should be "Float Single", and set "Ignore zero" in the Stats calculation.

The following is the equations in this step. The numbers given for the equations are corresponded to the numbers of functions in the model. The underlined constants must be changed for each image. All numbers necessary to change are given in the attached MS-Excel file "Materials of slope correction.xls". The equations in this model should not be changed except the constants listed below. ERDAS Imagine 8 has some bugs in the "Modeler", and a user must remember that an unexpected error might occur if the structure of an equation is changed, especially in complicated equations. If a user must change a structure of an equation, we recommend to validate the edited model carefully.

1 **0.15838***$n9_cos_slope
2 **0.1759***$n8_sin_slope*$n11_cos_aspect
3 **0.72203***$n9_cos_slope
4 **0.65012***$n8_sin_slope*$n11_cos_aspect
5 **0.97158***$n8_sin_slope*$n10_sin_aspect

6 $n16_temp - $n15_temp + $n14_temp * COS($n32_temp+0.0218166) + n13_temp*COS($n32_temp+0.0218166)+$n12_temp*SIN($n32_temp+0.0218166)

7 $n16_temp-$n15_temp+$n14_temp*COS($n31_temp-0.0218166)+$n13_temp*COS($n31_temp-0.0218166)+$n12_temp*SIN($n31_temp-0.0218166)

8 $n16_temp - $n15_temp + $n14_temp*(**-0.1980**) + $n13_temp*(**-0.1980**) + $n12_temp*(**-0.9802**)

9 $n16_temp - $n15_temp + $n14_temp*(**-0.1980**) + $n13_temp*(**-0.1980**) + $n12_temp*(**0.9802**)

10 $n15_temp-$n16_temp

11 $n13_temp+$n14_temp

12 ((2*$n19_temp*$n12_temp/($n20_temp**2))**2)-4*(1+($n12_temp**2)/($n20_temp**2))*(($n19_temp**2)/($n20_temp**2)-1)

13 (2*$n19_temp*$n12_temp/($n20_temp**2)+ ($n24_temp**0.5)) / (2*(1+($n12_temp**2)/($n20_temp**2)))

14 EITHER ($n22_memory) IF ($n22_memory>0.0001) OR (0.0001) OTHERWISE

15 (2*$n19_temp*$n12_temp/($n20_temp**2) - ($n24_temp**0.5)) / (2*(1+($n12_temp**2)/($n20_temp**2)))

16 EITHER (-1.5708) IF ($n27_memory < (-1)) OR (EITHER (1.5708) IF ($n27_memory > 1) OR (ASIN ($n27_memory)) OTHERWISE) OTHERWISE

17 EITHER (-1.5708) IF ($n28_memory < (-1)) OR (EITHER (1.5708) IF ($n28_memory > 1) OR (ASIN ($n28_memory)) OTHERWISE) OTHERWISE

18 EITHER (**-1.79195**) IF ($n34_memory > 0) OR (EITHER ($n32_temp) IF ($n45_memory>0) OR ($n31_temp) OTHERWISE) OTHERWISE

19 EITHER (**1.79195**) IF ($n36_memory >= 0) OR (EITHER ($n31_temp) IF ($n46_memory>0) OR ($n32_temp) OTHERWISE) OTHERWISE

20 EITHER($n52_memory) IF ($n52_memory>$n51_temp) OR($n51_temp) OTHERWISE

21 ($n16_temp*($n53_memory-$n51_temp)-$n15_temp*($n53_memory-$n51_temp)+$n14_temp*(SIN($n53_memory)-SIN($n51_temp))+$n13_temp*(SIN($n53_memory)-SIN($n51_temp))-$n12_temp*(COS($n53_memory)-COS($n51_temp)))***212.391**

The following is the explanation of numbers necessary to change.

In eq.1, 0.15838 is sind sinF which is used in Step 0.5
In eq.2, 0.1759 is sind cosF which is used in Step 0.5
In eq.3, 0.72203 is cosd cosF which is used in Step 0.5
In eq.4, 0.65012 is cosdsinF which is used in Step 0.5
In eq.5, 0.97158 is cosd which is used in Step 0.5
In eq.8, two (-0.1980) are cosine of 5min after sunrise angle
In eq.8, (-0.9802) is sine of 5min after sunrise angle
In eq.9, two (-0.1980) are cosine of 5min before sunset angle
In eq.9, (0.9802) is sine of 5min before sunset angle
In eq.18, (-1.79195) is sunrise angle
In eq.19, (1.79195) is sunset angle
In eq.21, 212.391 is Gsc related constant which value is calculated as "12*60/p*Gsc*dr" in W/m^2.

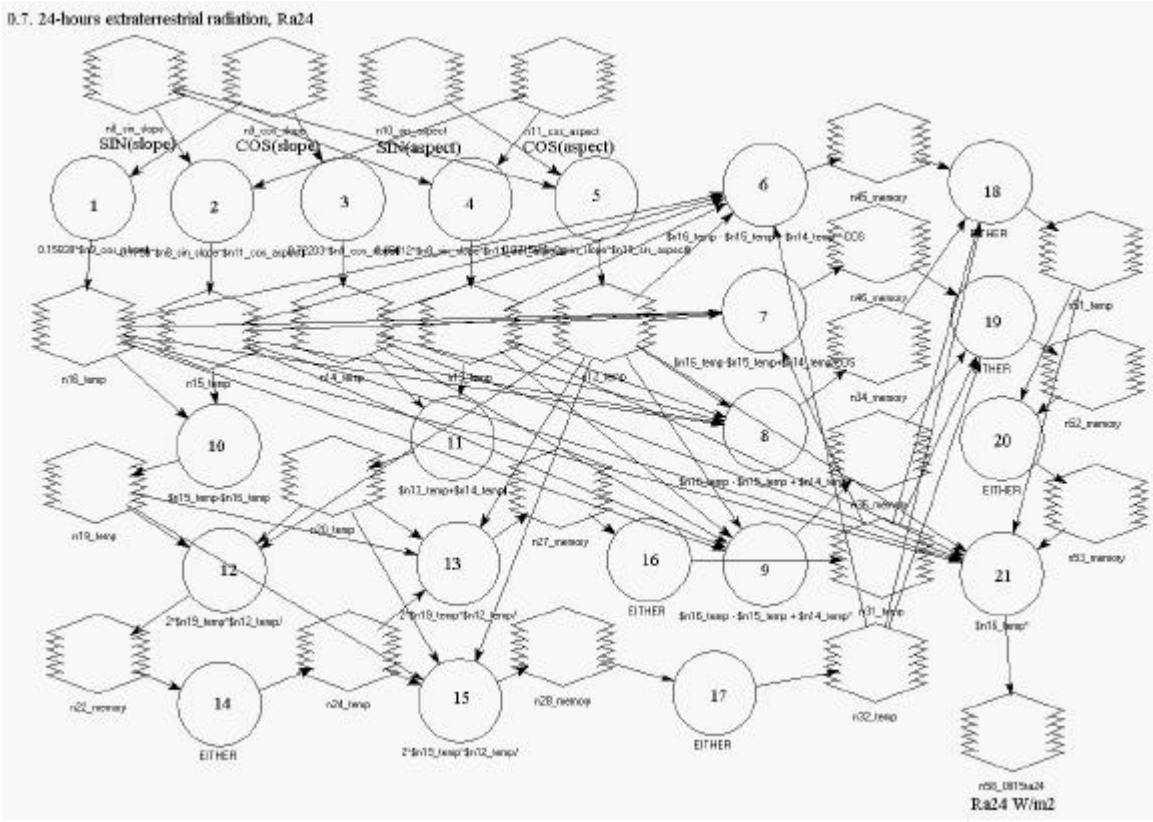

1. Spectral reflectance (unadjusted for transmittance)

Input image : Original Image, costheta0815
Output image : r1, r2, r3, r4, r5, r7
Use model : 01_reflectance

The following six equations are contained in the model, and the underlined constant 0.9762 in the equation should change for every acquisition due to changing zenith angles and sun-earth distances. Note that these reflectance values are not discounted for the effects of two-way transmittance of the atmosphere. This is done later during the albedo calculation. The data type of the output file should be “Float Single”, and set “Ignore zero” in the Stats calculation. For most Landsat 5 images,

r1 = (((-0.15+(15.21+0.15)*$n1_3831_150885(1)/255))*PI)/(195.7* costheta0815 *__0.9762__)
r2 = (((-0.28+(29.68+0.28)*$n1_3831_150885(2)/255))*PI)/(182.9* costheta0815 *__0.9762__)
r3 = (((-0.12+(20.43+0.12)*$n1_3831_150885(3)/255))*PI)/(155.7* costheta0815 *__0.9762__)
r4 = (((-0.15+(20.62+0.15)*$n1_3831_150885(4)/255))*PI)/(104.7* costheta0815 *__0.9762__)
r5 = (((-0.037+(2.72+0.037)*$n1_3831_150885(5)/255))*PI)/(21.93* costheta0815 *__0.9762__)
r7 = (((-0.015+(1.44+0.015)*$n1_3831_150885(7)/255))*PI)/(7.452* costheta0815 *__0.9762__)

The underlined constant 0.9762 is “inverse relative distance Earth-Sun, dr” (See. Example). The dr is also given by the attached MS-Excel file “Materials of slope correction.xls”.

The coefficients in the above equations for r will change for Landsat 7 images. For Landsat 7 images having “high gain” for channels 1-5 and 7, the above equations become:

r1 = (((-6.2+(191.6+6.2)*$n1_3831_150885(1)/255))*PI)/(1970* costheta0815 ***0.9762**)
r2 = (((-6.4+(196.5+6.4)*$n1_3831_150885(2)/255))*PI)/(1843* costheta0815 ***0.9762**)
r3 = (((-5.0+(152.9+5.0)*$n1_3831_150885(3)/255))*PI)/(1555* costheta0815 ***0.9762**)
r4 = (((-5.1+(157.4+5.1)*$n1_3831_150885(4)/255))*PI)/(1047* costheta0815 ***0.9762**)
r5 = (((-1.0+(31.06+1.0)*$n1_3831_150885(5)/255))*PI)/(227.1* costheta0815 ***0.9762**)
r7 = (((-0.35+(10.8+0.35)*$n1_3831_150885(7)/255))*PI)/(80.53* costheta0815 ***0.9762**)

These coefficients are larger in magnitude than those for LS5 since LS7 are expressed in W/m^2 per steradian per micrometer rather than in milliWatts/cm^2 per steradian per micrometer for LS5. For some Landsat 7 images, the gain used may shift from high to low, especially for channel 4. Therefore, the user needs to refer to the “header” for the image to obtain correct calibration coefficients to use.

Example of calculation of “dr” for Aug 15, 1985 Path038 & Row031.

“dr” is given as dr = 1+ 0.033 * cos (“DOY” * 2p / 365)
where dr is the inverse of the relative distance from the sun to the earth squared.
DOY is the Day of the year

In this equation, the unit of the angle (“DOY” * 2p / 365) is in radians

Since the DOY for Aug 15 is 227, dr is determined as,
dr = 1+ 0.033 * cos (227 * 2p / 365) = 0.9762

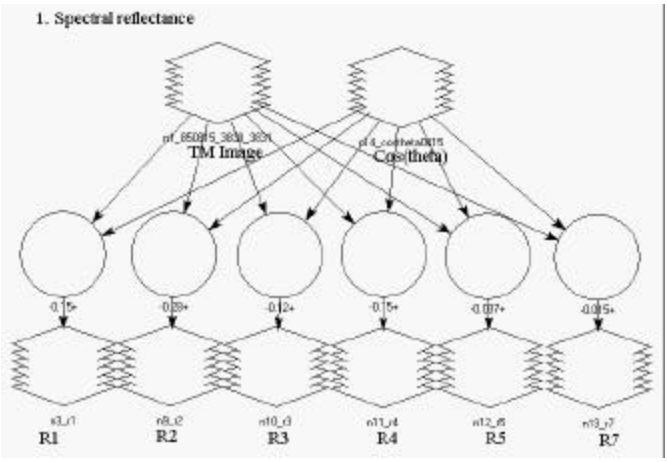

2. Surface albedo at the top of atmosphere (unadjusted for transmittance)

Input image : r1, r2, r3, r4, r5, r7
Output image : albedo_toa
Use model : 02_broadband_albedotoa

The following equation is contained in the model, and it does not need any change because they represent weighing coefficients which assign more weight in the spectral integration to the visible bands than to the near-infrared bands.
The data type of the output file should be “Float Single”, DO NOT “Ignore zero” in the Stats calculation.

For Landsat 5, albedo_toa =
$n1_r1*0.293+$n5_r2*0.274+$n2_r3*0.233+$n6_r4*0.157+$n7_r5*0.033+$n8_r7*0.011

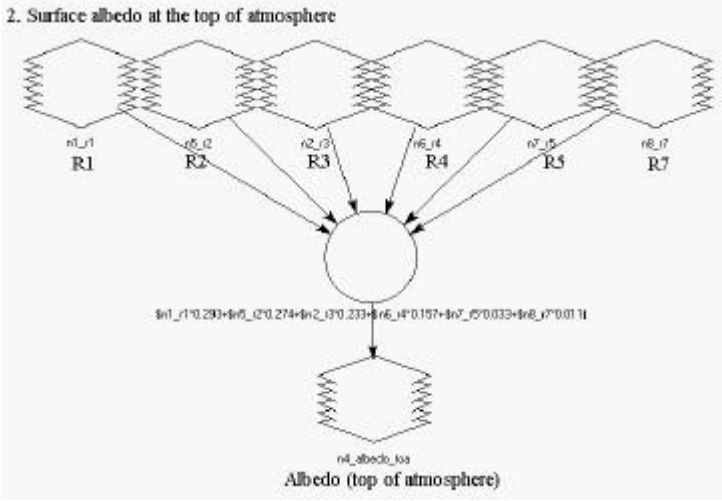

For Landsat 7, albedo_toa =
$n1_r1*0.293+$n5_r2*0.274+$n2_r3*0.231+$n6_r4*0.156+$n7_r5*0.034+$n8_r7*0.012

3. Surface albedo

Input image : albedo_toa, DEM
Output image : surface_albedo, trans
Use model : 03_surface_albedo

The following equations are contained in the model, and the underlined constant 0.0**3** in the equation should be adapted to account for atmospheric conditions for EACH image.
The data type of the output file should be “Float Single”, and DO NOT set “Ignore zero” in the Stats calculation.

One way transmittance t_{sw} = n7 = 0.75 + (2 * (10**(-5)) * $n5_dem)
surface albedo = ($n2_albedotoa - **0.03**) / ($n7_trans**2)

The underlined constant 0.03 is the reflectance of path radiance occurring at the top of the atmosphere "a_{path}".
The ($n7_trans**2) explains "two-way transmittance, t_{sw}^2", caused by the double path that reflected solar radiation has to be propagated. Two-way transmittance is required here, because the reflectances computed in steps 1 and 2 were unadjusted for transmittance in either direction. Since the t_{sw}^2 is automatically calculated by DEM file, this parameter will change automatically.

The a_{path} cannot be determined directly, so the user must determine the value by trial and error. The offset is obtained easily by studying the reflectance of dark targets such as seas. The slope is more controlled by the reflectance of bright targets such as bare land, snow and clouds. The two-way transmittance could also be determined from well-calibrated pyranometer data (these data, if used, should be traceable to the national or international solar standards).

Procedure for determining a_{path}.

First the user can assume the value as a_{path} = 0.03, and make an image of surface_albedo by running the model.

Next one can open the surface_albedo image, and check to seeif the results for albedo seem reasonable and appropriate.
Typically, surface albedo values are;
water=0.05, salts=0.50-0.60, desert=0.30-0.40, crops=0.15-0.25, forest=0.10-0.15

Other values are given in Appendix A and in various textbooks.
If the calculated values lie in the range of the usual values, initial estimates are probably appropriate.
If the calculated values fall outside the expected range, then value of a_{path} should perhaps be adjusted and the surface albedo re-estimated.
However, extreme caution should be used in adjusting these values. The value for t_{sw} should be confirmable by high quality pyranometer measurements.

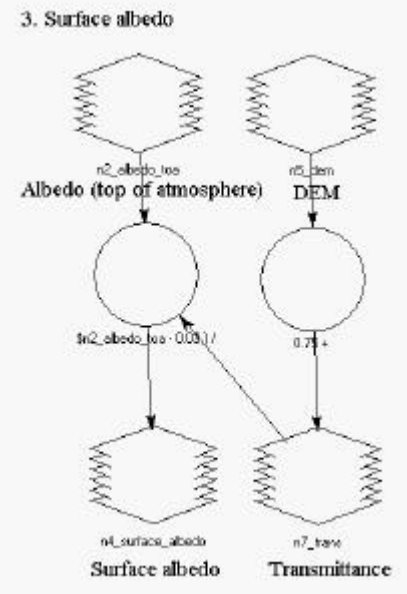

4. Normalized Difference Vegetation Index, NDVI

Input image : r3, r4
Output image : NDVI
Use model : 04_ndvi

The following equation is contained in the model, and the users does not have to change anything. The data type of the output file should be “Float Single”, and DO NOT set “Ignore zero” in the Stats calculation.

NVDI = ($n2_r4-$n1_r3)/($n2_r4+$n1_r3)

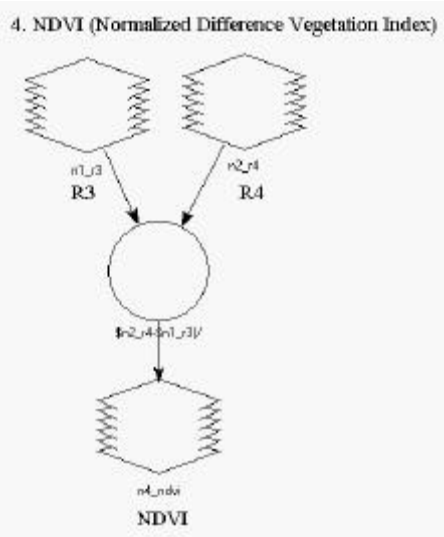

5. Thermal infrared surface emissivity

Input image : ndvi, surface_albedo
Output image : emissivity
Use model : 05_emissivity

There is one expression for emissivity and three other equations for adjusting for extraordinary conditions. The effective limits of emissivity are 0.9 <= emissivity <= 1.0. The user should not change any coefficient in the equations.

The data type of the output file should be “Float Single”, and set “Ignore zero” in the Stats calculation.

Emissivity: n2 = 1.009 + 0.047 * LOG ($n1_ndvi)
WaterFilter: n8 = EITHER 1 IF ($n1_ndvi < 0) OR $n2_memory OTHERWISE
SnowFilter: n10 = EITHER 1 IF ($n7_surface_albedo > 0.47) OR $n8_memory OTHERWISE
DesertFilter: Emissivity = EITHER $n10_memory IF ($n10_memory > 0.90) OR 0.9 OTHERWISE

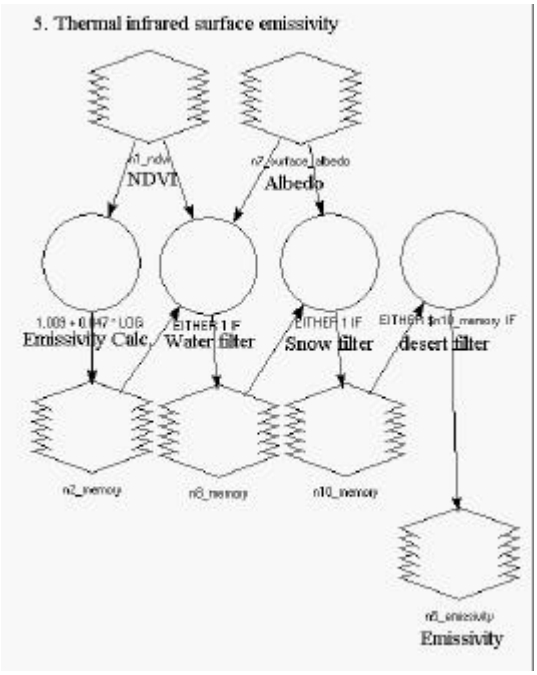

6. Surface temperature

Input image : original image, emissivity
Output image : surftemp
Use model : 06_surftemp

The following equations are contained in the model, and the user should not change any coefficients in the equations. This procedure for surface temperature uses the Planck approach. The Stephan-Boltzman constant does not apply since the full thermal spectrum is not utilized. The data type of the output file should be “Float Single”, and DO NOT set “Ignore zero” in the Stats calculation.

n3 = 0.1238+((1.56-.1238)*$n1_3831_150885(6)/255)
n5 = 1260/(log(61.6/$n3_memory+1))
T_0 = $n5_memory/(($n6_emissivity)**0.25)

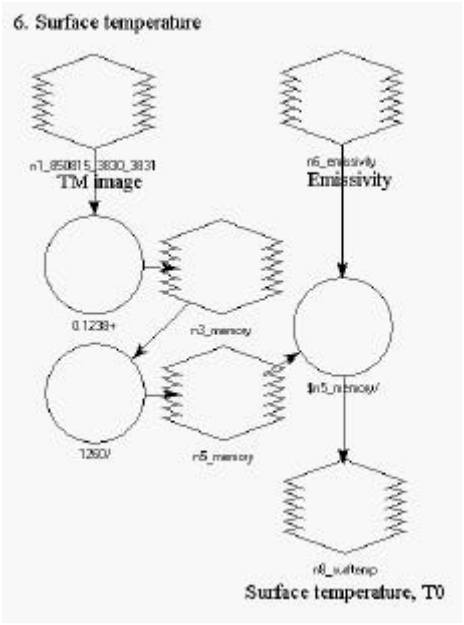

6.5. Apparent Surface Temperature at a Reference Elevation (corrected for the elevation effect (using a lapse rate) for calculation of sensible heat flux)

Input image : surftemp, DEM
Output image : surftemp_dem
Use model : 105_surftemp_dem

The following equation is contained in the model.
The data type of the output file should be “Float Single”, and set “Ignore zero” in the Stats calculation.

surftemp_dem = ($n1_dem-**1805**)*0.0065+$n4_surftemp

The underlined value 1805 is a reference elevation in m for low-lying areas in the Bear River basin where NDVI and H were identified. The user should change this value to one that is appropriate for the image area. It is appropriate to choose a representative elevation near the area of interest (AOI).

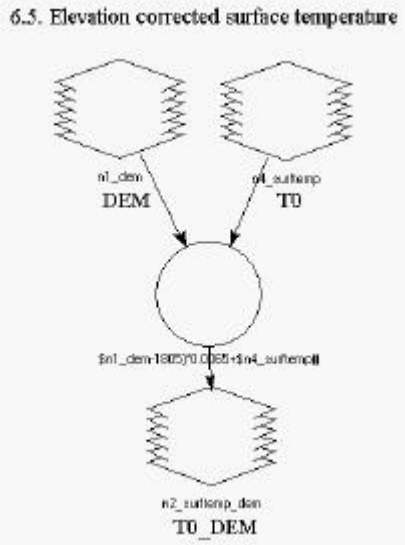

7. Net radiation

Input image : surface_albedo, emissivity, surftemp, costheta0815, trans
Output image : rn
Use model : 07_netradiation

The following three equations are contained in the model, and the user must change the underlined constants in the equation for EACH image. The data type of the output file should be “Float Single”, and set “Ignore zero” in the Stats calculation.

Lin: n14 = 1.08 * ((-LOG ($n10_trans))**0.265) * 5.67 * (10**(-8)) * (**289**4)

Rn = ((1 - $n3_surface_albedo) *1367*$n8_costheta0815***0.9762***$n10_trans) + $n14_memory - ($n2_emissivity* (5.67 * (10 ** (- 8))) * ($n1_surftemp ** 4)) - ((1 - $n2_emissivity) * $n14_memory)

where 1367 W/m^2 is the solar constant. The first underlined constant 289 is reference temperature Tref in K (See. Example). The second underlined constant 0.9762 is the “inverse of the square of the relative distance of the Earth-Sun, dr”. The same value from Step 1 should be used.

How to determine reference temperature Tref Reference temperature Tref (K) is the instantaneous air temperature at screen height, and it can be estimated as the surface temperature of well irrigated plots. In the Bear River basin Aug.15 image, we chose Tref as 289K which was the surface temperature of a well irrigated alfalfa field.

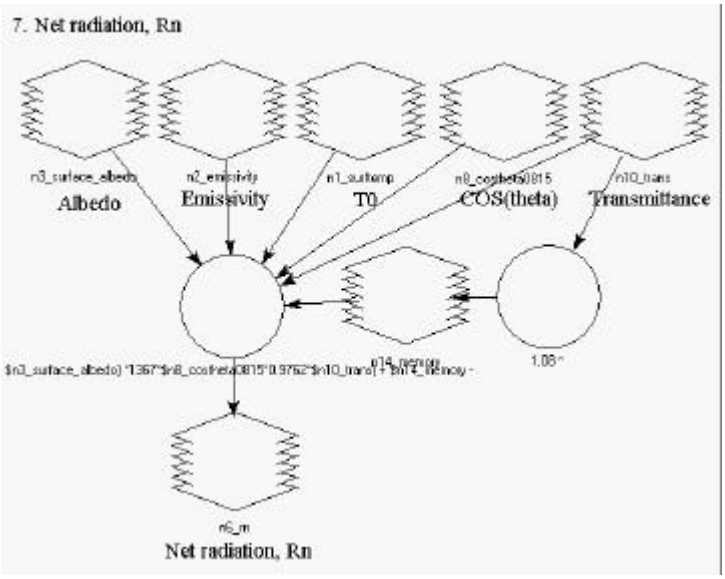

8. Soil heat flux

Input image : ndvi, rn, surftemp, surfsce_albedo
Output image : g0
Use model : 08_soilheatflux

The following three equations are contained in the model. The data type of the output file should be “Float Single”, and set “Ignore zero” in the Stats calculation. In this step, the soil heat flux G is predicted from NDVI and net radiation Rn, by applying a relationship from Bastiaanssen (1995, Fig. 6.8) that was based on data from four different sources. This relationship does not include a parameter for albedo that was proposed by Bastiaanssen et al. (1998), since the latter does not appear to produce reasonable estimates for the Bear River region. The algorithm from Bastiaanssen (1995) agrees relatively well with a leaf-area-index based prediction of G/Rn by Choudhury et al. (1987).

Filters for water surface and snow surface are used to apply different algorithms for G, since G in these surfaces are not possible to predict by NDVI. G for water bodies is predicted using an algorithm for deep, clear lakes that was derived during this study based on data taken from Yamamoto and Kondo (1968) and validated using data for Bear Lake, Idaho from Amayreh (1995). G for snow is predicted as 0.5 Rn. The Appendix A contains details and explanation. The user does not have to make any change in this model if he/she agrees with our assumptions.

The user MUST CHANGE the underlined coefficients **1** and **90**. These values are for G for water. If the date of an image is in between July to December, the equation of G for water becomes G = **1***Rn-**90**. For the period from January to June, G_{24} = **0.9***Rn-**40**. See Appendix A for details.

G calculation: n8 = 0.3*(1 - (0.98 * ($n1_ndvi ** 4)))*$n2_rn
Water Filter = n13 = EITHER (**1***$n2_rn-**90**) IF ($n1_ndvi<0) OR ($n8_memory) OTHERWISE

Snow Filter: G = EITHER (EITHER (0.5*$n2_rn) IF ($n15_surftemp<277) OR ($n13_memory) OTHERWISE) IF ($n10_surface_albedo>0.47) OR ($n13_memory) OTHERWISE

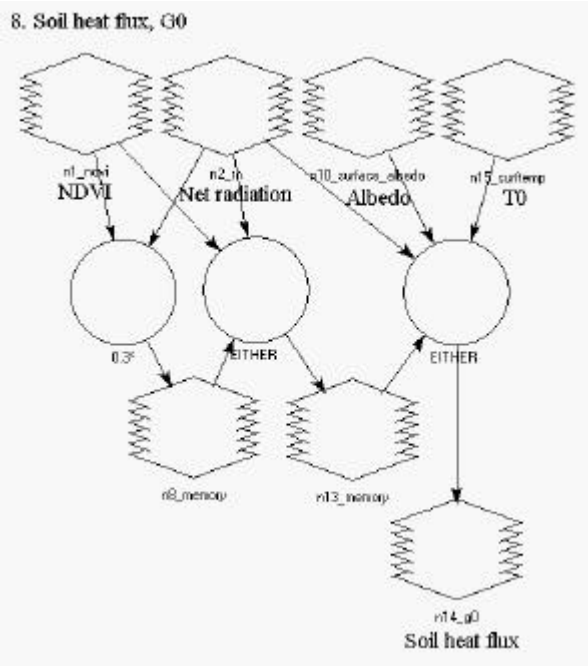

9. Surface roughness for momentum transport, z0m

Input image : ndvi, slope (in degree) derived from DEM
Output image : z0m
Use model : 09_ z0m

The following two equations are contained in the model. The user must change the underlined coefficients in the equation for EACH image. Units of z0m are m and units of slope in ERDAS are degrees. The data type of the output file should be "Float Single", and DO NOT set "Ignore zero" in the Stats calculation.

z0m calculation = n3 = EITHER (EITHER (EXP (**0.9648** * $n2_ndvi **- 3.3356**)) IF ((EXP (**0.9648** * $n2_ndvi **- 3.3356**)) < **0.246**) OR (**0.246**) OTHERWISE) IF ($n7_slope < **5**) OR (EITHER (EXP (**5.5895** * $n2_ndvi **- 3.2705**)) IF ((EXP (**5.5895** * $n2_ndvi **- 3.2705**)) < **4**) OR (**4**) OTHERWISE) OTHERWISE
Water Filter: zom = EITHER $n3_memory IF ($n2_ndvi> 0.0) OR 0.001 OTHERWISE

The coefficients "**0.9648**" and "**-3.3356**" are based on the actual growing conditions in fields. In the field area, we assumed that the maximum height of z0m is **0.246**m.
The coefficients "**5.5895**" and "**-3.2705**" are based on the actual growing conditions in forests in the Bear River basin, Aug. 1985. (See. Example). These coefficients are also given by the MS-Excel file "z0m.xls". In the forest area, we assumed that the maximum height of z0m is **4**m. Forests are differentiated from agriculture by assuming that all land surfaces having slope less than **5** degrees (about 8.5%) are agricultural or rangeland and slopes above **5** degrees are forested (potentially). This induces some error in pixels in agricultural areas that are along sides of channels and ditches, but the error is minor. Allen

(personal communication, 2000) found that using NDVI/albedo in the above equation provided better differentiation between tall trees and low growing vegetation.

Example for calculating linear constants

z0m is the surface roughness which can be calculated following standard ASCE procedures (Jensen et al., 1990) as;
z0m = 0.123 * (vegetation height in m)

For example, if the vegetation height is 0.5 m, z0m is 0.123 * 0.5 = 0.06 m

Note that if vegetation is sparsely populated, the equation z0m = 0.2*h might be better to use instead of z0m = 0.123*h.
In bear River Basin, z0m values were calculated using coefficient 0.123 for the field areas, and 0.2 for the mountainous areas.

To obtain a relationship between z0m and NDVI, we estimated the surface roughness at a few selected locations from which the crop height was assessed from a cropping calendar. At these 'anchor points', matching NDVI data were read from the image file.

The relationship between NDVI and surface roughness z0m is expressed as;
z0m = exp(a * NDVI + b), which a and b are constants.

Locations are selected from the NDVI image created during Step 4. Locations containing the vegetation of interest in the image are selected where the height of the vegetation can be approximated. NDVI values from several pixels of similar vegetation should be selected and averaged. For these NDVI values, the associated height should be approximated, based on the type of vegetation and time of year. The value for z_{0m} can then be calculated.
As an example, the following three sample pixels for the field areas in Bear River Basin on Aug. 15 1985 were chosen. The constants can be calculated as the following graph.

1. Burned rangeland : NDVI = 0.07, z0m = 0.037m, lnz0m = -3.30
2. Alfalfa : NDVI = 0.80, z0m = 0.074m, lnz0m = -2.61
3. Natural Vegetation : NDVI = 0.49, z0m = 0.062m, lnz0m = -2.79

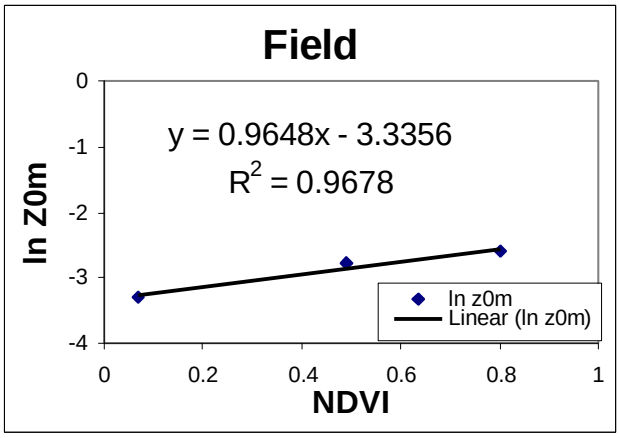

From the calculation, slope “a” was determined as “0.9648”, and intercept “b” was determined as “-3.3356”.

For the calculation of linear constants in forests, the samples for Natural vegetation and Trees were used.

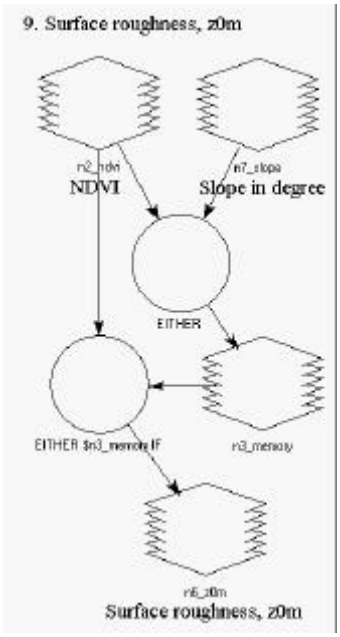

10. First guess of friction velocity u_*1 and aerodynamic resistance to heat transport rah1.

Input image : z0m
Output image : u_star1, rah1
Use model : 10_rah1
Other requirement : one point of wind speed and the vegetation height at the location where wind speed was observed.

The following two equations are contained in the model. The user must change the first underlined coefficient 5.3 for EACH image, and might need to change the other three underlined coefficients if assumptions on heights z_1, z_2 and z_{u*} are different (see appendix A).

The data type of the two output files should be “Float Single”, and DO NOT set “Ignore zero” in the Stats calculation.

u_star1 = **5.3***0.41/(log(**200**/$n1_z0m))
rah = log(**2** / **0.01**)/($n2_u_star1*0.41)

The first underlined coefficient 5.3 is estimated wind speed (m/s) at z_{u*} = 200m above the surface, u_{200}. (See the attached EXCEL file “windspeed.xls”. See also the following Example). The second coefficient z_{u*} = 200 is the blending height at which the estimated wind speed is assumed to be aerially constant. The height 200m was determined as the height at which wind speed is not affected by local variability in surface roughness and where the momentum flux is aerially constant. A large height is taken to minimize SEBAL model input, because wind speed from one routine weather station is sufficient (although more point data are always better). The third coefficient 2 and the fourth coefficient 0.01 are the upper and lower heights of the integration of the eddy diffusivity necessary for the calculation of the aerodynamic resistance to heat transport. A low value is intentionally chosen to cope with local scale variability, i.e. more variability occurs closer to the land surface. The integration heights are held constant to avoid problems resulting from unreliable estimates of the surface roughness length for heat transport.

Example of estimating wind speed at 200m using observed wind speed near surface level .

Field observation:
Wind speed = 2.3 m/s at 2 m.
The height of vegetation around the Met. Station is approximately 0.5m (which means that the surface roughness z0m at the point is 0.06m).

The basic equation is:
$u_x / u_* = 1 / 0.41 * \ln (z_x / z0m)$
where, u_x is wind speed at height x (m/s), z_x is height x which the wind speed u_x is observed (m),
u_* is friction velocity (m/s), z0m is surface roughness (m)

First, calculate u_* at the Met. Station by the field measurement data.
Since, u_x is 2.3 (m/s), z_x is 2 (m), and z0m is 0.06 (m),
$u_* = 2.3 * 0.41 / (\ln (2/0.06)) = 0.2689$ m/s

Next, calculate u_{200} at the Met. Station by calculated u_*
Since z_x is 200 (m), u_* is 0.2689 (m/s), z0m is 0.06 (m),
$u_{200} = (0.2689 / 0.41) * \ln (200 / 0.06) = 5.3$ m/s

This wind speed u_{200} = 5.3 m/s can be assumed as constant for whole image.

10. First guess of friction velocity, u*1, and aerodynamic resistance to heat transport, rah1

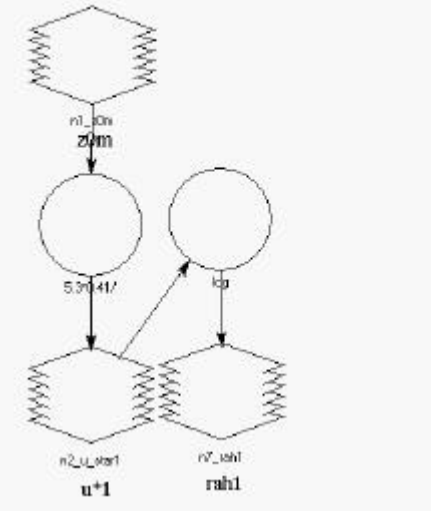

11. First guesses of sensible heat flux h1

Input image : surftemp_dem, rah1, surftemp, DEM
Output image : h1, air_density1
Use model : 11_h1

The following equations are contained in the model. **The user must change the two underlined coefficients** for EACH image.
The data type of the output file should be "Float Single", and DO NOT set "Ignore zero" in the Stats calculation.

dT1: n7 = **0.42658** * $n1_surftemp_dem - **123.28**
air temperature: n10 = $n8_surftemp-$n7_temp
air_density1 = 349.467*((($n10_memory-0.0065*$n11_dem)/$n10_memory)**5.26)/$n10_memory
H1 = $n13air_density1 * 1004 * $n7_temp / $n4_rah1

where air_density1, in kg /m^3, is the first estimate for air density for moist air, and 1004 J/kg/K is the air specific heat at constant pressure. The other two underlined constants "1.321" and "–381.9" are linear constants a and b (See. Example, Also see the attached "rah.xls"). Air density may change according to mean air temperature for the image and with elevation. The other two constants change for each step of the iteration cycle.

Example of calculate linear constants

In this example, procedures for finding the linear constants between dTa and To are explained. We recommend that the user read Appendix A for detail.

Open the elevation corrected surface temperature map (surftemp_dem.img).
The user should search for the coldest (= darkest) pixel that occurs in an agricultural area or other area known to have vegetation. One should avoid mountainous areas where impacts of slope and snow induce uncertainties in the estimates for R_n and G that are necessary for predicting H for this cold pixel. Generally, a well-watered agricultural field or marshland are good candidates for the "cold" pixel. The assumption of H ~ 0 will be made at this pixel. Water bodies should be avoided due to the problem of lag in stored heat (G) into the body that may not be available at the same instant as Rn, H and LE. Once the pixel has been selected, the user should note the temperature of the pixel as T_{cold}. The location of the pixel should be noted for future reference as well.
The value of the temperature in surftemp_dem.img is given in K. In Bear River basin in Aug.15, 1985, Tcold was 289.
Next, find the hottest (= brightest) pixel in a region where the land slope is known to be relatively flat (less than about 10%) and note the UTM and the temperature as T_{hot}
This step is difficult, since some searching and subjective decision-making are required.
The procedure presumes that there is no H from the coldest pixel and that there is no ET from the hottest pixel.
Therefore, the user should choose a location within the image where the latter assumption is plausible. Basically, a hot place is drier than a location with similar conditions but having a lower temperature. This is not always true because land uses are not constant within the image.

The best way to choose the hottest location (it is assumed that the "hottest" pixel is synonymous with the "driest" spot) is, by selecting a hot and possibly man-made place. However, if a man-made location is selected (for example a road or parking lot with asphalt cover), then one should confirm that the NDVI prediction and subsequent prediction of G are reasonable for that surface.
In the Bear River basin, we chose a large burned area in a rangeland region as the hottest location and T_{hot} was 330 K in Aug.15, 1985.

Next, open the net radiation map (netradiation.img), find the place where the user chose Thot, and record the value as Rnhot. Our Rnhot at the burned point was 471.73 W/m^2.
Next, open the soil heat flux map (soilheatflux.img), find the place where the user chose Thot, and record the value as G_0hot. Our G_0hot at the burned point was 141.52 W/m^2.
Next, open rah1 map (rah1.img), find the place where the user chose Thot, and record the value as rah1hot. Our rah1hot at the burned point was 51.05 s/m.

Now, calculate sensible heat flux at the hottest place Hhot. Note that the latent heat flux can be ignored (it is assumed to be zero at the hottest pixel) and that the sensible heat flux is therefore equal to the net available energy.
Hhot is calculated as;

Hhot = Rnhot – G_0hot

Therefore, our Hhot was, Hhot = 471.73 – 141.52 = 330.21 W/m^2.

Next, calculate dThot from the following equation.
The air density ? air is required to calculate dThot, and the air temperature is required for the calculation of ? air. Since the air temperature is unknown in this instance, we assume the air temperature is 20^{o}C.

$$dThot = \frac{Hhot \times rah1hot}{r_{air20C} \times 1004}$$

$$r_{air20C} = \frac{1000 \times P}{1.01 \times (20 + 273) \times 287}$$

$$P_{20C} = 101.3\left(\frac{293 - 0.0065z}{293}\right)^{5.26}$$

where, z is the representative elevation of the region in m

Now, the user has values for Tcold, Thot and dThot.
Under most conditions, the user can assume that dTcold = 0 over the well-watered (cold) pixel (i.e., H_{cold} = 0).

Then, by making linear relation between T and dT, the user can calculate a and b.
Our slope "a" was "0.4266", and our intercept "b" was "-123.28"

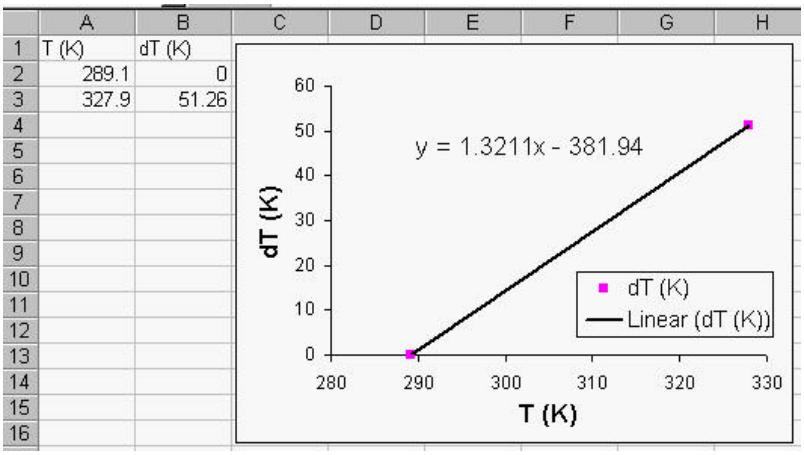

(*The values in the graph are different from our values. This is a sample)

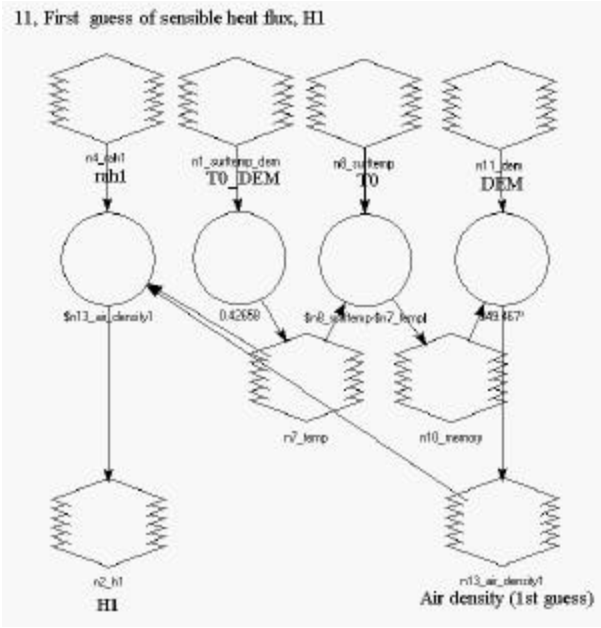

12. Friction velocity u_*2 and aerodynamic resistance to heat transport rah2.

Input image : surftemp, h1, u_star1, z0m, air_density1
Output image : u_star2, rah2
Use model : 12_rah2

The following step applies Monin-Obukov stability functions to the calculation of aerodynamic resistance. These functions were summarized in Allen et al., (1996).
The following seven equations are contained in the model. Seven constants are underlined which are kept constant for the application.

The underlined constant 5.3 in the sixth equation MUST BE CHANGED when different images are processed. The constant 5.3 is indicative of the regional wind speed at 200 m. During the iterations to determine u_* from windspeed, it should be held constant. Other underlined constants 0.01, 2, and 200 are the heights which were used in Step 10. The user does not have to change them unless he/she changed the height in Step 10.
The data type of the two output files should be “Float Single”, and DO NOT set “Ignore zero” in the Stats calculation.

n5 = EITHER (-1004 * $n30_air_density1 * ($n22_u_star1 ** 3) * $n1_surftemp) / (0.41 * 9.81 * $n3_h1) IF ($n3_h1 ne 0) OR -1000 OTHERWISE
n25 = EITHER ((1 - 16 * (**200** / $n5_temp)) ** 0.25) IF ($n5_temp < 0) OR 1 OTHERWISE
n12 = EITHER ((1 - 16 * (**2** / $n5_temp)) ** 0.25) IF ($n5_temp < 0) OR 1 OTHERWISE
n10 = EITHER (2 * LOG ((1 + $n25_memory) / 2) + LOG ((1 + $n25_memory ** 2) / 2) - 2 * ATAN ($n25_memory) + 0.5 * PI) IF ($n5_temp < 0) OR (-5***2** /$n5_temp) OTHERWISE
n11 = EITHER (2 * LOG ((1 +$n12_memory ** 2) / 2)) IF ($n5_temp < 0) OR (-5***2** /$n5_temp) OTHERWISE
u_star2 = (**5.3***0.41)/(log(**200**/$n28_z0m)-$n10_memory)
rah2 = (log(**2** / **0.01**)-$n11_memory)/(0.41*$n27_u_star2)

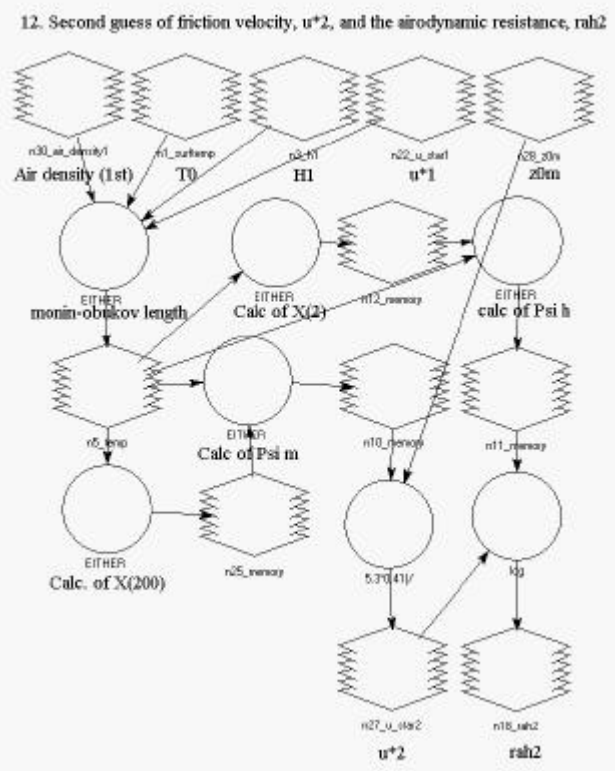

13. Make images of second guesses of sensible heat flux H2

Input image : surftemp_dem, rah2, surftemp, DEM
Output image : h2, air_density2
Use model : 13_h2

Basically this process is the same as Step 11. Only the coefficients are different.
The following equation is contained in the model. The user must change the two underlined coefficients for EACH image.
The data type of the output file should be “Float Single”, and DO NOT set “Ignore zero” in the Stats calculation.

dT2: n7 = **0.24098** * $n1_surftemp_dem – **69.644**
air temperature: n10 = $n8_surftemp-$n7_dt2
air_density2 = 349.467*((($n10_memory-0.0065*$n11_dem)/$n10_memory)**5.26)/$n10_memory
H2 = $n13air_density2 * 1004 * $n7_temp / $n4_rah2

The two underlined constants “0.24098” and “-69.644” are linear constants a and b (See. Example). These constants are also given in the MS-Excel file “rah.xls”.

Example of calculating updated constants a and b.

The basic concept for the calculation is the same as done in Step 11.
To calculate an updated a and b, the only thing that the user must do is to calculate an updated dT by using the rah2 and air_density1 values, instead of the rah1 value and temporary air density by assuming Tair=20^{o}C, for the hottest pixel selected from Step 11.

First, open the rah2.img map, and record the value from the hottest pixel selected in Step 11. We will call the value rah2hot. Our value for rah2hot for the example Aug 15, 1985 image was 23.492 s/m.
Next, open the air_density1 map, and record the value where the user chose as the hottest place in Step 11. We will call the value air_density1hot. Our value was 0.782kg/m^3

Next, calculate an updated dThot.
dThot can be calculated as

$$dThot = \frac{Hhot \cdot Rah2hot}{air\_density1hot \cdot 1004}$$

In this equation, Hhot is the value which was used in Step 11.
Since our Hhot was 330.21 W/m2, our updated dThot was

$$dThot = \frac{330.21 \cdot 23.492}{0.782 \cdot 1004} = 9.8803$$

Now, the user can calculate updated constants “a” and “b” by using values of Tcold (which was selected in Step 11), dTcold (which is zero), Thot and dThot.
Our slope “a” was “0.24098”, and our intersection “b” was “–69.644”.

14. Make images of third guesses for friction velocity u*3 and aerodynamic resistance to heat transport rah3.

Input image : surftemp, h2, u_star2, z0m, air_density2
Output image : u_star3, rah3
Use model : 14_rah3

This procedure is exactly the same as done in Step 12.
The user does not have to change any coefficient in the model unless the height values in Step 10 have been changed. Simply give the folder and name of input and output files, and run the model. The updated u_star and rah images are created automatically.

15-19. Internal Iterations for Stability (Continued)

Steps 15-19 are the same as done in Steps 13 and 14.

The user has to calculate the updated linear constants a and b in Steps 15, 17 and 19 by using updated rah and air_density values. Finally, converged image h5.img is obtained that is based on aerodynamic stability functions that reflect the impact of buoyancy caused by the heat flux.

20. Image of the instantaneous evaporative fraction.

Input image : rn, h5, g0
Output image : evapo_fr
Use model : 20_evapo_fr

The following two equations are included in the model. The user does not have to change any coefficient in the equations. The data type of the output file should be “Float Single”, and DO NOT set “Ignore zero” in the Stats calculation.

n7 = ($n1_rn-$n3_h5-$n13_g0) / ($n1_rn -$n13_g0)
evapor_fr = EITHER 0.0 IF ($n7_memory < 0.0) OR $n7_memory OTHERWISE

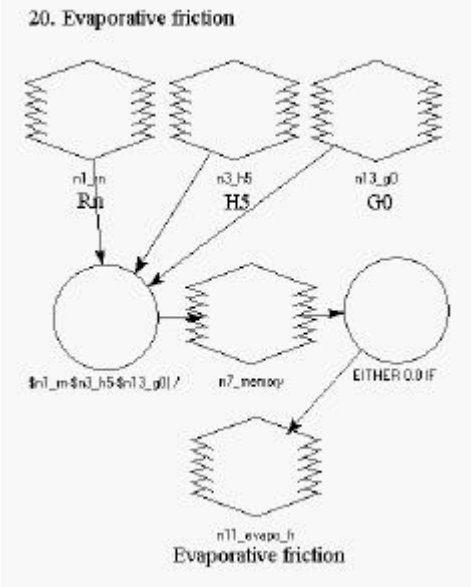

21. Image of 24 hour actual evapotranspiration.

Input image :surface_albedo, 0815ra24, cos_slope, trans, surftemp, ndvi, evapo_fr
Output image : ET24
Use model : 21_ET24

The following equations are included in the model. The 24hrs soil heat flux, G_{24}, is assumed to be zero for vegetated surfaces and will have a nonzero value for water bodies. The treatment of G_{24} for water is described in the Appendix A. On a snow surface, the heat used to melt a snowpack is G that is permanently invested in converting to liquid water. Therefore, $G_{24} > 0$, but the amount of the energy would be very small. Therefore, we suggest that a very gross approximation is that $G_{24} = 0$ for snow. This is a very approximate assumption and should be changed if better information is available. The fraction could also be changed with time of year.

The user MUST CHANGE the underlined coefficients 1 and 100. These values are for G_{24} for water. If the date of a image is in between July to December, the equation of G_{24} for water becomes G_{24} = **1***Rn-**100**. For the period from January to June, G_{24} = **0.9***Rn-**50**. See Appendix A for details.

The data type of the output file should be “Float Single”, and DO NOT set “Ignore zero” in the Stats calculation.

Rn24 = n3 = (1 - $n5_surface_albedo) * ($n13_0815ra24 / $n24_cos_slope) * $n14_trans -(110 *$n14_trans)
Latent heat of vaporization = n7 = (2.501 - 0.002361 * ($n8_surftemp - 273)) * (10 ** 6)
G24 Water Filter = n23 = EITHER (**1***$n3_temp**-100**) IF ($n15_ndvi<0) OR (0) OTHERWISE
ET24 = $n12_evapo_fr * (($n3_temp - $n23_memory) * 86400) / ($n7_memory)

This simplified formula for net outgoing long wave radiation is from Slob (deBruin (1987)). Ra24 is 24-hour extraterrestrial radiation and is computed for each pixel to take into account slope and aspect. It is computed as Ra24 = 1367 dr (integration of cos(theta)) / cos(slope). The integration of cos(theta) is taken over the period from sunrise to sunset, less any periods when the slope is shaded. The product is divided by cos(slope) to express the radiation on an equivalent horizontal plane.

The parameter n7 above is the latent heat of vaporization which is used to convert W/m^2 into mm of evaporated water. It is based on surface temperature.

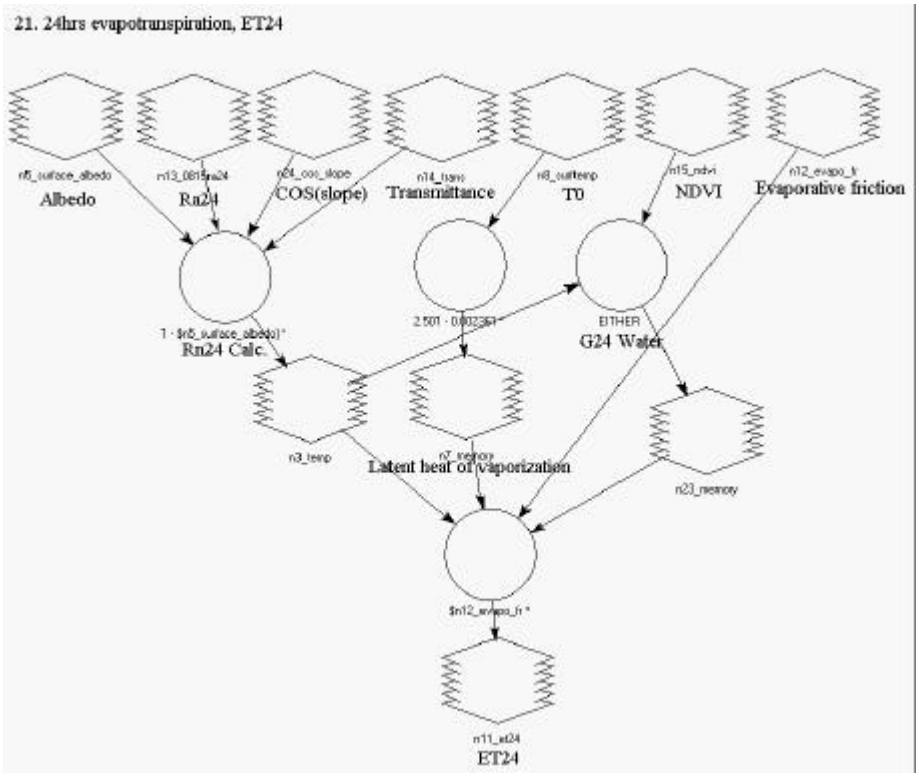
21. 24hrs evapotranspiration, ET24
Albedo
Ra24
COS(slope)
Transmittance
T0
NDVI
Evaporative friction
Rn24 Calc.
G24 Water
Latent heat of vaporization
ET24

References

Allen, R.G., Pruitt, W.O., Businger, J.A., Fritschen, L.J, Jensen, M.E., and Quinn, F.H. (1996). "Evaporation and Transpiration." Chapter 4, p. 125-252 in: Wootton et al. (Ed.), *ASCE Handbook of Hydrology*. New York, NY.

Amayreh, J.A. 1995. Lake evaporation: a model study. Ph.D. dissertation, Dept. Biological and Irrigation Engineering, Utah State University, Logan, UT. 178 p.

Bastiaanssen, W.G.M. 1995. Regionalization of surface flux densities and moisture indicators in composite terrain: A remote sensing approach under clear skies in Mediterranean climates. Ph.D. dissertation, CIP Data Koninklijke Bibliotheek, Den Haag, the Netherlands. 273 pages.

Bastiaanssen, W.G.M., M. Menenti, R.A. Feddes, and A.A.M. Holtslag. 1998. A remote sensing surface energy balance algorithm for land (SEBAL): 1. Formulation. *J. Hydrology* 212-213, p. 198-212.

Choudhury, B.J., Idso, S.B., and Reginato, R.J. 1987. Analysis of an empirical model for soil heat flux under a growing wheat crop for estimating evaporation by an infrared temperature based energy balance equation. *Agr. and For. Meteor* 39:283-297.

deBruin, H.A.R. , 1987. From Penman to Makkink. In: Hooghart, J.C. (Ed.), Proceedings and information: TNO Committee on Hydrological Research, Vol 39. Gravenhage, The Netherlands, p. 5-31.

Jensen, M.E., R.D. Burman, R.G. Allen (ed.). 1990. *Evapotranspiration and Irrigation Water Requirements*. Am. Soc. Civ. Engr. Manual No. 70. 332 p.

Yamamoto, G. and J. Kondo. 1968. Evaporation from Lake Nojiri. *J. Meteor. Soc. Japan*. 46:166-176.